A HYBRID CONTROL MODEL OF FRACTONE-DEPENDENT MORPHOGENESIS

A DISSERTATION SUBMITTED TO THE GRADUATE DIVISION OF THE
UNIVERSITY OF HAWAI‘I AT MĀNOA IN PARTIAL FULFILLMENT
OF THE REQUIREMENTS FOR THE DEGREE OF

DOCTOR OF PHILOSOPHY

IN

MATHEMATICS

AUGUST 2015

By
Aaron Tamura-Sato

Dissertation Committee:

Monique Chyba, Chairperson
George Wilkens
Daisuke Takagi
Yuriy Mileyko
Thomas Ernst

Acknowledgments

Special thanks goes to my advisor, Dr. Monique Chyba, for all of her advice, support, and the many opportunities she has given me to expand my appreciation for and knowledge of mathematics and mathematics education.

I would like to thank Dr. Frederic Mercier for his expertise and knowledge of biology and fractones, and giving me the opportunity to observe and perform practical biology research in his lab.

Thanks go also to Zachary Deweese for his contributions to the coding of the model implementation, and help with the visualization of the model data; and to Dr. Zou Rong for her contributions to the model code and assistance in the biology lab.

I would like to thank all members of my committee for their time, consideration, and advice in my research.

Finally, I would like to thank my parents and family for their boundless love and support.

This research received support from the NSF: NSF Award DGE-0841223.

Abstract

It has been hypothesized that the generation of new neural cells (neurogenesis) resulting from cell proliferation and differentiation in the developing and adult brain is guided by the extracellular matrix. The extracellular matrix of the neurogenic niches comprises specialized structures termed fractones, which are scattered in between stem/progenitor cells. Fractones have been found to bind and activate growth factors at the surface of stem/progenitor cells to influence their proliferation. We present a mathematical control model that considers the role of fractones as captors and activators of growth factors, controlling the rate of proliferation and directing the location of the newly generated neuroepithelial cells in the forming brain. The model is a hybrid control system that incorporates both continuous and discrete mechanics. The continuous portion of the model features the diffusion of multiple growth factor concentrations through the mass of cells, with fractones acting as sinks that absorb and hold growth factor. When a sufficient amount has been captured, growth is assumed to occur instantaneously in the discrete portion of the model, causing an immediate rearrangement of cells, and potentially altering the dynamics of the diffusion. The fractones in the model are represented by controls that allow for their dynamic placement in and removal from the evolving cell mass. These controls allows us to govern its developing shape. A version of the model has been implemented for computer simulation and initialized with real biological data. We hope to show the potential usefulness of such a model to verify the plausibility of the fractone hypothesis.

Table of Contents

List of Tables

List of Figures

Chapter 1

Introduction

The focus of this research is to construct a mathematical model of morphogenesis, the biological process by which we take on our particular shape. Morphogenesis is a complicated process. All creatures begin as a single fertilized egg, and grow cell by cell, taking on their particular form and anatomy. Morphogenesis is clearly a controlled process, as our growth is not random; infants grow in the womb at approximately the same rate, features develop at approximately the same time, and most humans are born with the same structures (limbs, eyes, organs, etc.) in the same locations. Yet morphogenesis is also a flexible process. Although they all start as a single cell, clearly newborns between species are not the same; puppies, kittens, fish fry, and human babies are all easy to distinguish. Even within species, differences are clear. Appearance and development between males and females is different. Among humans, we may have similar body structure, but some of us grow to be taller than others, other have longer limbs, and people of different ethnicities tend toward certain distinguishable features.

Where do these similarities and differences stem from? The obvious answer for a modern reader is DNA. That single cell that all living creatures start from is unique in terms of its DNA; unique between species, and unique even within species. DNA encodes all of the information for how development will occur. While extensive research is being pursued on the genetic code, our work does not examine the DNA itself, but rather how the DNA is expressed. If DNA is the blueprint for development, how does that development actually occur? DNA on its own cannot create the body. We know from years of experiments and measurements what the form of a developing embryo should be at any given time, but the dynamics of that growth and what drives it are less well understood.

It is important motivation to note that not all humans are born with all the usual features or have their bodies develop in the usual way. While some of these abnormalities are relatively

harmless, such as polydactylism (more than the usual number of fingers or toes), some of these abnormalities are detrimental to the health of the individual, either physically or mentally. The better we understand how the body develops during pregnancy and after birth, the better we will understand why problems occur. Our hope is that better understanding will lead to better treatments and preventative therapies to minimize the incidence and impact of these detrimental conditions. This approach is all the more important in light of the ongoing debate on the morality of genetic treatments. While it is true that genetic alteration may be able to prevent a host of diseases in the future, the ethical concerns must be taken seriously. However, therapies based on treating expression during development, while still potentially controversial, may be far more palatable as they are more in-line with modern medical practice.

Our model of morphogenesis seeks to study how the developing embryo is organized on a cellular level in order to grow into a specific morphology (shape). Our growth occurs through mitosis of individual cells, the splitting of one mother cell into two new daughter cells. It is only through repeated acts of mitosis over time that the cell mass can form. This growth, however, is not random, and so must be controlled by a governing mechanism.

It is currently uncertain how the embryo organizes and directs cellular growth. Several factors are believed to be involved, including the forces at play as cells push and pull on one another [12] [52]. Another known factor is that cellular growth can be caused or halted by the introduction of "growth factors", chemical signals that are detected by the cells through receptors on the cell surface [65]. Several growth factors exist, signalling cells to react in a particular way, such as undergoing rapid mitosis, halting mitosis altogether, or to migrate to a different area [6]. However, such chemical signals would typically diffuse freely around the cells, lacking the specificity and precision that may be required for proper development. One hypothesis for directed cellular growth is that small extracellular structures called "fractones", which are found attached to cells, direct the growth [32]. They do this by capturing specific growth factor with specialized receptors and concentrating it for presentation to the cells it is attached to. In this way, cells with fractones react with specificity to the presence of particular growth factors. Different fractones may target different growth factors, and thus the distribution of specific types of fractones throughout the developing embryos can direct the growth of the entire organism.

Experimental testing of this hypothesis is extremely difficult, however. Identifying fractones in a developing embryo requires killing of the subject, meaning that is currently impossible to examine how fractones affect development in vivo. For the same reason, it is also impossible to create a time series of development in the same organism. Because experimentation is so difficult,

we turn to mathematical models to simulate development. **The goal of our project is to we develop a mathematical model based on the new hypothesis of fractone-directed growth in order to verify its plausibility.**

Applying mathematical models to biology has a long history. Biological experimentation is difficult to design for many reasons. Biological experiments tend to be time-consuming and expensive, ethical and environmental issues abound, and control and repeatability are difficult to ensure. Mathematical models are able to avoid most of these difficulties.

Biological systems can be infinitely complex, whether we are discussing population dynamics or organ function or neurogenesis. The interactions between environment and species, hormones and enzymes, genetics and proteins are often not well understood by researchers and too complicated to model with complete detail. Models therefore simplify the system, taking into account only the most important details. Mathematical models have many advantages to biological research. Population models and epidemic models allow researchers to predict future behavior, helping them to advise policy and strategy for saving species or averting pandemics. Organ, genetic, and developmental models are an ethical alternative to actual experimentation which would be controversial at best.

The model we will develop in this paper simplifies the biology of neurogenesis, but focuses on the hypothesis that fractones guide development by either promoting or stalling mitosis in specific locations. While many cellular growth models have been developed in the past [4] [11] [14] [67], as the fractone hypothesis is relatively recent, to our knowledge no model incorporating fractones has been studied. The dynamics of the model are quite complicated, combining several different features necessary for examining the hypothesis in question.

Our objectives are to incorporate into the model the mechanism of fractones capturing growth factors and thereby directing the cellular growth, to implement and verify the behavior of the model, and to demonstrate that the model is readily capable of being applied to real-world data in order to study the fractone-governed morphogenesis hypothesis.

The model we use is a controlled hybrid automata [35]. The term "hybrid" refers to the how the model is a combination of discrete and continuous dynamics. In our model, diffusion of growth factor and capture by fractones is a continuous process, while the growth of cells is a discrete process, occurring instantaneously by assumption, and causing an immediate change to the geometry of the cell mass and therefore the mechanics of the diffusion. The hybrid automata system formalizes a way in which these dynamics can interact with each other.

While the model is a simplification of reality, it is still a complicated model with several parts. Two different growth factors undergo perturbed diffusion through the system space. The first growth factor we term the“positive” growth factor, meaning it promotes accelerated growth in cells of about one mitosis event every 6 hours. The second growth factor is a “negative” growth factor, meaning it will stop cells from undergoing mitosis. A third “neutral” growth factor is implicitly in the system, and although we do not track its diffusion or capture by fractones, we assume it is present and binding to receptors on the cells, triggering growth at a neutral rate of one mitosis event every 24 hours, even without a fractone directing it. The growth factors diffuse around the cells normally, except near fractones, which act like sinks, absorbing and concentrating growth factor near their associated cell. When enough positive growth factor is absorbed, and assuming insufficient negative growth factor was absorbed, the cell will undergo mitosis.

Mitosis creates two daughter cells from the mother cell instantaneously by assumption. In our algorithm, the direction of the growth is determined by the position of the fractone relative to the cell and according to a growth algorithm. The mitosis event causes a sequence of pushes among the cells in the mass and rearranges the position of the cells in order to make room for the new cells. This deformation of the cells also affects the fractones and growth factors in the system. This naturally alters the diffusion dynamics in the continuous phase of the model.

The locations of the fractones in the system are modeled by controls, which allow us to create, remove, and relocate fractones in the system. Since the fractones not only promote or inhibit growth but also determine the direction of growth in our model, the control allows us to steer growth in particular directions. It is through the understanding of these controls and the extent to which we can steer the growth that we will gain an idea of how well fractones can direct morphogenesis.

The meninges, a sheathe-like structure that covers the central nervous system even in early development, is also incorporated into the model. The meninges surrounds the cell mass and acts as the primary source of growth factor, producing it at discrete time intervals at a rate determined by a given function. All of these mechanisms described for diffusion and production of growth factors, the mitosis of cells, and the control functions must be incorporated into the model and then demonstrated to work the way we intend.

Our implementation of the model focuses on the process of neurulation, which is the early development of the spinal column, and leads to the creation of the brain and rest of the central nervous system. The stages of development in neurulation are common between most vertebrates, and is a critically important part of development. As part of this research, lab experiments were conducted to create images of mouse embryo brains at different times of development (although, as

mentioned, different embryos were used for each different time). Using these images, we created initial conditions for our model in order to verify it is capable of handling actual biological data. The model was implemented numerically in MATLAB in order to perform computer simulations of growth and verify expected behavior, and the biological data obtained was initialized successfully.

Our model tests a new theory of how cellular growth is directed in developing organisms. While several models of morphogenesis exist, all focusing on different mechanics, locations, and scales, none have addressed the hypothesis that fractones guide the growth. Our model offers an alternative way to study the role of fractones, which is otherwise very difficult to do through actual experimentation. Indeed, to our knowledge, no biological experiments have been performed to specifically test the role that a fractone plays in guiding development. **The contribution of this dissertation is the development of an innovative model for morphogenesis based on a fractone's governing principle. This demonstrates the applicability of hybrid control systems to complex biological processes. The model is validated by numerical simulations on real experimental data, and we are ready to receive further data in order to examine the extent to which fractones control morphogenesis.**

Chapter 2

Fractones And Morphogenesis

Images in this chapter are used with permission by Dr. Frederic Mercier.

Neurogenesis occurs in several stages, but we focus on a period called “neurulation” and the periods immediately subsequent to it. Prior to neurulation, vertebrate embryos form a long flat sheet, termed the neural plate. As neurulation begins, the edges of the plate begin to fold in toward each other forming the neural tube. While one end of the tube will remain relatively straight, the other end begins to fold itself up, also branching out laterally in some places. The straight end of the tube will eventually form the spinal cord, and the folded part, the brain. The areas of lateral growth form part of the ventricular system of the brain, which holds the cerebrospinal fluid responsible for protection of the brain and regulation of brain metabolites. The four ventricles of the brain are also primary sites of cellular growth.

The exact mechanisms that drive morphogenesis are not well known. Indeed, neurogenesis in adult brains was not believed to occur until relatively recently in 1992 [22] [31] when specific sites of cellular mitosis in the adult brain, called niches, were found. Recent research has discovered extracellular structures in these niches [42], [43] , and it has been proposed that these structure control the neurogenesis in the adult brain as well as during early development [32] [41]. Named ”fractones” for their branching shape, reminiscent of fractals (see Fig. 2.1), these structures are believed to absorb chemical signals called growth factors, and concentrate it for the cells [19]. The location and behavior of fractones therefore directs morphogenesis.

Fractones were first discovered in 2002 by Dr. Frederic Mercier, Dr. John Kitasako, and Dr. Glenn Hatton. While studying the ventricles of rat brains, they discovered small extravascular - away from the blood vessels - bulbs in the subependymal layer (see Fig. 2.2). These bulbs tended to be located near groups of replicating cells. Tests revealed that they were in fact basal lamina structures. The basal lamina is a layer of the extracellular matrix upon which stem cells or epithelial

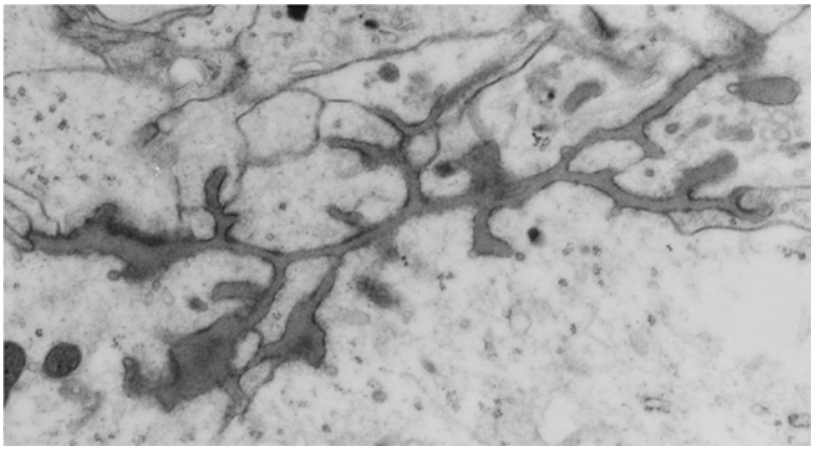

Figure 2.1: *An individual fractone taken by transmission electron microscopy. Note the branching morphology that lends it its name.*

cells are located (epithelium is the tissue which covers and lines many structures and organs of the body). The extracellular matrix has traditionally been thought of as more of a support structure for the body, however more recent studies have found that it may play a larger role in controlling development [20] [57]. The basal lamina is believed to make a significant contribution to morphogenesis and development early in life, but its contributions during adulthood are not clearly known [7] [25] [64]. The discovery of these basal lamina structures near replicating cells in the subventricular zones under study by Mercier, et al. was a significant find, as it suggested a mechanism by which neural stem cell growth was regulated.

The basal lamina bulbs Dr. Mercier, et al. found measured approximately 1-4 μm in diameter, and were located in a regular distribution close to the walls of the lateral and third ventricles (see Fig. 2.3), as well as along the developing spinal cord [42] [43]. Under transmission electron microscopy, it was seen that these bulbs had a complex branching morphology and were also connected to several cells in the ependyma and subependymal layer (where most cell growth occurs) on one side and blood vessels on the other via thin stem-like structures. As the basal lamina is thought to contribute to morphogenesis, it was hypothesized that these "fractones" were directly influencing the cells they formed connections with (see Fig. 2.4).

In 2007, this hypothesis was supported by experiments that found fractones exist in adult humans and have heparan sulfate proteoglycans (HSPG), which capture growth factors (specifically FGF-2) for presentation to cells. The fractones were found to capture and store these growth factors, and that cell proliferation preferentially occurred near fractones rather than blood vessels. Of

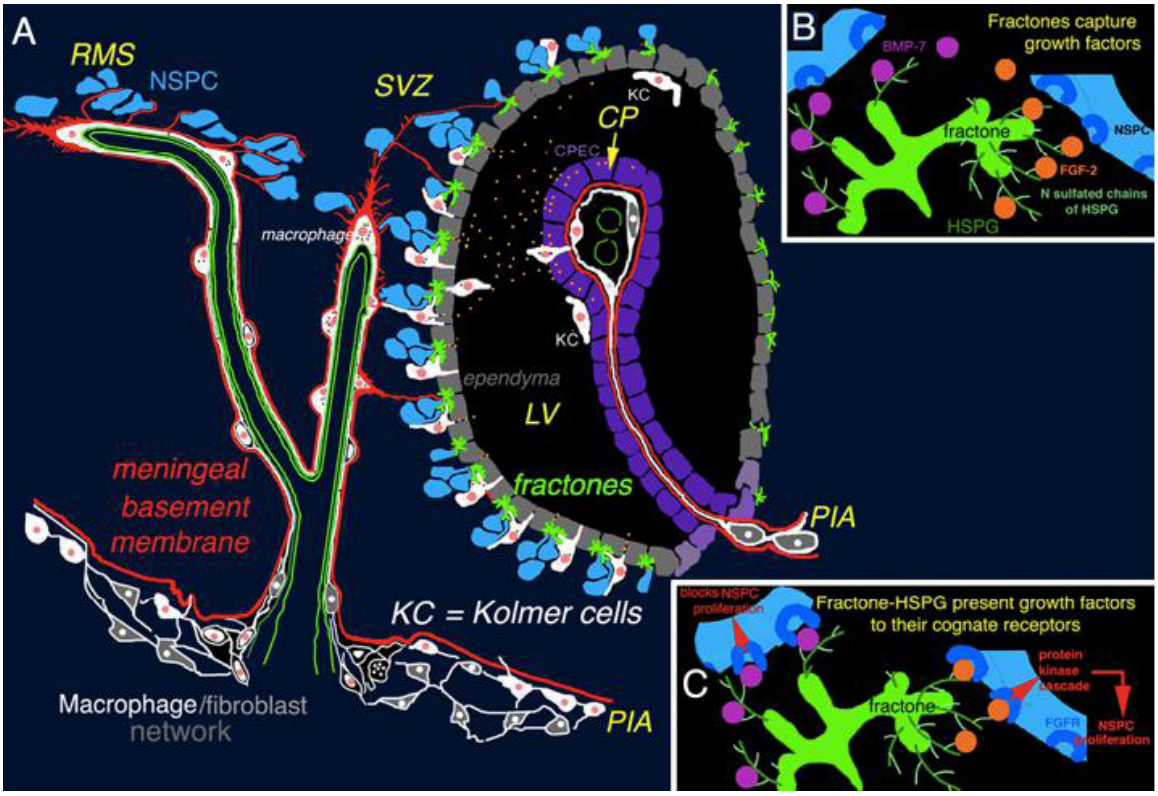

Figure 2.2: *Diagram of the anatomy of the brain near the lateral ventricle. CP: Choroid Plexus. SVZ: Subventricular Zone. RMS: Rostal Migratory Stream. NSPC: Neural Stem and Progenitor Cell. LV: Lateral ventricle.*

important note is that not all fractones were found to have HSPG, suggesting that fractones may be specialized in the types of growth factors they will bind [32]. As a result of this study, it is thought that several types of fractones may exist, each targeting specific growth factors, which are bound, stored, concentrated, and presented to nearby cells, thus triggering a reaction according to the type of growth factor.

There are many growth factors that are known and their interactions are complex. Different combinations of growth factors can signal different reactions in the cells. Cells typically detect and capture growth factor through various specialized receptors on the exterior of the cell. The specific types of growth factor present will signal cells to replicate, to stop replicating, to migrate, or even to kill themselves (a process called apoptosis). Growth factors may also be responsible for directing stem cells to differentiate into specific types of cells. All of these actions are critical to morphogenesis as it allows cells to create the structures of the body. Growth factor is produced

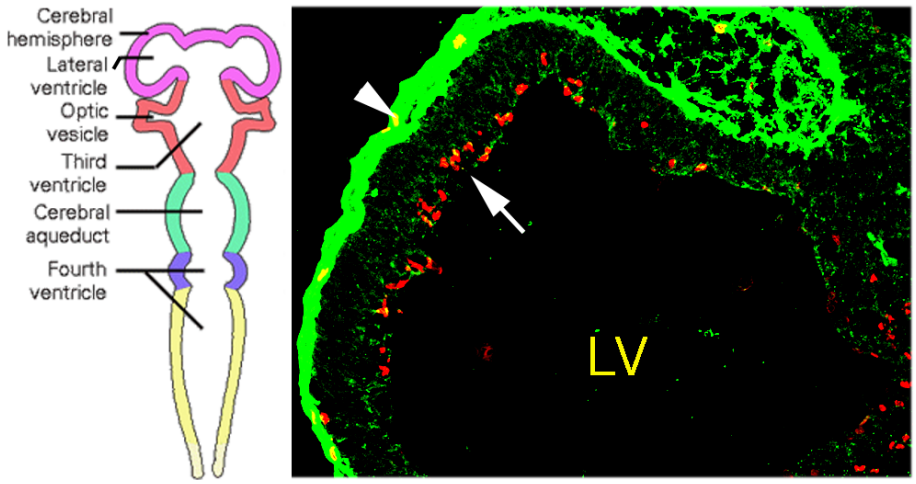

Figure 2.3: *Left: Diagram of the ventricular system of the brain. Studies have focused on fractones in the lateral and third ventricles, as well as the cerebral aqueduct. Right: Image of the lateral ventricle (LV). Around the surface of the ventricle (arrow) in red are cells that have recently undergone mitosis and the green puncta are the fractones. Note that mitosis occurs at the edge, among the fractones. The surface of the brain (arrowhead) is also shown.*

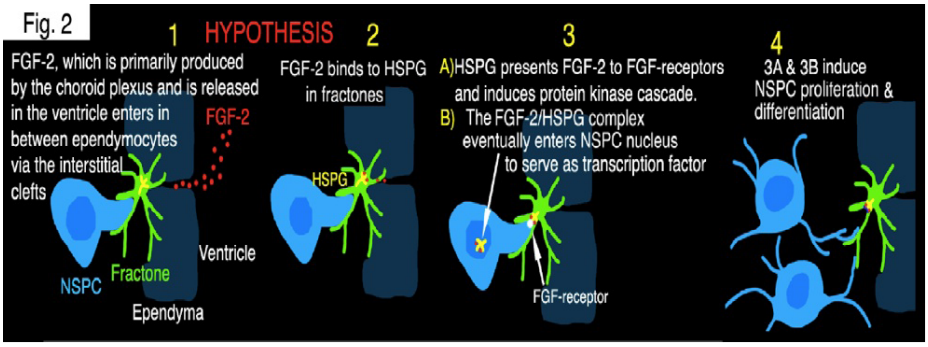

Figure 2.4: *Diagram describing the hypothesized process by which fractones regulate neurogenesis.*

from many sources, including the extracellular matrix and meninges, a sheath-like covering for the brain which has more recently been theorized to play a significant role in development [17]. The timing and location of growth factor production offers some determination as to what actions will occur and where, but fractones allow a much finer control than relying on simple diffusion of growth factors.

Two growth factors are explicitly introduced in our model, with a third implicitly present. The first growth factor represents a positive growth factor like fibroblast growth factor 2 (FGF-2). This positive growth factor promotes what we will term "accelerated growth" every 6 hours. The second growth factor represents a negative growth factor and will inhibit growth. Sufficient quantities of the second growth factor absorbed by a fractone will halt all mitosis for cells adjacent to the fractone. In our model, the two growth factors will diffuse through the system and be gathered by the fractones. The third growth factor, which may represent something like Epidermal Growth Factor (EGF), is not explicitly modeled, but assumed to be present in the system and absorbed through the receptors directly on the cell, as opposed to absorption by the fractone. The third growth factor is assumed to be responsible for causing cell growth at a slower rate than the positive growth factor. Thus without fractones, cells will still replicate, but will do so at a much slower speed. We will refer to this slower growth as "neutral growth" in order to reduce the confusion with the accelerated growth directed by fractones.

Studies have since found fractones in many areas of the brain and neural tube (see Fig. 2.5), often clustered in areas of high mitotic activity. However, fractones can also be found in areas where little cell replication occurs. This lends credence to the theory that growth factors are specialized; some fractones may target growth factors which stop mitosis from occurring. The type of fractone present is therefore just as important as where and when fractones are found during development. In our model, two fractone types will be used since there are two growth factors we explicitly track. The "positive fractone" will absorb positive growth factor at a much higher rate than negative growth factor, and "negative fractones" will do just the opposite.

2.1 Lab Experimentation

As part of my research, I spent time in the lab of Dr. Frederic Mercier to familiarize myself with the biology of fractones and assist with an experiment. One of the developmental disorders we have focused on as part of examining the role of fractones is autism (see papers by Mercier et al [45] [44]). While many researchers are looking into the genetic cause of autism [1] [23] [27] [46], we focus on the developmental cause. By looking at the morphological differences in the brains of autism patients [30], we hope to trace this back to a developmental issue in neurogenesis, the formation of the brain. Through experimentation, we sought to determine the morphological differences and fractone differences in the brains of B5 wild-type control mice and BTBR type mice, which serve as an autism model. Because autism is a human disorder and its diagnosis is

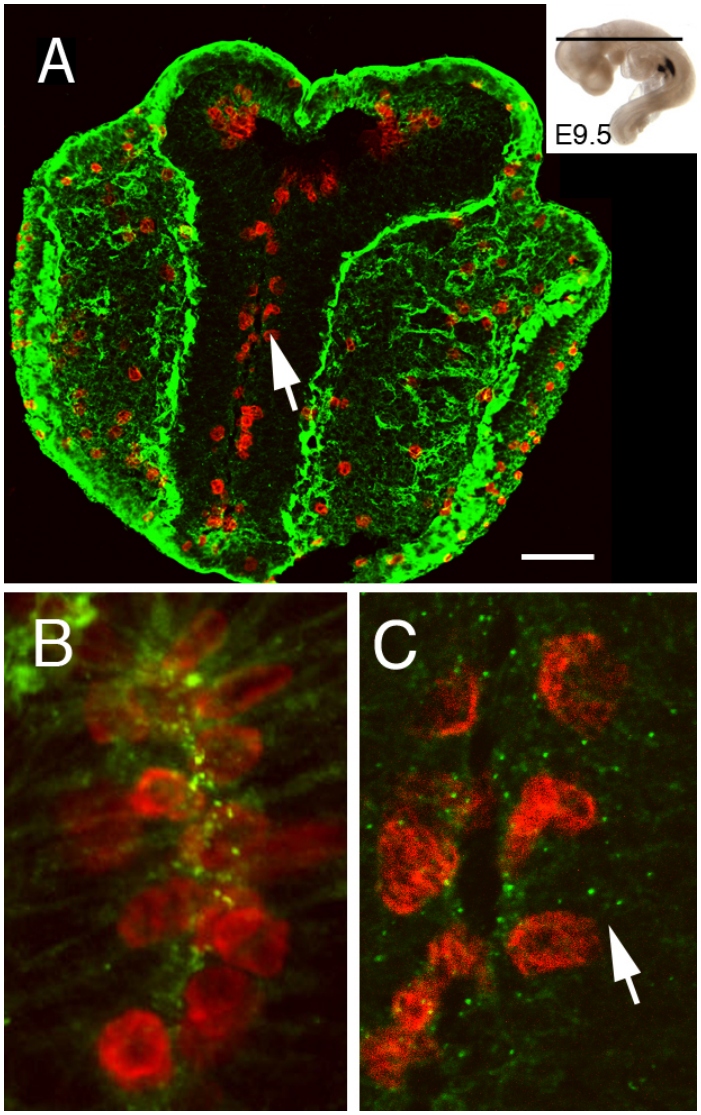

Figure 2.5: *(A) Cross-section of a whole mouse embryo during the neurulation process, 9.5 days after fertilization. In red are cells undergoing mitosis (phosphorylated histone-3 immunocytochemistry). Taken by flourescence microscopy. (B): 8.5 days after fertilization, all proliferating cells directly contact fractones (the green puncta). (C) 9.5 days after fertilization, additional fractones surround non-proliferating cells, suggesting that fractones may also confine the proliferation zone.*

somewhat debatable, we note that BTBR mice are chosen as our autism model because they display similar behavioral traits as humans diagnosed with autism.

The experimental technique is given in more detail in [45]. What follows is a brief explanation of the procedure. Staining the slides was done with an immunochemistry technique. A primary antibody is applied to the tissue, which attaches only to specific sites. A secondary antibody is then applied which adheres to the primary antibody. The secondary antibody has a fluorescent tag attached to it that allows it to be easily seen under microscope. We used a primary antibody which attaches to laminin, which is one of the proteins found in the basal lamina. In our experiments, bisbenzidine, a chemical stain, was also used that targets the nuclei of cells. As a result we get an image (see Fig. 2.6), which shows the laminin-tagged blood vessels and fractones, as well as the cells.

Slides were prepared in the following manner. The brains were removed from the adult mice and frozen, then sliced with a Leica CM1900 cryostat machine to 25 μm. Slices were placed on glass slides and frozen for preservation. To prepare the slides, they were first placed in an acetone solution to fix for 2 minutes, then removed and rinsed in a bath of phosphate buffered saline (PBS) solution for holding. PBS is a solution that closely matches the natural conditions within the body. The slides were then rinsed in distilled water and had a solution of PBS and gelatin applied. After another rinse in PBS, the primary antibody (L9393, 1/1,000, Sigma-Aldrich) was applied. The gelatin helps the primary antibody to adhere and remains stable. The excess antibody was then rinsed with PBS and another round of PBS and gelatin applied. After a PBS rinse, the secondary antibody, Alexa-Fluor, goat anti-rabbit, was applied. After rinsing, a solution of bisbenzidine "Hoechst 33258" (2 μg/ml, Sigma-Aldrich, Saint Louis, MO) is applied. After a final rinse, the slides are held in PBS solution until covered, using a commercial product or glycerol as a mounting solution.

Slides were examined, and images taken with 10x and 20x PlanApo dry objectives using a DFC350FX digital camera mounted on a DMIL epifluorescence microscope (Leica Microsystems, Bannockburn, USA). Fractones in the ventricles were counted by the researchers manually.

In comparing samples from BTBR and B6 mice, it was found that B6 (control) mice has more and larger fractones when compared to BTBR mice. The fewer fractones in BTBR mice is hypothesized to cause developmental problems during neurogenesis. In particular, it was found that the lateral and third ventricles were much less developed when comparing B6 and BTBR specimens of the same age.

Another morphological difference is found with the falx cerebri, a cleft in the middle of the brain, is much longer in the BTBR mouse. The extended length is thought to disrupt the corpus callosum, a bundle of neural fibers that connects the left and right hemispheres of the brain.

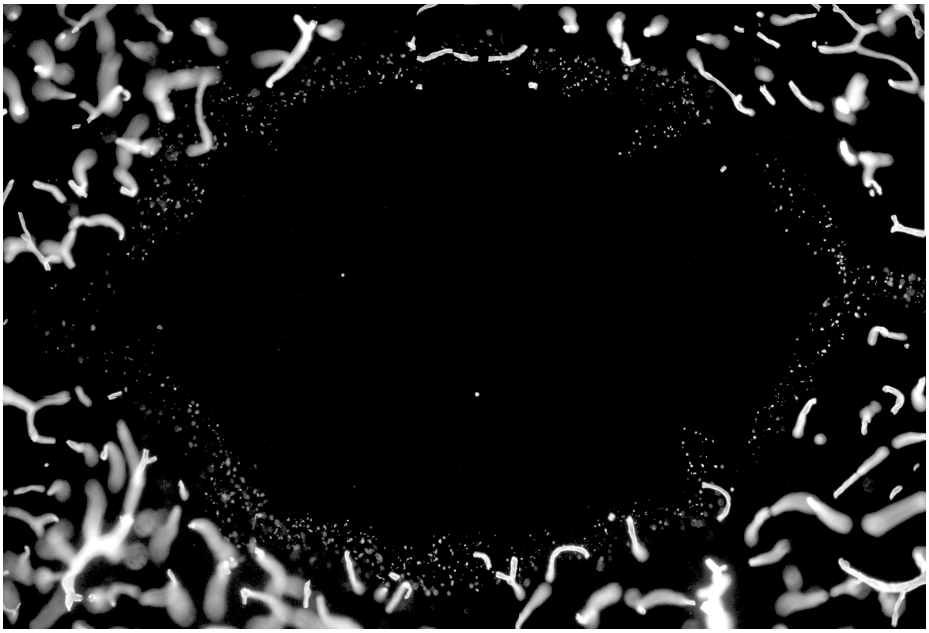

Figure 2.6: *Image of the cerebral aqueduct in an adult mouse taken by 20x PlanApo objective lens. The aqueduct connects the third and fourth ventricles together. Fractones are visible as the small puncta arranged around the aqueduct. The larger elongated shapes surrounding aqueduct are blood vessels.*

The enlarged falx cerebri may therefore interfere with communication between the two sides of the brain. It is an open question as to how this abnormal growth occurs, but it is suspected that a over abundance of fractones may drive the excessive growth.

These previous studies were conducted with adult specimens. But as the hypothesis is that fractones guide development at all ages, it is necessary to examine a series of younger subjects. Lab experimentation is underway for a more comprehensive study of fractone numbers and locations in the mouse embryo over time. That data will be passed to us for study with our mathematical model.

Chapter 3

Model History

Among the first mathematical models of diffusion mechanics applied to biology comes from the work of Alan Turing, who proposed that the natural patterns and markings observed in nature - such as stripes or spots - could arise through basic reaction-diffusion mechanisms [62]. The sort of model proposed by Turing is relatively simple. Differential equations model "morphogens" (a placeholder name for any molecule or object) diffusing through space and chemically reacting with one another. So a very basic model in a ring of two morphogens, X and Y, with concentrations at position $r \in \{1, \ldots, N\}$, X_r and Y_r, would be given by:

$$\frac{dX_r}{dt} = aX_r + bY_r + \mu\left(X_{r+1} - 2X_r + X_{r-1}\right)$$
$$\frac{dY_r}{dt} = cX_r + dY_r + \nu\left(Y_{r+1} - 2Y_r + Y_{r-1}\right)$$

where μ is the diffusivity constant and a, b, c, d are marginal reaction rates describing the rate of chemical reaction between the two morphogens, and where X_{N+1} and Y_{N+1} are identified to X_1 and Y_1, respectively Note that the last term in each equation is standard 1D diffusion. It is relatively simple to extend the system to more than two morphogens and to diffusion in two or three dimensions.

Since Turing's work on morphogenesis modeling, several models of cell growth and embryonic development have been created [67]. Mathematical models have helped to illustrate how growth may occur, backing up the hypotheses of biologists and expanding our knowledge of medicine and physiology. Recently, with the acceleration of gene studies and the race to cure cancer, cell models have become even more important as a virtual testing ground for theories and treatment protocols [4]. Cancer cell models can predict tumor growth as well as capillary growth that is necessary to support cancerous cells in growing tumors [2] [59]. Models allow a fast and

cheap environment free of ethical concerns in which to test protocols before employing them on actual living organisms.

Cellular growth has been modeled in several different ways, each with their own purpose. Models typically choose to look at cellular growth on one of three scales: tissue-level, cell-level, and molecule-level. Tissue-level models examine the growth, motion, and folding of entire sheets or spheres of cells. These sorts of models are common for cancer research models which study the growth rate of tumors [66], and are also used in morphogenesis models to study what physical forces are involved in folding entire sheets of tissue in order to form the particular shapes that are observed in developing embryos, such as the neural tube [12] [14] [15] [26].

Cell-level models look at individual cells, how they interact with each other in terms of adhesion of cell to one another, moving past one another, how they stretch and undergo mitosis with neighbors present, and how populations of individual cells spread, evolve, and take on shapes [47] [54]. Many cell-level models base themselves on discrete two-dimensional grids, like a square checkerboard grid or a hexagonal grid. Sometimes a single cell can take on several tiles of a grid, and the model focuses on the dynamics of cell stretching, morphing, and growing in size. Other times, cells are only a single tile large, and the model focuses and the spread of a population of cells as they all undergo mitosis. A simple and famous example of such a model is Conway's Game of Life, which uses only four rules for cell growth and death to demonstrate that even relatively simple mechanics can give rise to complex dynamics.

Molecule-level models consider the chemical signals that are released by cells and detected by cells through the presence of receptors on cell exteriors. These chemical signals can instruct cells to perform many different actions, such as to undergo or halt mitosis, to migrate, to differentiate into particular types of cells (such as a muscle cell or a brain cell), and even to kill themselves, a process called apoptosis that is vital to embryonic development. Models at this level consider the diffusion and capture of these chemical signals, and let these mechanics govern when, where, and at what rate cell mitosis occurs [65].

As may be expected, some recent models are multi-scale, applying the mechanics of these different scales together [10] [21] [63]. In a natural way, the molecule-level mechanics govern the cell-level mechanics which in turn can govern the tissue-level mechanics. Many models start at a cellular level and extend to a tissue-level [11]. The drawback of modeling on multiple scales is the sheer size and complexity of the system that arises. Tissues can be comprised of millions of cells (the human body has on the order of 10^{13} cells [8]), and if each one of those cells is controlled

by chemical signals that must be captured by a receptor, then the model becomes computationally intensive.

The model presented in this paper is multi-scale, considering diffusion dynamics of chemical growth factors and their capture by fractones. The captured growth factor then triggers behavior changes in the capturing cell, directing a cell to either undergo mitosis immediately or halt all mitosis forever. Replicating cells push their neighbors according to an algorithm, evolving the shape of the cell mass. While it is easy to see how this could be taken to a tissue-level, we are restricted by the complexity of the system to consider only relatively small masses of cells.

The model that we present now was initially based on previous work done by Dr. Monique Chyba and her graduate student, John Rader [13] [53]. We have since taken this model and over several iterations expanded its functionality and complexity in several areas.

Chapter 4

Fractone Based Model

Our model is based on a hybrid automata [24] [34] [35] [51] [49] [50] [61]. The traditional hybrid automata combines continuous and discrete dynamics. We follow the notations used by Lygeros, Johansson, et al [29] [28] [36] [37] [38] [39], who define a general hybrid automata with a finite number of continuous and discrete variables (See Appendix A). Our system, however, models its diffusion over a functional space, and thus we alter the definitions to accommodate while retaining the same general idea. Our continuous dynamic is the diffusion and capture of growth factor, while the discrete dynamic is the cellular growth which, by assumption, occurs instantaneously. This assumption is made in order to simplify the growth dynamics, which would otherwise be made complicated by the motion of the slow growth of the daughter cells as they develop to full size. The growth factors diffuse around the cells in the system, which obstruct diffusion by assumption, until a fractone captures enough positive growth factor, at which point growth occurs instantaneously, changing the cell configuration and therefore the diffusion dynamics. The assumption that cells block diffusion is made since cells typically require receptors in order to interact with growth factors. Models exist which deal with this growth-factor-receptor interaction [18], however we assume that the majority of growth factor capture for our two growth factors will occur via fractones.

In addition to the hybrid and discrete dynamics, we incorporate control parameters [3] [9] [16] [69] , which represent the fractones. Thus the fractones are controlled by the user, and where they exist, they disrupt the diffusion mechanics by acting as sinks. Mitosis that occurs at a neutral rate of once every 24 hours, which is not fractone-driven, introduces a stochastic element as well, as the direction of this random growth is chosen randomly. For a brief survey of stochastic elements in hybrid models, see [60]. We note that this random choice of direction is an assumption in the model, as even this non-fractone directed growth is likely controlled in some way in the developing organism.

The details of our model are as follows: We define the ambient space $A \subseteq \mathbb{R}^3$. The ambient space represents the physical space in which the embryo develops, such as the amniotic sac. We assume that this physical space is large enough or grows fast enough so as not to block or influence the growth of the organism.

4.1 Discrete Configuration Space

The discrete portion of the model describes the physical and chronological distribution of cells, meningeal cells, and fractones in the ambient space. Although cells can take a variety of shapes and sizes, and to a degree tend to be malleable, we simplify our model by assuming cells are ellipsoids of the same volume, and do not deform after creation. Our definition of cells as ellipsoids of fixed volume but variable semi-axis length has been used in previous models [48] [33] [58] [71]. For our model, we use an average cell size, relying on measurements taken of developing rat embryos showing the neuron soma size to be approximately $72 - 81$ μm^2 in size [40] and averaged 9 μm cell diameters of yeast cells [71], and set $s = 3$ μm, $S = 6$ μm, and $V = \frac{4}{3}\pi(4.5)^3$ μm^3.

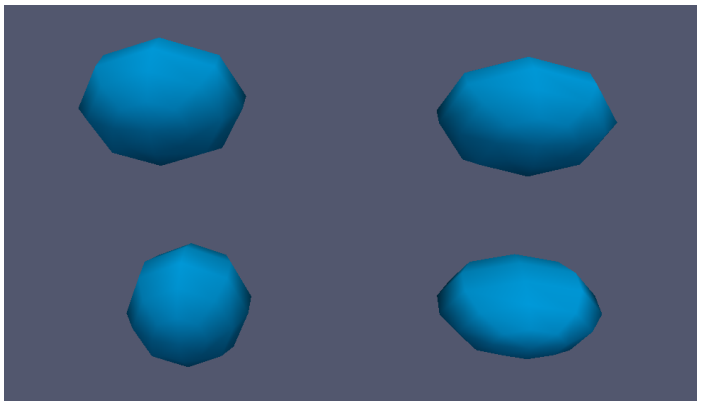

Figure 4.1: *Four example cells. All cells have equal volume, and axial radii between* 3 *and* 6.

Definition We define a *cell body* as an ellipsoid of fixed volume V and semi-axis lengths r_1, r_2, r_3, with $s \leq r_i \leq S$, $i \in \{1, 2, 3\}$, for constants $V, s, S \in \mathbb{R}$. We note that while cell bodies in the system must all have the same volume V, they may each have different semi-axis lengths.

Although mitosis in our model occurs instantaneously, we must account for the time it takes a daughter cell to develop to full maturity before it can undergo mitosis. This time between cell division in an embryo varies depending on the type of cell, age, and species. In a developing rat

embryo, this time can vary between 3 to 14 hours [5]. For our model, we use an approximate 6 hour cell cycle as an assumption. We introduce a "cell time" for each cell that tells us at what time the cell was created, measured in minutes since the model was initialized, and this allows us to track the age of the cell determine when the cell is mature enough to replicate. It is important to note that when mitosis occurs, the mother cell splits into two daughter cells, thus the parent cell ceases to exist and two daughter cells are created, both with cell times set to the time of mitosis.

Definition We define a *cell time*, $t_c \in \mathbb{R}$, and pair it with a cell body, c_b, to define a *cell*, $c = \{c_b, t_c\}$.

We wish to restrict the possible sets of cells to those that make physical sense; cells shouldn't overlap with each other in space. Thus we introduce the concept of an "admissible" set of cell bodies. We define this over cell bodies rather than cells because it is a purely geometric notion and the cell time has no relevance in its definition.

Definition To determine if a given set of cell bodies, $C = \{c_i\}$, is *admissible*, choose a constant $\epsilon \in \mathbb{R}$. For each cell, c_i, with cell body semi-axis lengths r_{1i}, r_{2i}, r_{3i} we assign a concentric ellipsoid, $\hat{c}_i$, with semi-axis lengths $r_{1i} + \epsilon$, $r_{2i} + \epsilon$, and $r_{3i} + \epsilon$ respectively. Let $\hat{C} = \bigcup_i \hat{c}_i$. If $\hat{C}$ is a compact connected space and $c_i \cap c_j = \emptyset$, $\forall i, j$, $i \neq j$, then the configuration is admissible.

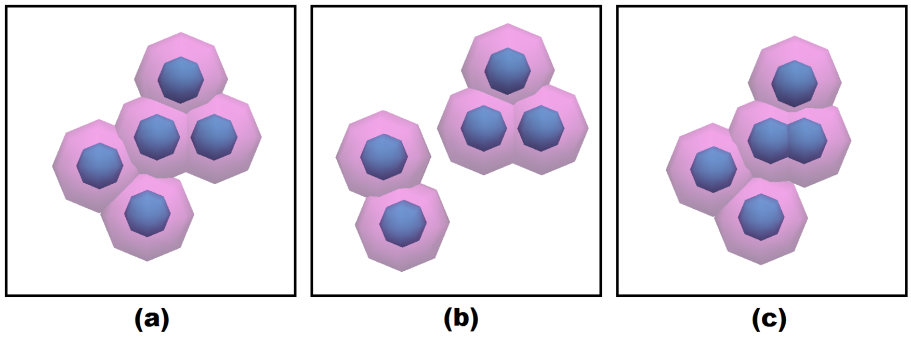

Figure 4.2: *Examples of an (a) admissible set of cell bodies and (b-c) two inadmissible sets of cell bodies. In blue, the cell bodies. In pink, the associated $\hat{C}$. The set in (b) is not admissible since $\hat{C}$ is not connected. The set in (c) is not admissible since two of the cell bodies intersect.*

The choice of epsilon determines how far apart cells may be in an acceptable set of cells. Distances greater than 2ϵ between cell boundaries will cause holes to appear in $\hat{C}$. In our model, we use $\epsilon = 4.5$ μm, the same length as the radius of a spherical cell. Examples of admissible and inadmissible sets of cell bodies can be found in Figure 4.2.

The second component in the discrete portion of our model is the meninges. For clarity, we will always refer to meningeal cells as such and embryonic cells, as described previously, as just "cells". Meningeal cells are located on the exterior of a developing set of cells, and are the source of growth factors in our model. To simplify the dynamics of the model, meningeal cells undergo no mitosis and their age is therefore unimportant. Furthermore, we assume that meningeal cells are of uniform volume and spherical shape.

Definition We define the *meningeal cell* centered at $(x_0, y_0, z_0) \in A$ as

$$\overline{B_{\epsilon/2}(x_0, y_0, z_0)} = \left\{ (x, y, z) \in A | (x - x_0)^2 + (y - y_0)^2 + (z - z_0)^2 \leq \left(\frac{\epsilon}{2}\right)^2 \right\}$$

With the choice of the meningeal radius as half of ϵ means that a meningeal cell in our model has a sphere of radius of 2.25 μm, with a volume one-eighth that of a spherical cell. As with sets of cells, we wish to restrict the location of meningeal cells to an admissible set.

Definition Given an admissible set of cells, C, and a set of meningeal cells, $C_m = \{c_{mp}\}$, which we will call the *meninges*, C_m is *admissible* if the center of each meningeal cell lies on the boundary,$\partial\hat{C}$, of $\hat{C}$, and $c_{mi} \cap c_{mj} = \emptyset, \forall i, j, i \neq j$.

Since the radius of a meningeal cell is $\frac{\epsilon}{2}$ and the center of a meningeal cell in an admissible set lies on the boundary of $\hat{C}$, which is located a minimum distance ϵ from cell bodies, it follows that a meningeal cell will never intersect a cell.

Since the developing organism is primarily a group of cells surrounded by meninges, we define their combination:

Definition Given an admissible set of cells, C, and admissible meninges, C_m, we define the pair as a *cell mass*, $M = \{C, C_m\}$.

The third component of the discrete portion of the model are the fractones. From chapter 2, we know fractones have a tree-like shape when viewed with electron microscopy, however, for this paper, we do not study the fractone's specific geometry, its receptors, or its means of attachment to cells, but only its specific hypothesized role in development. We thus model fractones as small spherical structures found next to cells that will absorb growth factors through diffusion. Our fractones are balls with radius one-ninth that of a spherical cell. In our model this means a fractone has a diameter of 1 μm, which is on the smaller end of the previously mentioned 1-4 μm diameter found experimentally. As before, we wish to restrict the location of fractones to be tangent to cells. Recall that two ellipsoids a and b are tangent if $a \bigcap b$ has exactly one point.

Definition We define the *fractone* centered at $(x_0, y_0, z_0) \in A$ as $\overline{B_r(x_0, y_0, z_0)}$ where $r = \frac{1}{9}\sqrt[3]{\frac{3}{4\pi}V} = 0.5$. Given an admissible set of cells, C, a set of fractones, $\{f_q\}$, is *admissible* if every fractone is tangent to at least one cell body and $f_i \cap f_j = \emptyset, \forall i, j, i \neq j$.

We note that the fractone has a small enough diameter that admissible fractones will never intersect with meningeal cells.

To simplify the model, we consider only two types of growth factors: a positive growth factor and a negative growth factor. When a sufficient quantity of these growth factors is absorbed by the fractones, they trigger accelerated growth of cells or prevent mitosis, respectively. We also only consider two types of fractones: positive fractones and negative fractones. Positive fractones collect positive growth factor a greater rate than negative growth factor, while negative fractones do the opposite. It is important to note that in reality, many growth factors are present during development and several types of fractones with different sensitivities may exist. As such our model can be easily extended to incorporate more types of growth factors and fractones.

The combination of cells, meningeal cells, and fractones are combined to form the basis of the discrete portion of the model, which we call a "biological structure".

Definition W define a *biological structure* as a triple, $\{M, F^+, F^-\}$, as a cell mass, M, paired with two admissible sets of fractones, F^+ and F^-, which represent the positive and negative fractones, respectively, in the system.

We let **Q** be the set of all possible biological structures in A. Then **Q** is the state space of the discrete dynamic of our model. We note that two distinct elements of **Q** may have the same set of cell bodies and fractones in A, but the temporal parameters of the biological structures may differ, and one or more of the cells will have different cell times.

4.2 Distance Metrics

As part of our analysis of the system, it is useful to define a metric measuring how close two biological structures are to one another. In comparing two different organisms of the same species and age, we expect some differences between them - the exact length and width of limbs, for example - but the general shapes ought to be similar; limbs should not be growing from different places or missing altogether. Thus when defining a metric to distinguish two biological structures,

it is better to choose one that weighs a few extreme differences more than many smaller ones. Our metric is based off of the Hausdorff distance [55]. This was chosen because Hausdorff distance cares much more about outliers in the relative geometric positions of cells than groups of cells that are just slightly non-overlapping. We first define a metric for groups of cells.

Definition For two biological structures, $q_a, q_b \in \mathbf{Q}$, with $q_a = \{M_a, F_a^+, F_a^-\}$, $q_b = \{M_b, F_b^+, F_b^-\}$, with $\{C_a, C_{ma}\} = M_a$ and $\{C_b, C_{mb}\} = M_b$, and cell bodies and cell times $\{c_{ar}, t_{ar}\} \in C_a$, $\{c_{bs}, t_{bs}\} \in C_b$, and sets of cell bodies $E_a = \{c_{ar}\}$ and $E_b = \{c_{bs}\}$, we define the *directed Hausdorff distance* between E_a and E_b, $d(E_a, E_b)$, by:

$$d(E_a, E_b) = \max_{(i_a,j_a,k_a)\in E_a} \min_{(i_b,j_b,k_b)\in E_b} \|(i_a, j_a, k_a), (i_b, j_b, k_b)\|$$

where $\|\cdot\|$ is the standard Euclidean distance: $\sqrt{(i_a - i_b)^2 + (j_a - j_b)^2 + (k_a - k_b)^2}$.

Thus $d(E_a, E_b)$ gives the minimum distance from the point $(i_a, j_a, k_a) \in E_a$ to any point in E_B, where (i_a, j_a, k_a) is the point in E_a furthest from any point in E_b. It is important to note that the directed Hausdorff distance is not commutative, so to make an appropriate metric, we make a refinement:

Definition We define the *Hausdorff distance*, D_H, by:

$$D_H(E_a, E_b) = \max(d(E_a, E_b), d(E_b, E_a))$$

See Fig. 4.3 for an example illustrating D_H.

As mentioned, although two biological structures may share the same cell bodies, the age of the cells may still distinguish them, and it is important for our metric to take this into account, as cell age may have relevance in future embryonic growth. Each discrete state we simulate is a snapshot of the distribution of cells in an organism at a particular time, and presumably that organism goes on living and growing.

Definition We define the *directed age distance*, d_a of two biological structures, using the same notation as the previous definitions. For a given set of cell bodies E_i, let I_i be the set of coordinates for the center $\{(x_{ir}, y_{ir}, z_{ir})\}$ of each cell $c_{ir} \in E_i$.

$$d_a(C_a, C_b) = \max_{C_a} \min_{C_b} [\|(x_{ar}, y_{ar}, z_{ar}), (x_{bs}, y_{bs}, z_{bs})\| + \kappa(|t_{ar} - t_{bs}|)]$$

for $\kappa \in \mathbb{R}$. For our model, we use $\kappa = 4.5$. This is chosen so that a 1 minute difference in age is equivalent to spherical cells being a radius length off-set.

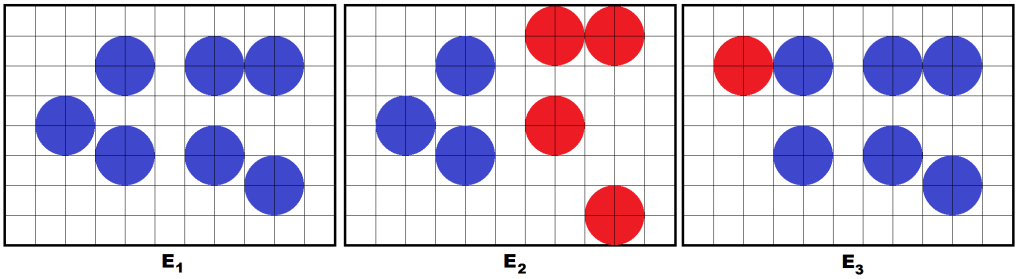

Figure 4.3: *Three collections of 2D cells, E_1, E_2, E_3. Cells shown in red in E_2 and E_3 are those that differ in position from E_1. If the grid shown is 1 unit in length, then $D_H(E_1, E_2) = 1$ and $D_H(E_1, E_3) = 2$ and $D_H(E_2, E_3) = 2$. Note that $D_H(E_1, E_3) > D_H(E_1, E_2)$, demonstrating that a smaller distance can be achieved even if more cells are out of position as long as the the difference in cell positions is relatively small.*

We further define the *age distance*, D_a of two biological structures,

$$D_a(C_a, C_b) = \max\left(d_A(C_a, C_b), d_A(C_b, C_a)\right)$$

The relative positions of the fractones are also important to measure since different fractone positions suggest that growth has occurred in a different pattern, even if the cell bodies are in similar positions. We therefore define a metric for comparing the fractones of two systems.

Definition We define the *directed Hausdorff fractone distance*, d_F, of two sets of fractones, F_a, F_b,

$$d_F(F_a, F_b) = \max_{(i_a,j_a,k_a)\in F_a} \min_{(i_b,j_b,k_b)\in F_b} \|(i_a, j_a, k_a), (i_b, j_b, k_b)\|$$

We further define the *Hausdorff fractone distance*, D_F, of two sets of fractones, F_a, F_b,

$$D_F(F_a, F_b) = \min\left(d_F(F_a, F_b), dF(F_b, F_a)\right)$$

Definition For $q_a, q_b \in Q$, using the previous notation, we define $B_a = \{C_a, F_a^+, F_a^-\}$ and $B_b = \{C_b, F_b^+, F_b^-\}$. Thus B_a and B_b represents all of the information in q_a and q_b except for the meninges. We define the biological structure distance, D_B, between B_a, B_b, as:

$$D_B(B_a, B_b) = D_H(E_a, E_b) + D_A(C_a, C_b) + D_F(F_a^+, F_b^+) + D_F(F_a^-, F_b^-)$$

Proposition 4.2.1 *D_B is a metric on the set of all B_i*

Proof We note that D_F is a Hausdorff metric on the set of all possible sets of fractones, and D_H is a Hausdorff metric on the set of all possible sets of cell bodies, E_i.

Let B_a, B_b be any two sets formed from $q_a, q_b \in Q$. By its definition it is clear that $D_B(B_a, B_b) \geq 0$ since the terms in the sum, D_h, D_A, and D_F are all non-negative. It is also clear that D_B is symmetric since D_F and D_H are symmetric by virtue of being metrics, and similarly $\max(dA(C_i, C_j), dA(C_j, C_i)) = \max(dA(C_j, C_i), dA(C_i, C_j))$.

If $B_a = B_b$, then it is clear that $D_B(B_a, B_b) = 0$ by the previous definitions.

For the converse, if $D_B(B_a, B_b) = 0$, then since each of its terms is non-negative, this implies that $D_H(E_a, E_b) = 0$, $D_A(C_a, C_b) = 0$, $D_F(F_a^+, F_b^+) = 0$, and $D_F(F_a^-, F_b^-) = 0$. Since D_F is a Hausdorff metric, this implies that $F_a^+ = F_b^+$ and $F_a^- = F_b^-$.

Since $D_A(C_a, C_b) = \max(d_A(C_a, C_b), d_A(C_b, C_a))$, $D_A(C_a, C_b) = 0$ if and only if both $d_A(C_a, C_b) = 0$ and $d_A(C_b, C_a) = 0$. $d_A(C_a, C_b) = 0$ only if for every cell $c_{ar} \in C_a$ there exists a cell $c_{bs} \in C_b$ such that the center of the cell bodies are the same, $\|(x_{ar}, y_{ar}, z_{ar}), (x_{bs}, y_{bs}, z_{bs})\| = 0$, and the cell times are the same, $|t_{ar} - t_{bs}| = 0$. There is a similar result for $d_A(C_b, C_a) = 0$. Note this does not imply that $C_a = C_b$, as only the cell centers and cell times are guaranteed to be the same. However, since $D_H(E_a, E_b) = 0$, and D_H is a Hausdorff metric on the set of E_i, we know that the cell bodies must the the same, $E_a = E_b$, and therefore $C_a = C_b$. Thus we can conclude that if $D_B(B_a, B_b) = 0$ then $B_a = B_b$.

Finally we need to show that for any B_c formed from some $q_c \in Q$, $D_B(B_a, B_b) \leq D_B(B_a, B_c) + D_B(B_c, B_b)$. Since D_F and D_H are Hausdorff metrics, we know that $D_F(F_a^+, F_b^+) \leq D_F(F_a^+, F_c^+) + D_F(F_c^+, F_b^+)$ and $D_F(F_a^-, F_b^-) \leq D_F(F_a^-, F_c^-) + D_F(F_c^-, F_b^-)$ and $D_H(E_a, E_b) \leq D_H(E_a, E_c) + D_H(E_c, E_b)$. Thus we need only show that $D_A(C_a, C_b) \leq D_A(C_a, C_c) + D_A(C_c, C_b)$.

Without loss of generality, let $d_A(C_a, C_b) > d_A(C_b, C_a)$. $d_A(C_a, C_b)$ is by:

$$(\|(x_{a1}, y_{a1}, z_{a1}), (x_{b1}, y_{b1}, z_{b1})\| + \kappa(|t_{a1} - t_{b1}|))$$

for the cells $c_{a1} \in C_a$ and $c_{b1} \in C_b$ which satisfy the maximum and minimums in the definition of the directed age distance. We note that there may be several choices of the pair c_{a1} and c_{b1} that give the same maximum distance in the system, but without loss of generality we may choose any pair.

Let

$$d_A(C_a, C_c) = (\|(x_{a1}, y_{a1}, z_{a1}), (x_{c1}, y_{c1}, z_{c1})\| + \kappa(|t_{a1} - t_{c1}|))$$

for appropriate cells $c_{a1} \in C_a$ and $c_{c1} \in C_c$. Then note that since the directed age distance, $d_A(C_c, C_b)$, maximizes over the cells in C_c:

$$d_A(C_c, C_b) \geq (\|(x_{c1}, y_{c1}, z_{c1}), (x_{b2}, y_{b2}, z_{b2})\| + \kappa(|t_{c1} - t_{b2}|))$$

where $c_{b2} \in C_b$ is chosen to minimize the distance to c_{c1}. Therefore

$$d_A(C_a, C_c) + d_A(C_c, C_b) \geq (\|(x_{a1}, y_{a1}, z_{a1}), (x_{c1}, y_{c1}, z_{c1})\| + \kappa(|t_{a1} - t_{c1}|))$$

$$+ (\|(x_{c1}, y_{c1}, z_{c1}), (x_{b2}, y_{b2}, z_{b2})\| + \kappa(|t_{c1} - t_{b2}|)) \geq (\|(x_{a1}, y_{a1}, z_{a1}), (x_{b2}, y_{b2}, z_{b2})\| + \kappa(|t_{a1} - t_{b2}|))$$

And since c_{b1} was chosen to minimize the distance to c_{a1} over all the cells in C_b, we conclude

$$(\|(x_{a1}, y_{a1}, z_{a1}), (x_{b2}, y_{b2}, z_{b2})\| + \kappa(|t_{a1} - t_{b2}|)) \geq d_A(C_a, C_b)$$

Thus $D_A(C_a, C_b) \leq d_A(C_a, C_c) + d_A(C_c, C_b)$, and therefore $D_A(C_a, C_b) \leq D_A(C_a, C_c) + D_A(C_c, C_b)$.

Since $D_B(B_a, B_b)$ is symmetric, non-negative, obeys the triangle inequality, and is zero if and only if $B_a = B_b$, D_B is a metric on the set of all B_i. ∎

We note that while D_B is a metric on the set of all B_i, it is not a metric on Q since two distinct $q_a, q_b \in Q$ may have the same fractones and cells but different meninges. Thus it is possible for the (analogous) $D_B(q_a, q_b) = 0$ but $q_a \neq q_b$. However, since $D_B(q_a, q_b) = 0$ if $q_a = q_b$, and symmetry, non-negativity, and the triangle equality still clearly hold, D_B is a pseudometric on Q. Further note that our metrics do not consider the growth factor distributions. This is because our primary goals for this research revolve around the cellular distributions instead of the growth factor distributions. Indeed, determining growth factor distributions on such small scales in a developing embryo would require a significantly different experimental set-up.

4.3 Continuous Dynamic

Growth factors diffuse around cells and meningeal cells and cannot pass through them, while being absorbed by fractones. We define the diffusion mechanics for two growth factors, but the model can be extended naturally to more than two growth factors.

For a given $q \in \mathbf{Q}$, growth factors will diffuse only through a subspace of A which we will call the "diffusion space". This diffusion space extends a certain radius around the exterior of the set of cells. In fact, the same $\hat{C}$ we used to determine if a set of cells is admissible, is used. Any "holes" in $\hat{C}$ are incorporated into the diffusion space, as growth factor could realistically be assumed capable of diffusing across cavities in a developing embryo. Cells and meningeal cells are removed from the diffusion space as we assume there is no diffusion of our two growth factor across the cell membranes. The particular geometry of the diffusion space extends out so that the center

of the spherical meningeal cells lie on its boundary. This is done because the meninges acts as an external sheathe for the developing organism, and growth factor would not be expected to diffuse across it. Examples of biological structures and diffusion spaces can be found in Figure 4.4.

Definition For a given cell mass, $M = \{C, C_m\}$, let C_H represent the union of the connected components in $A \setminus \hat{C}$ that are separated from the boundary of A (ie. they are disjoint from the other's closure [56]). Let $\hat{M} = (\cup c_b) \bigcup (\cup c_{mp})$ be the union of all cell bodies and meningeal cells. Then we define the *diffusion space* as $D = \left(C_H \bigcup \hat{C}\right) \setminus \hat{M}$.

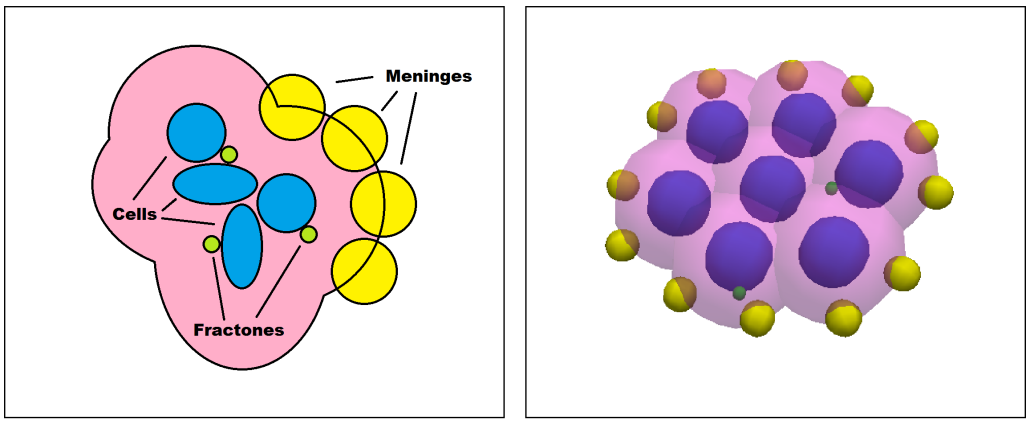

Figure 4.4: *(a) A 2D figure of a biological structure and diffusion space and (b) a 3D figure of a biological structure with diffusion space. Cells are in blue, fractones in green, meninges in yellow, and diffusion space in pink (although the diffusion space also includes the fractones).*

The growth factor concentrations in our model are given by $X(x,t) = \{X_1(x,t), X_2(x,t)\}$, the set of 2 growth factor concentrations at $x = (x_1, x_2, x_3) \in \mathbb{R}^3$ at time t. The growth factor distribution $X_l(x,t)$ lies in $\mathbf{X}_0$, the set of all functions $X_0(\cdot) : A \to \mathbf{R}_{\geq 0}$. The units of $X_l(x,t)$ are arbitrary molarity units, which we will term "concentration units". By our assumptions, growth factor should only be located in the diffusion space, and not in cells or meningeal cells, so we impose the constraints that $X_l(x,t) = 0$ when $x \notin D$. We denote the set of possible growth factor distributions for our 2 growth factors $\mathbf{X} = \mathbf{X}_0 \times \mathbf{X}_0$.

Growth factor is introduced into the diffusion space through the meninges. It is assumed to be produced by the meninges and is added to the diffusion space near the border of any meningeal cells. The amount of growth factor produced by the meninges is given by a growth factor production

function, $g(t)$. For obvious reasons, we restrict $g(t) \geq 0$. In practice, we set $g(t)$ as a constant function, a sinusoidal function, or a square wave, which are all assumptive of how growth factors might be produced by the meninges. To define the volume in which the growth factor will be added, we set $\epsilon_g = 0.5$ (an arbitrary choice), and for each meningeal cell, c_{mp}, centered at (x_0, y_0, z_0), define $D_{mp} = \overline{B_{\epsilon/2+\epsilon_g}(x_0, y_0, z_0)} \cap D$. Then at time t, an amount of growth factor equal to $g(t)$ is distributed uniformly into each D_{mp}.

The 3D diffusion of growth factor in the system is described by the operator f_{ql}, which is dependent on the biological structure $q \in \mathbf{Q}$ and growth factor, l. In the absence of fractones and meningeal cells, diffusion occurs in the diffusion space according to the heat equation as follows:

$$f_{ql}(q, X, t) = \frac{\partial}{\partial t} - \kappa_l \left(\frac{\partial^2}{\partial x_1^2} + \frac{\partial^2}{\partial x_2^2} + \frac{\partial^2}{\partial x_3^2} \right) = 0$$

where κ_l is the diffusion constant.

When meningeal cells are present, growth factor is added to the system according to the chosen $g(t)$, and when fractones are present, diffusion is perturbed. The fractones act as sinks, with growth factor only flowing into fractones, and never out. To model the fractones, we introduce the control $u : A \times \mathbb{R} \to \{0, 1\}$, $u(x, t) = \{0, 1\}$. Thus if at time t, $x \in \gamma_i$, for some fractone γ_i, $u(x, t) = 1$. Otherwise, $u(x, t) = 0$. Then f_{ql} is an operator on (q, X, t, g, u) that describes this perturbed diffusion with a growth factor source.

The introduction of u makes our model into a control system. In more detail, the biological structure q provides information on the diffusion space, where all diffusion occurs. The control u provides information of fractone locations, which should always correspond properly with the fractone locations in q. Where fractones exist, the diffusion space appears empty of growth factor when calculating the diffusion mechanics. Fractones do store growth factors - they merely make them unavailable for diffusion. Thus the control u has an influence on the diffusion mechanics. Based on the diffusion space, the growth factor production function g, and fractone locations, f_{ql} describes the motion of the system through the functional space $X(x, t)$. The perturbed diffusion will be made explicit in the numerical implementation in the following chapter, which recharacterizes the PDE as a system of ODEs.

To initialize the model, we need a starting point that includes the initial biological structure and the initial distribution of growth factors. In practice, we obtain these initial conditions from biological experimentation. Using the previously described procedure, we can obtain images of the relative locations of cells and fractones. The initial conditions are dependent on the age of the embryo and location under study. The initial conditions for the discrete dynamics and continuous

dynamics are given in $Init \subseteq \mathbf{Q} \times \mathbf{X}_0 \times \mathbf{X}_0$.

Example Consider an initial condition starting at time $t = 0$ with one cell centered at $x = (x_1, x_2, x_3) = (0, 0, 0)$, no meninges, a distribution of the first growth factor concentration which grows from 0 to 20 concentration units as we move from the boundary of the cell to the boundary of the diffusion space, and a distribution of the second growth factor which is 0 everywhere in the diffusion space (see Figure 4.5).

Then we have the singleton set of initial conditions given by $Init = \{q, X_1, X_2, 0\}$, where

$$X_1(x,t) = \begin{cases} \frac{20}{4.5}\left(\sqrt{x_1^2 + x_2^2 + x_3^2} - 4.5\right) & (x_1, x_2, x_3) \in B_9(0,0,0) \setminus B_{4.5}(0,0,0) \\ 0 & \text{Otherwise} \end{cases}$$

and

$$X_2(x,t) = 0$$

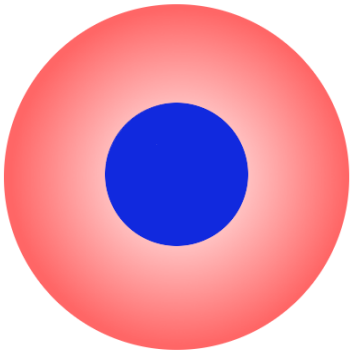

Figure 4.5: *An example initial condition with a single cell (in blue) and distribution of a single growth factor in the diffusion space surrounding it. The growth factor concentration is represented by the color intensity of the red; close to the cell, the concentration is* 0 *concentration units, and at outer boundary of the diffusion space, it is* 20 *concentration units.*

The connection between the discrete and continuous dynamics are modeled through several mathematical structures: the domains, edges, guard conditions, and reset maps. First, the domain, Dom, assigns to each $q \in \mathbf{Q}$ all of the growth factor distributions that could occur without a mitosis event. Each mitosis event changes the biological structure, and the possible changes that

could physically occur are represented in the set of edges, $E \subseteq \mathbf{Q} \times \mathbf{Q}$. An element $(q_1, q_2) \in E$ represents the instantaneous change in the discrete dynamic from biological structure q_1 to biological structure q_2. Note in our system, not every element of Q is connected to every other element. The existence of an edge between two biological structures determines the "rules" for growth, and is represented in our model by our control and the algorithm for pushing cells.

To determine which edge is traversed and when, each edge is assigned a guard condition. For an edge (q_1, q_2), when this guard condition is met, growth occurs instantaneously and we instantly switch from biological structure q_1 to the new biological structure, q_2. In our model, there are two sorts of guard conditions, one for the accelerated growth and one for the neutral growth. The guard conditions for accelerated growth represent those growth factor distributions where a fractone has absorbed sufficient positive growth factor, and the guard conditions for neutral growth represent when sufficient time has passed for a cell to undergo neutral growth.

When growth occurs and new cells are created, growth factor will be redistributed in the system due to the physical forces related to the motion and growth of the new cells. This is modeled in our system by a deformation algorithm, which is represented mathematically by the "reset map". For each edge, the reset map determines how the growth factor distribution changes when the guard condition is met. Thus, although we call the diffusion the "continuous dynamic", each mitosis event may cause a discontinuous jump in the growth factor distribution over time.

It is important that our initial conditions always start us within the domain of the initial biological structure, and that our reset maps similarly always redistribute the growth factors so that we are within the domain of the new biological structure. This way, we are always within $Dom(q_1)$ for some $q_1 \in \mathbf{Q}$, and as we reach an extreme of $Dom(q_1)$, we meet a guard condition for some edge $(q_1, q_2) \in E$, which triggers mitosis and a discrete switch to the new biological structure, q_2, and the reset map ensures we are in $Dom(q_2)$. Thus we are always in $Dom(q_i)$ for some $q_i \in \mathbf{Q}$.

More formally, we define the domain by $Dom(\cdot) : \mathbf{Q} \to P(\mathbf{X}_0) \times P(\mathbf{X}_0) \times \mathbb{R}_{\geq 0}$, where $P(\mathbf{X}_0)$ denotes the set of all subsets of $\mathbf{X}_0$. For a $q \in \mathbf{Q}$, $Dom(q)$ maps to the set of all growth factor distributions of our two growth factors and all times in which cellular growth has not occurred.

The guard conditions are given by $G(\cdot) : E \to P(\mathbf{X}_0) \times P(\mathbf{X}_0) \times \mathbb{R}_{\geq 0}$. For a given edge (q_1, q_2), $G((q_1, q_2))$ maps to the set of all growth factor distributions of our two growth factors and times at which mitosis, either accelerated or neutral, would be triggered, and lead to the biological structure deforming from q_1 to q_2. See Figure 4.6 for a visual representation of how the domains, edges, and guard conditions interact.

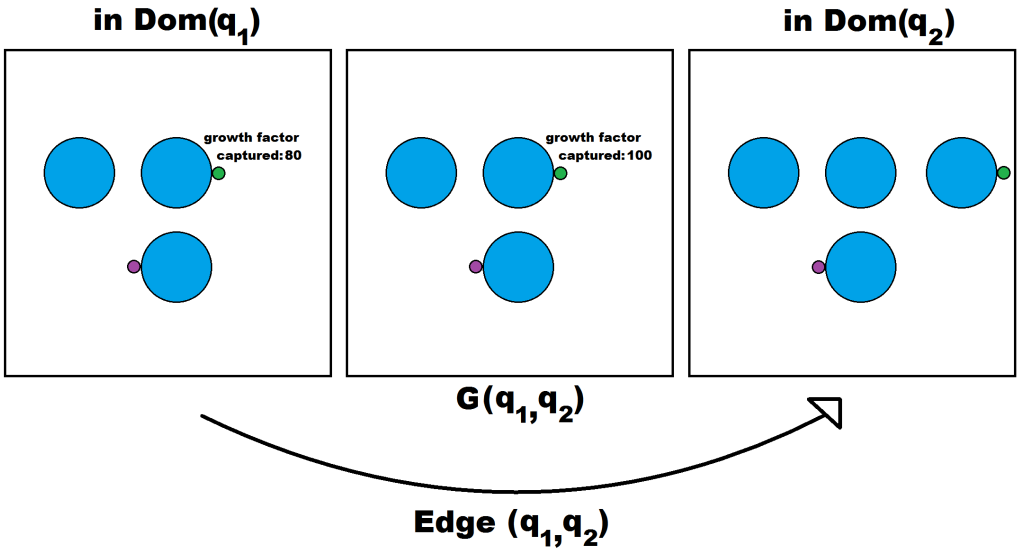

Figure 4.6: *The interaction of the domain, guard conditions, and edges of our model. Left to right, we begin in the domain of biological structure* q_1*. The guard condition for edge* (q_1, q_2) *is then met when the positive fractone captures* 100 *concentration units of growth factor. This triggers growth and we instantaneously switch discrete states to biological structure* q_2*.*

The reset maps are given by $R(\cdot,\cdot) : E \times \mathbf{X}_0 \times \mathbf{X}_0 \rightarrow \mathbf{X}_0 \times \mathbf{X}_0$. As mentioned, upon triggering a growth along edge E, the values of X are changed, representing the pushing of growth factor due to the growth. For mitosis occurring at time t_m along edge (q_1, q_2), $X(x, t_m) = R((q_1, q_2), X_1(x, t_m^-), X_2(x, t_m^-))$, where t_m^- is the limit as t approaches t_m from the left.

By putting all of this together, we define the hybrid control system

$$H = (\mathbf{Q}, \mathbf{X}, f_{ql}, u, g, Init, Dom, E, G, R)$$

Example Given a biological configuration, q, as shown in Fig. 4.7, with two growth factors, cell bodies c_1, c_2, c_3, cell times t_1, t_2, t_3 respectively, positive fractones γ_1, γ_2, negative fractone γ_3, and diffusion space D, growth will occur when one of the positive fractones absorbs enough positive growth factor or the time reaches the neutral growth time of one of the cells. c_3 will only undergo neutral growth if the negative growth factor absorbed by γ_3 exceeds the threshold. The thresholds are arbitrarily chosen, as our growth factor concentrations are in arbitrary units. These thresholds

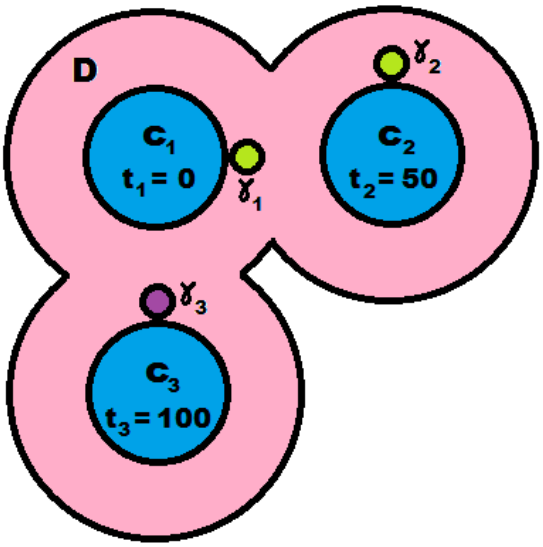

Figure 4.7: *An example biological configuration with cells, c_1, c_2, c_3, in blue; positive fractones, γ_1, γ_2, in green; negative fractone, γ_3, in purple; and diffusion space in pink. Corresponding cell times t_1, t_2, t_3 for c_1, c_2, c_3, respectively, are shown.*

represent the level of growth factor concentrations at which the cells react to the growth factor, either undergoing mitosis for positive growth factor or halting all mitosis for negative growth factor. For an accelerated growth threshold of $\tau_1 = 100$, a negative growth threshold of $\tau_2 = 80$, and neutral growth time delay of 360 minutes,

$$Dom(q) = \Big\{(X_1(x,t), X_2(x,t), T) \,|\, \int_{\gamma_1} (X_1(x,t) - X_2(x,t))\, dV < 100, \int_{\gamma_2} (X_1(x,t) - X_2(x,t))$$
$$dV < 100, T \neq 360, 410, 460, \text{ or } \int_{\gamma_1} (X_1(x,t) - X_2(x,t))\, dV < 100,$$
$$\int_{\gamma_2} (X_1(x,t) - X_2(x,t))\, dV < 100, \int_{\gamma_3} X_2(x,t) dV \geq 80, T = 460\Big\}$$

Growth of c_1 would be represented by an edge, e_1, with guard condition:

$$G(e_1) = \Big\{(X_1(x,t), X_2(x,t), T) \,|\, \int_{\gamma_1} (X_1(x,t) - X_2(x,t))\, dV \geq 100 \text{ or } T = 360\Big\}$$

4.4 Mitosis and Deformation Mechanics

The guard conditions in the above example is typical, and when it is met, mitosis occurs, causing an instantaneous change in the discrete state (along some edge). The edges define the

growth algorithm. As has been stated, we do not model the actual growth of the daughter cells - all daughter cells are formed at full adult size immediately. When a cell undergoes mitosis, the daughter cells are formed along the axis of the tangent vector to the surface of the ellipsoid at the point where the fractone is tangent to the cell. In this way, the fractones determine the general direction of growth. Daughter cell cell bodies are separated by a set distance d_m when placed. The new cells have the same geometry and orientation as the parent cell by simplifying assumption, and when it is created it may force pushing of neighboring cells that may cascade into a deformation of the entire cell set. The directions of each push is determined by the direction of the tangent vector to the surface of the ellipsoid being pushed at the point of collision. The algorithms for growth and pushing are given explicitly in the next chapter for a simplified system of cells aligned to a grid.

4.5 Evolution of the System

We make the following definitions to describe the evolution of the system over time. We denote the evolution of a discrete state by $\hat{q}(\cdot) : \mathbb{R} \to \mathbf{Q}$ which is a map to the discrete state the system is in at time t, and we denote the evolution of a continuous state by $\hat{X}(\cdot) : \mathbb{R} \to \mathbf{X}_0 \times \mathbf{X}_0$ which is a map to the continuous state we are in at time t.

We want to restrict our set of control functions to always agree with the fractone locations of whatever discrete state we are in, and also want to ensure that the control is properly defined over the entire time that the discrete state is evolving. We therefore make the following definition.

Definition For any $T \in \mathbb{R}_{\geq 0}$, a control, u, defined on $[0, T]$ is *admissible* for the evolution of the discrete state $\hat{q}$ defined on $[0, T]$ if $u(x, t) = 1$ if and only if x lies in a fractone in biological structure $q = \hat{q}(t)$ for all $x \in A$ and $t \in [0, T]$.

Then we define a specific evolutions of a system with an admissible control as follows:

Definition For a given admissible control, u, defined on $[0, T]$ and initial conditions $(q_0, X_0) \in \mathbf{Q} \times \mathbf{X}$, we define an "end-point" on $[0, T]$ as a specific evolution of the system, $(\hat{q}(t), \hat{X}(t))$, with $\hat{q}$ and $\hat{X}$ defined on $[0, T]$ and $\hat{q}(0) = q_0$, $\hat{X}(0) = X_0$.

Because of the random nature of the neutral growth there may exist multiple end-points on $[0, T]$ with the same control and initial conditions. We define the set of all such end-points as follows:

Definition For any $T \in \mathbb{R}_{\geq 0}$, and a given hybrid control system H with admissible control $u(x,t)$ defined on $[0,T]$, and initial conditions $(q_0, X_0) \in Init$, we define the *end-point set*, $\Lambda_H(q_0, X_0, u, T)$, as the set of all possible end-points on $[0,T]$.

Since the random neutral growth tends to complicate the system by adding a stochastic element and many end-points for a given control, we will often consider a simpler system by removing the random growth mechanic. In this simplified system the growth of cells occurs only when a fractone absorbs sufficient growth factor, and the evolution of the system is now completely determined by the initial conditions and control used. This means that $\Lambda_H(q_0, X_0, u, T)$ now only has a single end-point, which we will call the "end-point map" on $[0,T]$, and denote by $\chi_H\left(t, q_0, X_0, u(\cdot), T\right) = \left(\hat{q}(t), \hat{X}(t)\right)$.

Now, instead of specifying a control and initial position, we consider the "evolution set" of a hybrid control system H at T, which is the set of end-point maps for all admissible controls defined on $[0,T]$.

Definition Define the *evolution set* of H at T by $Evol_H(T) = \bigcup_{U,Init}\{\chi_H\left(t, q_0, X_0, u(\cdot), T\right)\}$, where U is the set of all admissible controls defined on $[0,T]$.

Since we want to consider the evolution of the system at any time, we expand the definition of the evolution set of H at T to consider all end-point maps defined on any $T \geq 0$.

Definition Define the *evolution set* of H by $Evol_H = \bigcup_{T\geq 0} Evol_H(T)$.

We further define the set of "reachable" states, which covers all possible $(q, X) \in \mathbf{Q} \times \mathbf{X}$ that can be reached by end-point maps in an evolution set. We start with the discrete and continuous states we can reach at a specific time:

Definition Define the set of all *reachable* states of H at T by

$$Reach_H(T) = \left\{(q, X) \in \mathbf{Q} \times \mathbf{X} | q = \hat{q}(T), X = \hat{X}(T) \text{ for some } (\hat{q}, \hat{X}) = \chi_H \in Evol_H(T)\right\}$$

And naturally, we define the set of all discrete and continuous states H can reach at any time:

Definition Define the set of all *reachable* states of H by

$$Reach_H = \bigcup_{T\geq 0} Reach_H(T)$$

Finally, since we are often interested in the development 24 hours from the start of the model, we give special notation to the reachable states of H at $T = 1440$ (since there are 1440 minutes in a day).

Definition Define the set of *end structures* of hybrid system H by $End_H = Reach_H(1440)$

Further definitions of sets describing the evolution of general hybrid automata, but not specifically relevant to our model, can be found in Appendix A.

4.6 Controllability and Optimization

The elimination of the neutral growth in the system means that $Reach_H$ is set of all discrete and continuous states that the system can be "steered" to by careful selection of the control. This leads to a natural questions about controllability of the system. Given an initial set of cells and a final target set of cells, is it possible to evolve the system from the initial state to the final one through manipulation of the fractones? There are a couple of considerations to note here. First, our primary interest is in the cells, not the meninges, so the meningeal cells are largely disregarded. Second, since we are considering biological growth, we must grow at a particular pace and reach our target at a particular time, with a certain degree of accuracy. This accuracy, however, need not be perfect. We will therefore consider a 24 hour timeframe and give a bound, δ, on the distance between our final set of cells and our target set of cells.

Formally stated, the question of controllability is: Given an initial admissible set of cell bodies, E_0; a target admissible set of cell bodies, E_f, with $E_0 \subset E_f$; an initial growth factor distribution, $x_0 \in \mathbf{X}_0$; and ignoring random neutral growth, can we find a control $u(x,t)$ and initial $q_0 \in \mathbf{Q}$, where q_0 has the set of cell bodies E_0, such that for the resulting hybrid control system H, $\exists (q_f, X_f) \in End_H$, where q_f has the set of cell bodies, E, and $D_H(E, E_f) \leq \delta$? Generally, we will allow the cells to be a little more than one cell-width off from the target. Since a spherical cell in our model is 9 μm in diameter, we typically let $\delta = 12$.

Our on-going research revolves around this question of controllability as we hope to simulate the development of embryos over time using the hypothesis that fractones guide growth. Given experimentally-determined maps of developing embryos at different times, we hope to be able to find the control that takes us from one map to another. For example, if we know the location of cells in a portion of a developing rat embryo seven days after fertilization and eight days after fertilization, we hope to be able to find the distribution of fractones (the control) such that our simulation

takes us from day seven's cell map to a reasonable approximation of day eight's cell map. Finding such a control, and verifying its biological plausibility, would lend credence to the hypothesis that the development is guided by the fractones.

The literature on hybrid systems has limited results on controllability of a system as large and complicated as ours. Most papers focus on classes of hybrid control systems that are not applicable to ours [29] [28] [68] or look at general hybrid control models but propose algorithms to determine controllability that, while compelling, are in practice infeasible for the complexity of our model [70].

Although it is beyond the scope of this paper, the related question of optimality is mathematically interesting and potentially biologically relevant. Biological mechanisms often become quite efficient by some measure through the natural course of evolution (although exceptions abound). Comparison between results for optimal controls of various cost functions defined on the system, $J(H,t)$, may reveal general strategies adopted by the developing organism for efficient growth.

Assuming a target set of cell bodies is reachable from a given initial set of cell bodies, the question of optimality asks: what is the control that will evolve the system to a state near the target while minimizing some cost function, $J(H,t)$? This cost function could measure several factors, including time, accuracy, or the number of fractones we use in the system, on the assumption that the creation or destruction of fractones would require energy from the developing organism. Thus, formally stated, our optimality problem is: Given an initial set of cell bodies, E_0; a target set of cell bodies, E_f, which is reachable in the sense that a discrete state with such cell bodies $q_f^* \in textQ$ is in $Reach_H$; an initial growth factor distribution, $x_0 \in \mathbf{X}_0$; and ignoring random neutral growth, find the control, $u(x,t)$, and initial $q_0 \in \mathbf{Q}$, where q_0 has the set of cell bodies E_0, such that for the resulting hybrid control system H, the cost function $J(H,t)$ is minimized.

We remark that removing the neutral growth from the system is a significant change to the dynamics of the system. However understanding the behavior of the system without neutral growth is a first step to understanding the dynamics with it. The next step would be to evaluate how significantly the results from the simplified system are perturbed by the reintroduction of the neutral growth, and whether the question of controllability we have stated can be altered to compensate, perhaps through relaxing the bound on the distance between the final set of cells and the target set by an acceptable amount.

Chapter 5

Computer Model

To examine our questions and simulate our model, we rewrite the model described in the chapter 4. The model takes place in a discretized ambient space, A, which is a subspace of $\mathbb{Z}^3$. Thus our ambient space is essentially on a grid, and we refer to each element of the grid as a unit, representing a $1 \times 1 \times 1$ cube in space, which we scale to 1 μm^3. Time passes discretely in uniform time steps such that 24 hours is represented by 200 time steps. One time step is therefore 432 seconds. As with most numerical processes, the diffusion dynamics can be more accurately approximated if we reduce the size of a time step. We choose 200 steps per 24 hour period in order to run the simulation in a timely manner.

The conversion of the model occurs naturally for most of the components of the model described in chapter 4. However, some changes and simplifications are made. We define several spaces in the discretization, starting with the cell space, $Cell(t)$, which is the set of all units (i, j, k) that represent cell bodies at time t. Cell bodies are considered to be $9 \times 9 \times 9$ unit cubes, and are placed in the ambient space such that their distance and orientation are regular. Specifically, the centers of each cell body must align to a $6 \times 6 \times 6$ unit grid in the ambient space. Geometrically, this means that cells have at least 3 units of space between each other. This spacing is used to allow sufficient diffusion of growth factor through the system. The size of the cube is chosen because the spherical cells in the original model have a diameter of 9 μm. The grid alignment of the cells and the uniform cube geometry are used to simplify the mechanics of the system.

Similar to $Cell(t)$, we define the meninges space, $Men(t)$, which is the set of all units (i, j, k) that represent meningeal cells at time t. Meningeal cells are $9 \times 9 \times 9$ unit cubes, just like cell bodies, and are similarly aligned to the same $6 \times 6 \times 6$ unit grid as the cells are. We note that this is a departure from the meningeal cells described in chapter 4, which were significantly smaller in size. However, in our new model, meningeal cells do not enter the diffusion space, and

so their relative size is unimportant. The most significant consideration for the meningeal cells is merely that they cover the exterior of the set of cells. Treating them as the same size and shape as cells simplifies the implementation of the model. Meningeal cells are placed around the exterior of the cell mass according to a meninges-creating algorithm that searches through all the cells in the ambient spaces, recognizes which cells are on the exterior of the mass, and places a meningeal cell 3 units away from it on the exterior, assuming there is no overlap with an existing meningeal cell. See Fig. 5.1 for examples of cells and meninges in the ambient space.

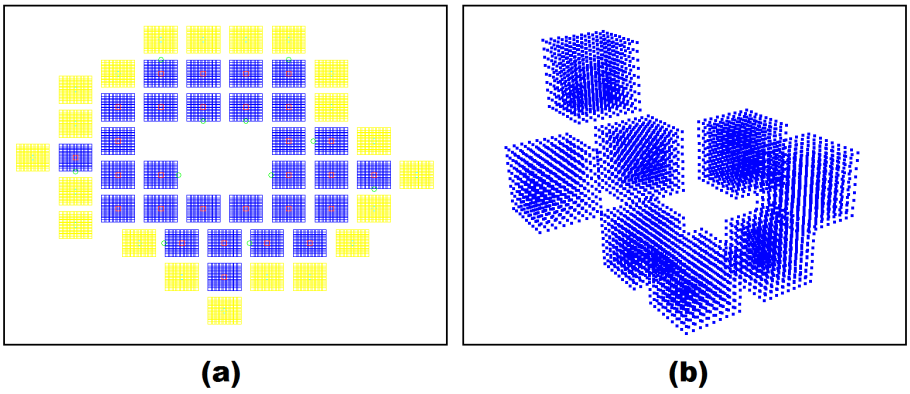

Figure 5.1: *Example distributions of cells. (a) 2D view of cells with meninges. Note the alignment of cells to the grid and the placement of meninges around the exterior of the set of cells. (b) 3D view of a set of cells.*

The fractone space, $Frac(t)$, is the set of all units (i, j, k) that represents positive and negative fractones at time t. $Frac(t)$ can be split into $Frac^+(t)$ and $Frac^-(t)$, respectively. Fractones are $1 \times 1 \times 1$ unit cubes (thus a single unit in size), and must be located exactly 5 units from the center of a cell. This places fractones directly adjacent to cells, and centered on one of the cell's 6 faces. We say a fractone is "associated" to a cell if it is directly adjacent to it. We note that because of the spacing between cells, a fractone can only be associated to one cell. While a cell can have multiple positive fractones or multiple negative fractones associated to it, we do not allow a cell to have both positive and negative fractones associated to it. This is done to simplify the mechanics of the model since positive and negative fractones encourage different behavior in a cell (the effect of the positive and negative fractones is described in the next section).

Positive and negative fractones are modeled by control functions $u^+_{i,j,k}(\cdot) : \mathbb{R}_{\geq 0} \to \{0, 1\}$ and $u^-_{i,j,k}(\cdot) : \mathbb{R}_{\geq 0} \to \{0, 1\}$, respectively, for each $(i, j, k) \in A$. As in section 4.4, we wish to restrict the set of possible controls to a set of admissible ones. For a control $u^+_{i,j,k}$ to be admissible,

$u^+_{i,j,k}(t) = 1$ if and only if a positive fractone is present in unit (i, j, k) at time t and is equal to 0 otherwise. There is a similar restriction for admissibility for $u^-_{i,j,k}$.

5.1 Growth Factors and Diffusion

As in section 4.3, growth factor will diffuse through the system, only now the diffusion is described by a set of ODEs. We define the free space, $Free(t)$, as the set of all units (i, j, k) within 3 units of a cell body boundary and any "holes" in that resulting volume, as we defined in section 4.3 for the diffusion space. Any units that belong to cells, meninges, or fractones are not allowed in $Free$.

The diffusion space of our discretization, $Diff(t)$, is therefore the union of $Free(t)$ and $Frac(t)$, and is the space where perturbed diffusion of growth factors occurs. Generally, units in $Free(t)$ diffuse freely without the perturbation (except for those that neighbor a fractone), and units in $Frac(t)$ cause perturbed diffusion.

The amount of growth factor in the diffusion space at time t is now described by $x^+_{i,j,k}(t)$ and $x^-_{i,j,k}(t)$, which record the amount of positive and negative growth factors, respectively, in unit (i, j, k) at time t. By $x^+(t)$, we denote the associated matrix of positive growth factors, where the (i, j, k)-th entry of $x^+(t)$ is $x^+_{i,j,k}(t)$ (and similarly for $x^-(t)$).

Growth factor is generated by the meninges, as described in section 4.3, except now it is added only every t_{prod} units of time. This could be every 1 time step for a more continuous addition of growth factor, but for our simulations, we set $t_{prod} = 10$ time steps, so growth is added to the system only every 10 time steps. The growth factor production function $g^+(t)$ determines the amount of positive growth factor added to each unit in the diffusion space a distance 1 unit from a meningeal cell. Negative growth factor is added similarly for growth factor production function $g^-(t)$. See Fig. 5.2 for an example of a growth factor production function and its cumulative addition to the system.

Growth factor moves through the diffusion space by perturbed diffusion. When growth factor is far from a fractone, it will diffuse normally. However, near a fractone, growth factor will be captured and stored. This is represented in our model by the standard diffusion equation, however terms are added so that units occupied by fractones will always appear to be empty of growth factor. Fractones therefore always pull in growth factor and growth factor never leaves. The amount of positive (and similarly negative) growth factor absorbed by the fractone is modified by the absorption rate α^+_k (similarly α^-_k), where $k = 1$ represents a positive fractone and $k = 2$ represents

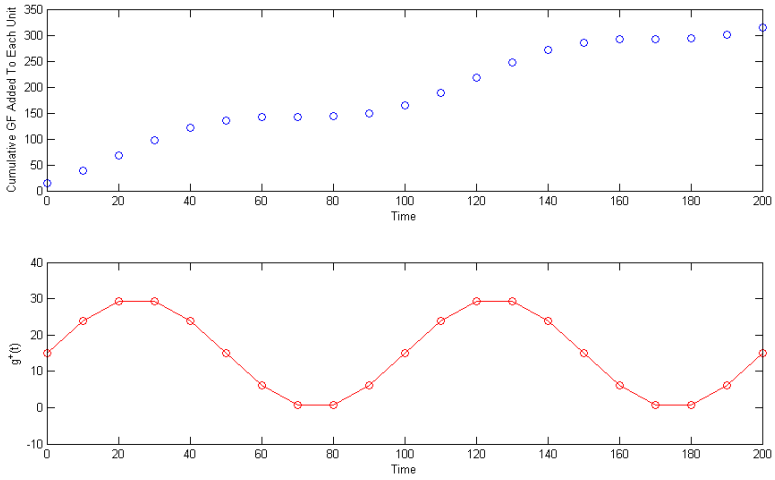

Figure 5.2: *Top: Cumulative growth factor added to a unit over time for growth factor production function,* $g^+(t)$. *Growth factor is added every* 10 *time steps, represented by the circles. Bottom:* $g^+(t) = 15\left(\sin(\frac{\pi}{50}t) + 1\right)$.

a negative fractone. A positive fractone would usually have a higher absorption of positive growth factor than negative growth factor. The equations for the perturbed diffusion therefore appear as follows, where ν^+ is the diffusion constant for the positive growth factor.

When far from a fractone, diffusion occurs freely, according to:

$$\dot{x}^+_{i,j,k}(t) = \nu^+ \sum_{\substack{(\delta,\beta,\gamma)\in\Delta \\ (i+\delta,j+\beta,k+\gamma)\in Diff(t)}} \left(x^+_{i+\delta,j+\beta,k+\gamma}(t) - x^+_{i,j,k}(t)\right) \tag{5.1.1}$$

where $\Delta = \{(1,0,0),(-1,0,0),(0,1,0),(0,-1,0),(0,0,1),(0,0,-1)\}$.

However, in units adjacent to a fractone, diffusion is perturbed and the unit with the fractone always appears empty. When (i,j,k) is not a fractone, this changes the diffusion to:

$$\dot{x}^+_{i,j,k}(t) = \nu^+ \sum_{\substack{(\delta,\beta,\gamma)\in\Delta \\ (i+\delta,j+\beta,k+\gamma)\in Free(t)}} \left(x^+_{i+\delta,j+\beta,k+\gamma}(t) - x^+_{i,j,k}(t)\right)$$

$$+\nu^+ \sum_{\substack{(\delta,\beta,\gamma)\in\Delta \\ (i+\delta,j+\beta,k+\gamma)\in Frac(t)}} u^+_{i,j,k}(t)\left(x^+_{i,j,k}(t) - x^+_{i+\delta,j+\beta,k+\gamma}(t) - \alpha^+_k x^+_{i,j,k}(t)\right)$$

And when (i,j,k) is a fractone, the diffusion becomes:

$$\dot{x}^+_{i,j,k}(t) = \nu^+ u^+_{i,j,k}(t) \sum_{\substack{(\delta,\beta,\gamma)\in\Delta \\ (i+\delta,j+\beta,k+\gamma)\in Free(t)}} \alpha^+_k \left(x^+_{i+\delta,j+\beta,k+\gamma}(t)\right)$$

Both this free and perturbed diffusion can be combined into an affine control system:

$$\dot{x}^+ = F_0(x(t)) + \sum_{(i,j,k)\in \text{Diff(t)}} F^{(i,j,k)}(x(t))u^+_{i,j,k}(t)$$

where the drift F_0 represents the free diffusion - the (i,j,k)th component of this vector field is given by the right hand side of equation 5.1.1 - and the control vector fields $F^{(i,j,k)}$ describe the perturbed diffusion when a fractone is present in unit (i,j,k) - the (i,j,k)th component of this vector field is given by:

$$\nu^+ \sum_{\substack{(\delta,\beta,\gamma)\in\Delta \\ (i+\delta,j+\beta,k+\gamma)\in Free(t)}} \left(x^+_{i,j,k}(t) - x^+_{i+\delta,j+\beta,k+\gamma}(t) + \alpha^+_k x^+_{i+\delta,j+\beta,k+\gamma}(t)\right)$$

and component $(i+\delta, j+\beta, k+\gamma)$, $(\delta,\beta,\gamma)\in\Delta$, is given by :

$$\nu^+ \left(x^+_{i,j,k}(t) - x^+_{i+\delta,j+\beta,k+\gamma}(t) - \alpha^+_k x^+_{i+\delta,j+\beta,k+\gamma}(t)\right)$$

All other components are zero. The diffusion equation for the negative growth factor is analogous.

5.2 Mitosis and Displacement Algorithm

Two types of mitosis may occur in the model. Accelerated growth occurs when a fractone collects sufficient positive growth factor. For our model we trigger accelerated growth when the amount of positive growth factor exceeds the amount of negative growth factor in the fractone by the threshold value of τ_1, a parameter whose value we set. For accelerated growth, the direction of mitosis is determined by the location of the fractone. For example, if a fractone lies to the left of a cell, then the mitosis will occur in the left direction. We note that this is a significant assumption on the behavior of the fractone, and in reality the direction of the push may be governed by many other factors. However, in our model, we wish to give the fractone as much control over the growth as possible. See the following section for more details on the growth algorithm.

Neutral growth occurs once a day (200 time steps) when a cell is old enough, determined by its cell time t_c. When the time in the model exceeds t_c by 200 time steps, neutral growth will occur unless a negative fractone has captured a sufficient amount of growth factor. For the cells in the initial cell mass, t_c is assigned randomly during the set-up of the model, and takes on an integer value between -200 and 0 time steps. When cells are created as the model progresses, t_c is assigned as the time of mitosis, as described in section 4.1.

Neutral growth will occur unless an associated fractone to the cell has collected more than a threshold value τ_2 negative growth factor. τ_1 and τ_2 are both set arbitrarily at 100 in our simulations. The direction of neutral mitosis is random. The choice to make neutral growth occur in a random direction was done because absent the fractone, the mechanism that determines the direction of growth is unknown. On a biological note, it is worth remembering that the actual growth cannot be random - it must be governed by something. Although we will often analyze simulations with neutral growth turned off, biologically it is an important part of development that must be considered when we attempt to simulate actual biological maps.

Growth of any kind may occur only once every 6 hours (50 of our time steps), as explained in section 4.1. Note that when mitosis occurs, the parent cell ceases to exist and two daughter cells are created, so this 6 hour limit will never interfere with normal mitosis (since a cell must be 24 hours old before it undergoes mitosis). Accelerated growth, however, is delayed until 6 hours have passed, even if an associated fractone has collected enough growth factor to reflect the biology.

When mitosis is triggered, growth occurs in our model as follows: For a mother cell undergoing mitosis and growing to the right, centered at $(0, 0, 0)$,

1. If the full $12 \times 12 \times 12$ space to the right of the mother cell is in the free space, then the mother cell splits, leaving one the daughter cell centered at $(0, 0, 0)$ and creating one cell centered at $(12, 0, 0)$. Any associated fractones to the right, above, or below the mother cell transfer to the daughter cell centered at $(12, 0, 0)$ while any associated fractones to the left of the mother cell remain with the daughter cell centered at $(0, 0, 0)$. See Figure 5.3.

2. If there is already an existing cell centered at $(12, 0, 0)$ or $(18, 0, 0)$, the division of the mother cell into two daughter cells deforms the existing mass of cells to the left and to the right. More precisely, the mother cell vanishes and the two daughter cells are created, centered at $(-6, 0, 0)$ and $(6, 0, 0)$. Associated fractones to the mother cell on the right, above, and below transfer to the daughter cell centered at $(6, 0, 0)$. The other fractones transfer to the daughter cell centered at $(-6, 0, 0)$. Existing cells that overlap these new cells undergo displacement (see below).

If mitosis triggered by a fractone is to the left, above, below, in front of, or behind the mother cell the deformation of the existing mass of cells is done in an analogous fashion.

Cell growth and displacement can cause cells to overlap with each other. The displacement algorithm gets rid of this overlap by pushing cells that overlap apart. The algorithm is as

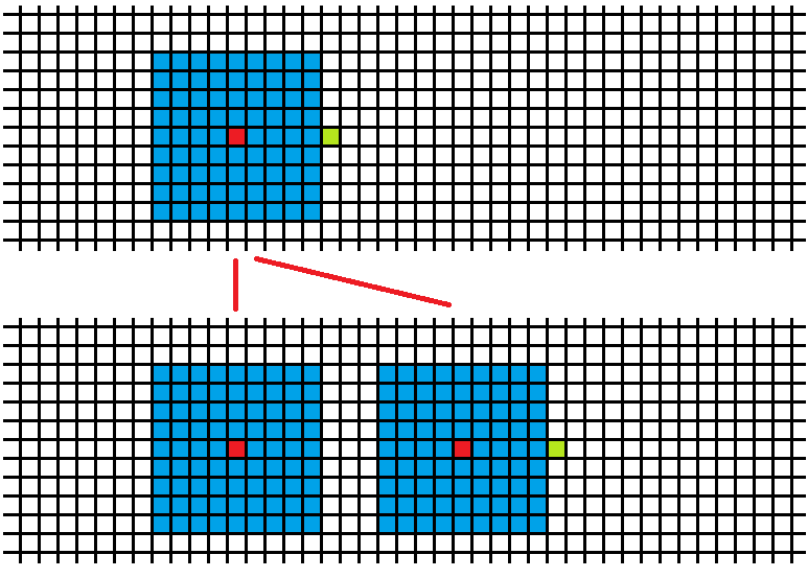

Figure 5.3: *An example of a cell in our system undergoing mitosis with no blocking cells. While a two dimensional example, the three dimensional algorithm is analogous. Cells are shown in blue with a red center unit. Fractones are shown in green. When the fractone absorbs enough positive growth factor, it triggers mitosis. Since the fractone is on the right of the cell, the direction of the growth is to the right. The mother cell splits into two daughter cell, one remaining in the same position and the other* 12 *units to the right.*

follows: Assume a cell centered at $(0, 0, 0)$ grows to the right and creates a new cell centered at $(12, 0, 0)$.

1. If a cell is an off-set neighbor of the parent cell in one dimension, ie. at locations $(12, 6, 0)$, $(12, -6, 0)$, $(12, 0, 6)$, $(12, 0, -6)$, then the cell will be translated over 6 units perpendicular to the direction of the push. For instance, a mitosis event occurring on a mother cell centered at $(0, 0, 0)$ deforming the existing mass to the right pushes a cell centered at $(12, 6, 0)$ to a new position at $(12, 12, 0)$. All fractones transfer with it. See Figure 5.4 for an example of this.

2. if a cell is an off-set neighbor in two dimensions at $(12, 6, 6)$, $(12, 6, -6)$, $(12, -6, 6)$, or $(12, -6, -6)$, then the neighboring cell will be pushed to the following respective locations: $(12, 12, 6)$, $(12, 6, -12)$, $(12, -6, 12)$, $(12, -12, -6)$. See Figure 5.5 for an example of this.

3. If a cell is an off-set neighbor in three dimensions at $(18, 6, 6)$, $(18, 6, -6)$, $(18, -6, 6)$, or $(18, -6, -6)$, then the neighboring cell will be pushed to the following respective locations: $(18, 12, 6)$, $(18, 6, -12)$, $(18, -6, 12)$, $(18, -12, -6)$. See Figures 5.6 and 5.7 for an example of this.

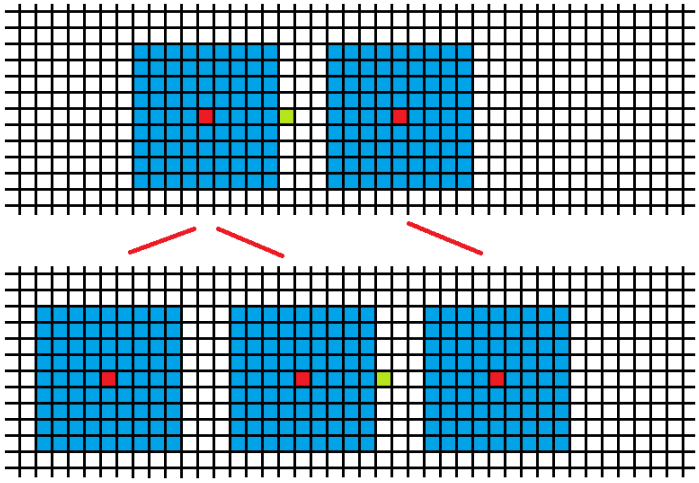

Figure 5.4: *An example of mitosis with a blocking cell directly in the path of the growth direction. The blocking cell is displaced* 6 *units and the mother cell undergoing mitosis splits into two daughter cells, one shifted* 6 *units in the direction of growth and the other* 6 *units in the opposite direction of growth.*

Note that one displacement of a cell may trigger another displacement, causing a chain reaction of displacements which generates the mass deformation. We note that if multiple mitosis events should occur during the same time step, then accelerated growth goes first, starting with the cell whose associated fractone has absorbed the most positive growth factor, and working down. After the accelerated growth, neutral growth will occur, in order of their cell centers from left to right(x-axis), bottom to top (y-axis), and front to back (z-axis).

Growth and displacement of cells additionally affect the distribution of growth factor. Indeed, during a mitosis event the dimension of the cellspace increase which is equivalent to a decrease of the dimension of the diffusion space. Growth factor therefore needs to be redistributed in the new diffusion space. Growth factor sandwiched between moving cells is merely translated the appropriate 6 units over. However, when displacement occurs without triggering further displacement in the same direction, the displaced growth factor is redistributed so that 80% of any displaced growth factor is evenly distributed one unit away from the boundary of the new cell space in the

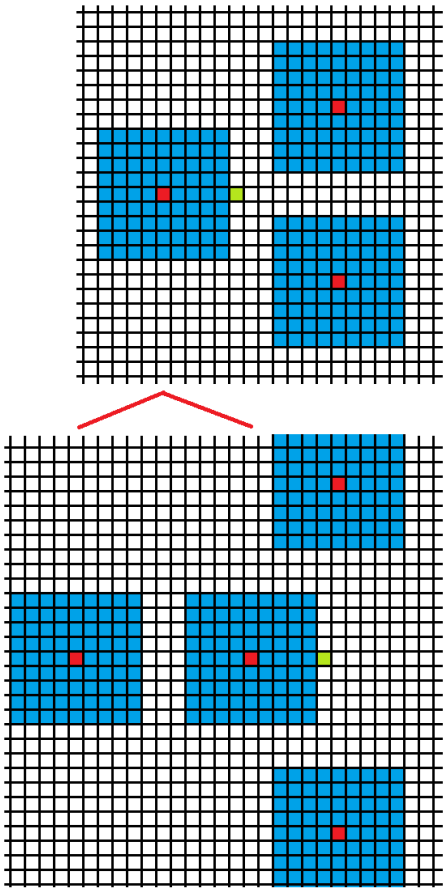

Figure 5.5: *An example of mitosis with blocking cells offset from the direction of growth. The blocking cells are shifted* 6 *units perpendicular to the growth, while mother cell undergoing mitosis splits into two daughter cells, one shifted* 6 *units in the direction of growth and the other* 6 *units in the opposite direction of growth.*

direction of the deformation and 20% is evenly distributed two units away. This creates a wave of growth factor redistribution that moves with the growth of the mass of cells (see Fig. 5.8 and Fig. 5.9).

Growth and displacement may also affect the location of the meninges. After each mitosis event and the corresponding pushes, the meninges are redistributed by the meninges-creating algorithm in the exact same way as when the system was first initialized. This way, the meninges is always located on the exterior of the set of cells and grows and stretches as needed as the cell mass grows.

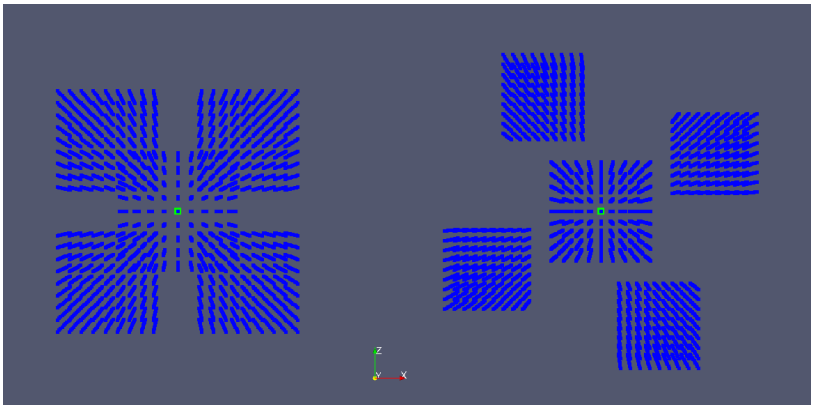

Figure 5.6: *3D pushing algorithm for pushing into cells offset in two dimensions. A mother cell (front) is growing back into four cells offset in two dimensions. The four blocking cells are pushed in four different directions, perpendicular to the direction of growth, determined by their relative position to the mother cell.*

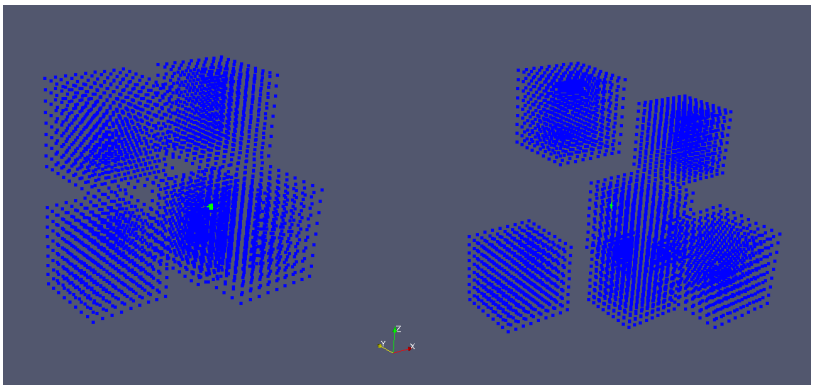

Figure 5.7: *3D pushing algorithm from an alternate angle.*

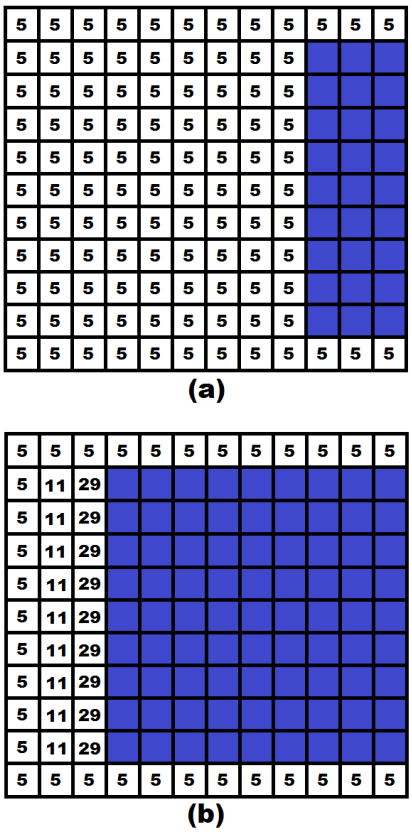

Figure 5.8: *The push dynamics that show a concentration of growth factor along the leading edge of a push. (a) Two-dimensional diffusion space before the push, showing a uniform distribution of* 5 *concentration value in the diffusion space. In blue, is the edge of the cell. (b) Diffusion space after the push. 80% of the pushed growth factor is placed adjacent to the cell, and 20% two units away. The distribution and values in the three-dimensional system are similar.*

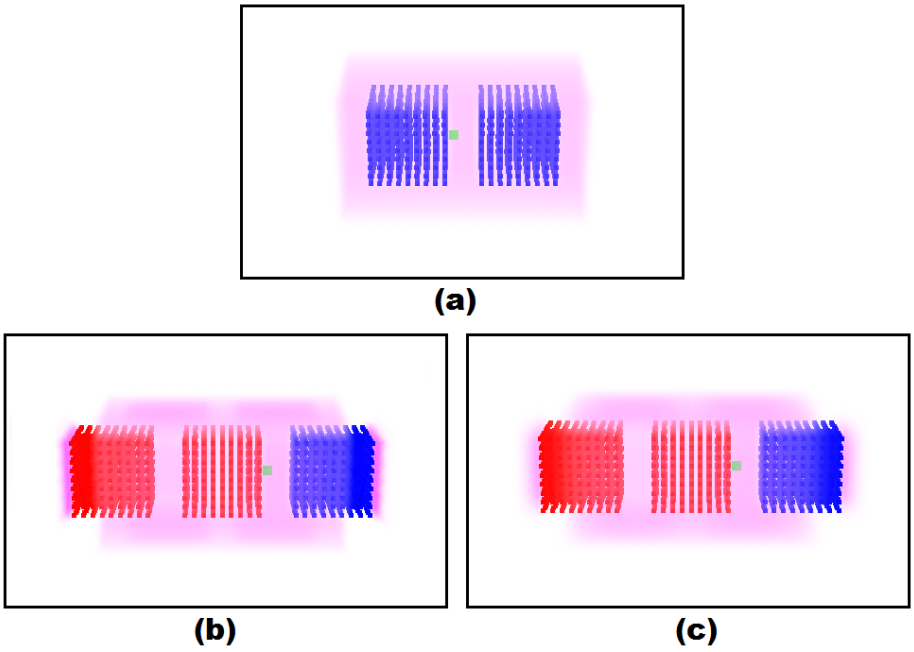

Figure 5.9: *3D image of a simple mitosis event with positive growth factor concentration shown at* 5 *time step interval. Blue: Cell. Red: Proliferating Cell. Green: Fractone. Pink: Positive Growth Factor (intensity proportional to concentration). (a) Initial set up with growth factor uniformly distributed in the diffusion space (notice it extends* 3 *units out from the borders of each cell). (b) Mitosis event occurs, splitting the mother cell into two daughter cells* 6 *units to the left and right of the mother's position. Resulting growth also pushes the non-proliferating cell to the right. Notice the redistribution of the growth factor due to the push on the far left and right. (c)* 5 *time steps later, growth factor has begun to diffuse in the now larger diffusion space.*

5.3 Computer Model Operation

The model is run using Matlab R2010b. The progression of the model is shown in figure 5.10.

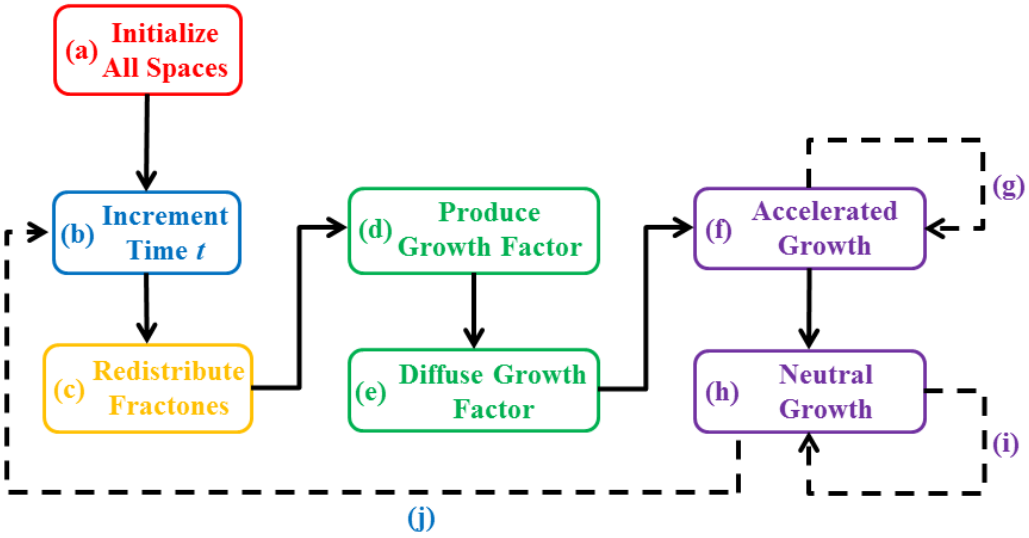

Figure 5.10: *A flowchart of the model phases, labeled (a) through (j). Dashed arrows represent conditional flows. All phases are described in the text.*

In more detail, each phase of the program operates as follows:

Initialize All Spaces (figure 5.10(a)): This phase occurs only once at the very start of the program. It generates a discretized representation of the cell spaces in three-dimensional arrays by reading a provided map of our starting configuration. Each element in the array represents one unit in our ambient space and is assigned a number that corresponds to one of the previously discussed spaces. For example, elements labeled with a 1 belong to the free space, and elements labeled with a 3 represent positive fractones. In addition, the growth factor concentrations in the diffusion space are set. For our model, we initially filled the diffusion space with a uniform distribution of growth factor (typically 10 growth factor concentration units for each type of growth factor). Growth times for normal growth of cells are also set during this phase.

Increment Time (figure 5.10(b)): Diffusion in the model occurs discretely with small time steps. This phase simply increases the model time by one time step.

Redistribute Fractones (figure 5.10(c)): The program then checks the controls if any fractones need to be redistributed at time t. If so, fractones are removed or added to the system. Otherwise, no changes occur.

Produce Growth Factor (figure 5.10(d)): Growth factors, both positive and negative, are added to the system near the meninges, as described in section 5.1.

Diffuse Growth Factor (figure 5.10(e)): Positive and negative growth factors undergo perturbed diffusion according to the diffusion equations in section 5.1.

Accelerated Growth (figure 5.10(f)): All positive fractones in the system are checked for their growth factor concentrations. If the difference of the positive growth factor minus the negative growth factor exceeds the set threshold, τ_1, then accelerated growth will occur according to the algorithm in section 5.2. The cellspace is reconfigured due to the growth that occurs during this phase. If multiple fractones have exceed the threshold, then multiple accelerated growths occur, in order of greatest net growth factor concentrations to least (figure 5.10(g)).

Normal Growth (figure 5.10(h)): All cells are checked for whether they have reached maturity for neutral growth. Any cell that reaches its neutral growth time is checked for associated negative fractones with negative growth factor. If a fractone has negative growth factor which exceeds τ_2, then the neutral growth will not occur. Otherwise, growth occurs according to the algorithm described in section 5.2. The cellspace may be reconfigured during this phase due to growth. If multiple neutral growths should occur, they occur left to right(x axis), bottom to top (y axis), and front to back (z-axis) (figure 5.10(i)). At the end of this phase, if $t = 200$, then the program stops as we have completed a 24 hour simulation (figure 5.10(j)).

Depending on the size of the simulation run, the computation time varies. For an ambient space that is $400 \times 400 \times 400$ units, and about 200 cells, it takes approximately 45 minutes for 200 time steps to pass.

Chapter 6

Results

In this section, we first verify the computer model. The model is complicated and each individual process needed to be tested. In addition, since the second phase of the project will require tuning of parameters, it was important to verify that the behavior of the model is as expected and to recognize the potential impact of changing parameter values. Next, we consider the application to biology and verify that our model is ready to accept biological data when it becomes available. Finally, we examine the question of controllability and achieving an admissible control that takes us on a trajectory from a given initial set of cells to a given target set of cells.

6.1 Verification of Model Behavior

Several test cases were performed to verify the behavior of the model and examine the impact of the parameter values. Some cases do not use the random neutral growth in order to more easily examine the parameter impact; the set-up used will be explained in each case. Meninges is present surrounding the cells during the tests, but are not shown in the following figures as they would otherwise obscure the results.

6.1.1 Case 1: Uniform Growth

In Figure 6.1(a), a symmetrical octahedron cell mass was created initially. This octahedron is generated with a $5 \times 5 \times 5$ cube center and a square pyramid on each face of the cube. Each cell in the middle $3 \times 3 \times 3$ block of cells is assigned one fractone on a random side, with an even probability for each side. Each of the results in 6.1(b-d) was generated by a different assignment of fractones. Neutral growth is switched off so that only growth directed by fractones occurs. The model was run for 24 hours (200 times steps) in each case, with fractones not redistributed by a control and only moving as per the growth and pushing algorithms. A uniform 15 growth factor

Test	D_H	D_F^+	D_a	D_B
b	43.681	72.25	1146.6	1262.6
c	42	54.571	1136.8	1233.4
d	43.681	51.614	1133.5	1228.8

Table 6.1: *Table of distances for the three tests of uniform growth without neutral growth. Tests (b), (c), (d) refer to the images in Fig. 6.1.*

concentration units was added to units neighboring meningeal cells (not shown in figures) every 10 time steps. Absorption constants of 0.9 and 0.2 for the positive fractones were set for positive and negative growth factor, respectively.

We would expect roughly uniform growth over time. Figures 6.1(b-d) show the results after 24 hours of growth (200 time steps). The results are as expected, although notice in all cases long strands of cells seem to grow. These long strands of cells occur when fractones are aligned along the same axis, causing pushing and growth along the same axis. Figure 6.1(b) shows this behavior in particular.

Additionally, we can calculate the distances between the initial and final sets of cells. The results are shown in table 6.1. The distance metrics used are as described in section 4.2. Recall, that D_H is the Hausdorff distance between the set of cells. D_F is the Hausdorff distance between the set of fractones. D_A is the age distance, a modified Hausdorff distance that accounts for both distance between cells and their relative ages. D_B is the sum of all of these distances.

The distance results show that despite the random distribution of the positive fractones, the amount of growth is roughly the same - well within even a cell radius of length. Thus no test simulation grew much more than any other. The age distances are so large because they are comparing new cells born during the simulation to the old initial cells which were initialized with cell ages between -200 and 0.

We repeat the experiment, but now with the neutral growth active. The age of each cell in the initial set is randomly chosen during initialization. Thus each test has randomized fractone locations as well as randomized times for neutral growth of each cell. We again expect uniform growth in all directions for each test. Three test were run and the results are shown in Fig. 6.2

The Hausdorff distance, D_H between the cells was calculated for the test with neutral growth between the initial and final cell positions (see Table 6.2). Because the ages were randomized between tests, we do not calculate the age distance. According to the Hausdorff distances between the sets of cells, which are all fairly similar, the growth is fairly uniform, as intended. We note that

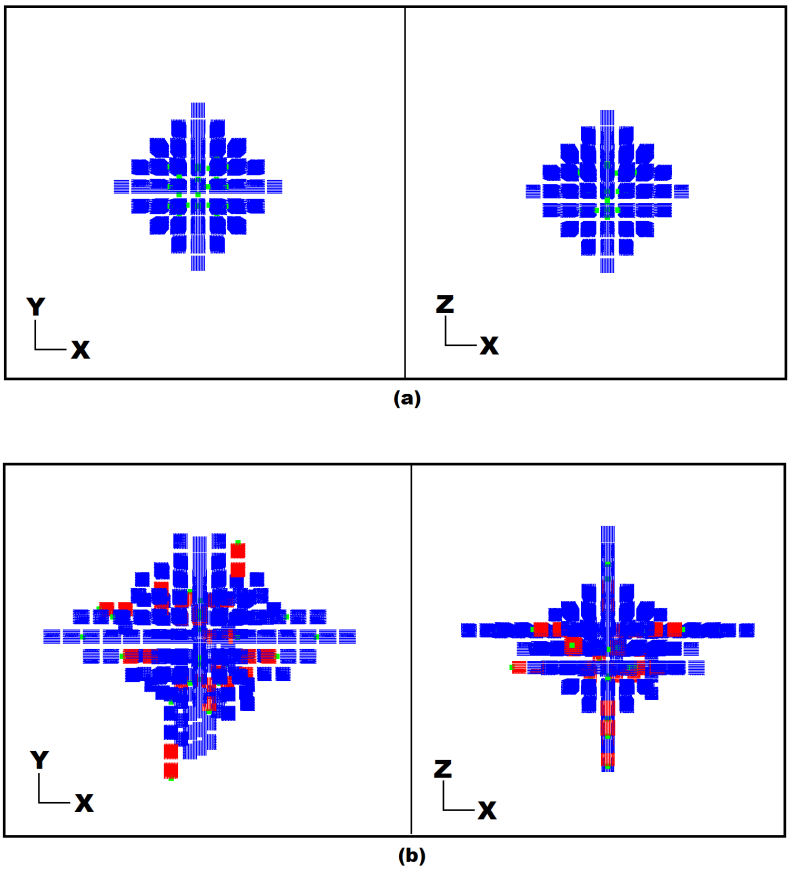

Figure 6.1: *(a) The initial cell structure, a three-dimensional octahedral structure. Fractones are randomly distributed in the center of the cell mass. (b) Examples of growth after 24 hours (200 time steps). In blue, non-proliferating cells, those which have not grown within 6 hours (50 time steps); in red, proliferating cells, those which have grown within 6 hours (50 time steps); in green, fractones, shown enlarged for visibility. Right images are* 90 *degree rotations of the left images around the* x*-axis.*

test (b) has a larger Hausdorff distance than test (c) despite Fig. 6.2 showing test (c) with a long strand of cells. Not clearly visible in the image of test (b) is a long strand of cells that is further from the closest point of the initial octahedron than the strand in test (c), which is actually fairly close to one of the "vertices" of the initial octahedron.

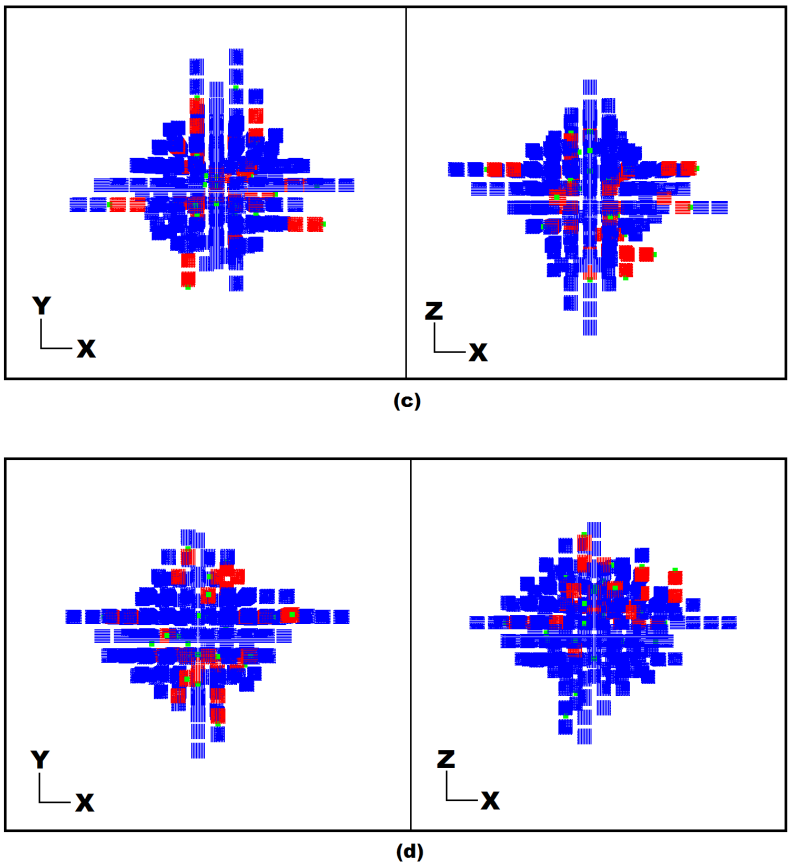

Figure 6.1: *(c-d) Examples of growth after 24 hours (200 time steps). In blue, non-proliferating cells, those which have not grown within 6 hours (50 time steps); in red, proliferating cells, those which have grown within 6 hours (50 time steps); in green, fractones, shown enlarged for visibility. Right images are* 90 *degree rotations of the left images around the* x*-axis.*

Test	D_H
a	55.3170
b	48.3740
c	43.2670

Table 6.2: *Table of Hausdorff Distances for the three tests of uniform growth with neutral growth. Test (a), (b), and (c) refer to the images in Fig. 6.2.*

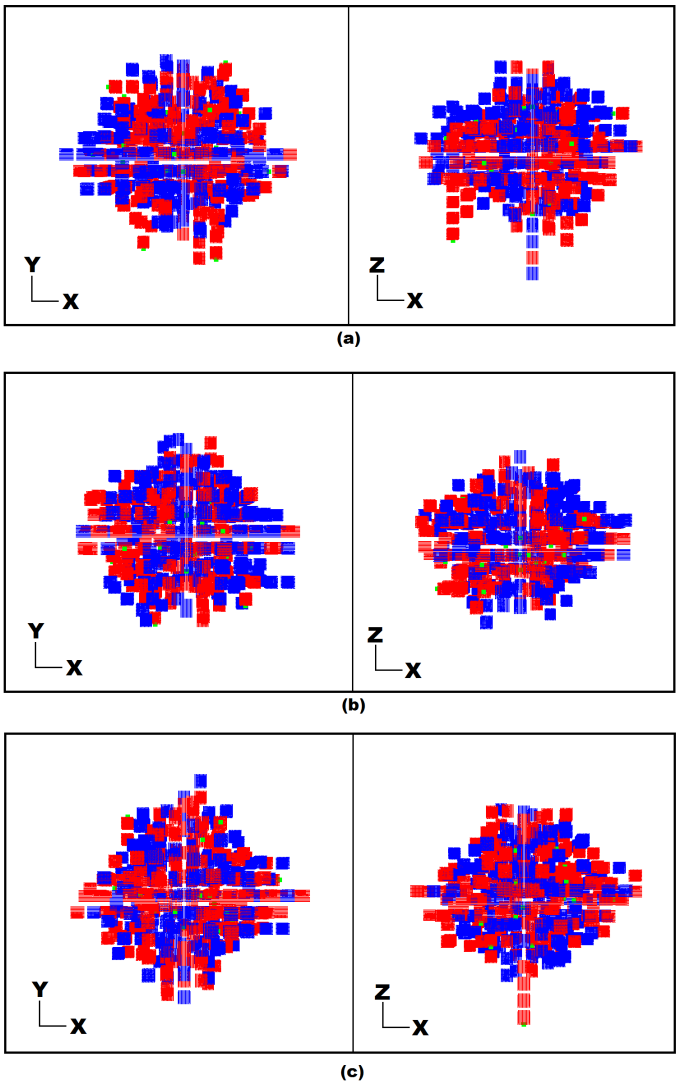

Figure 6.2: *Two views of final cell configurations for uniform growth test with neutral growth. (a-c) Three example final configurations after* 24 *hours (200 time steps) with neutral growth active. The initial set-up is the same as in Fig. 6.1(a). In blue, non-proliferating cells, those which have not grown within 6 hours (50 time steps); in red, proliferating cells, those which have grown within 6 hours (50 time steps); in green, fractones, shown enlarged for visibility.*

6.1.2 Case 2: Directed Growth

To demonstrate this strand behavior as well as the ability for fractones to direct growth along a particular axis, we run one more simulation using the same set up as Case 1, except we change the fractone distribution. Now each cell in the center $3 \times 3 \times 3$ block has a 50% chance of having one fractone placed on a face perpendicular to the x-axis and a 50% of no fractone at all. By our algorithm then, all growth should be along the x-axis, and this is seen in Fig. 6.3. To best demonstrate thiss directed growth, we turn off the neutral growth.

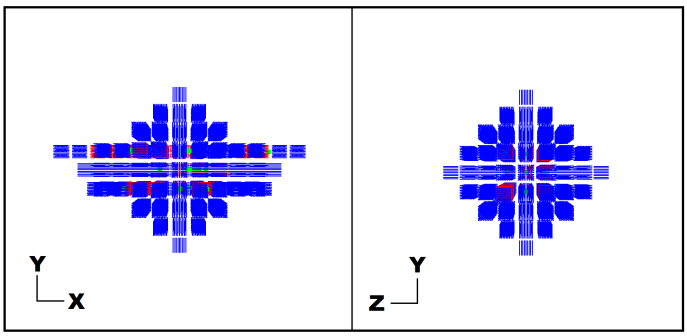

Figure 6.3: *Example of growth with fractones placed along one axis only. Same initial cell set-up as in Fig. 6.1. The right image is rotation of the left image 90 degrees around the y-axis. In blue, final non-proliferating cell positions after 24 hours; in red, final proliferating cell positions; in green, fractones (enlarged for visibility).*

6.1.3 Case 3: Accelerated and Blocked Growth

To demonstrate the relative effects of positive and negative fractones, we show three further test cases. In all three cases, the initial cell configuration is a $7 \times 9 \times 4$ rectangular prism. In Fig. 6.4, two randomized patches of fractones, one of positive and one of negative, are created. As can be seen in the left image of Fig. 6.4(a), the initial set-up has positive fractones randomly distributed adjacent to cells on the right and negative fractones randomly distributed to cells on the bottom left. As stated in chapter 5, we do not allow a cell to have both positive and negative fractones. The growth factor production and initial growth factor concentration was the same as in Case 1. The absorption constants for positive fractones were 0.9 and 0.2 for positive and negative growth factor, respectively. For negative fractones, the absorption constants were 0.2 and 0.9 for positive and negative growth factor, respectively. Neutral growth is active, and the initial cell ages are set randomly so that growth will occur sometime within the 24 hour runtime.

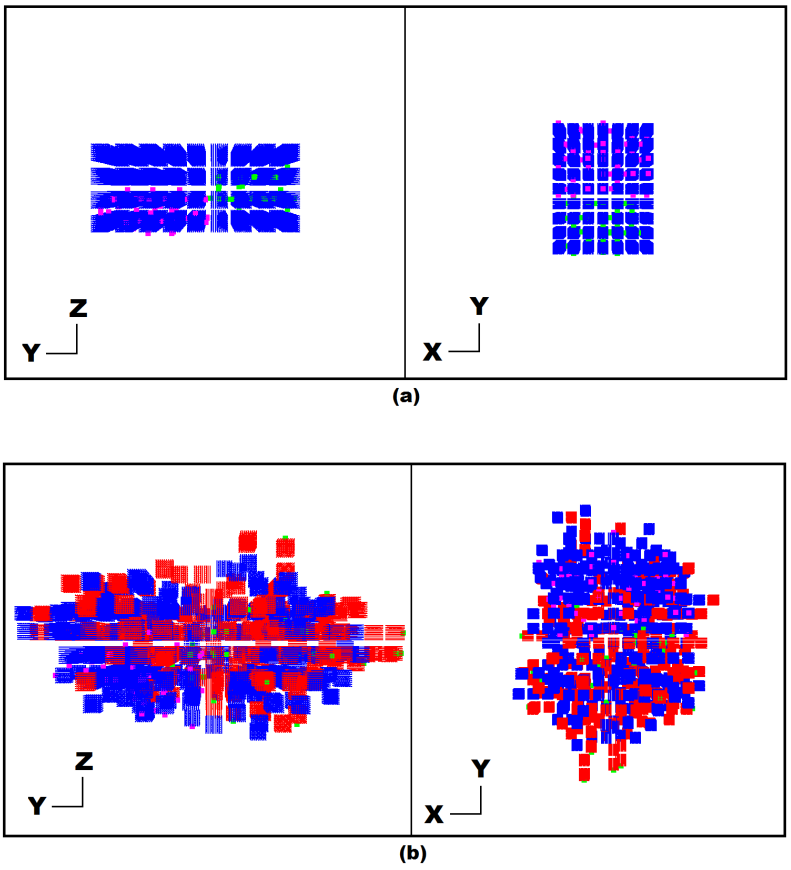

Figure 6.4: *Two views, left and right, with positive axes as labeled of a test for relative growth as directed by positive and negative fractones with neutral growth. (a) The initial cell mass, a rectangular prism of cells with dimensions* $7 \times 9 \times 4$ *cells. Positive fractones and negative fractones are randomly distributed in exclusive zones as shown. Fractones size is enlarged for visibility. (b) Examples of growth after 24 hours (200 time steps). In blue, non-proliferating cells; in red, proliferating cells; in green, positive fractones; in pink, negative fractones.*

Near the positive fractones, we expect lots of growth, while near the negative fractones we expect very little growth. In the area with no fractones, we expect moderate growth from the neutral growth of cells. Three test cases were generated with a different randomized fractone distribution, and the results after 24 hours (200 time steps) of growth are shown in Fig. 6.4(b-d). The growth pattern is as expected, however the random neutral growth somewhat masks the effects.

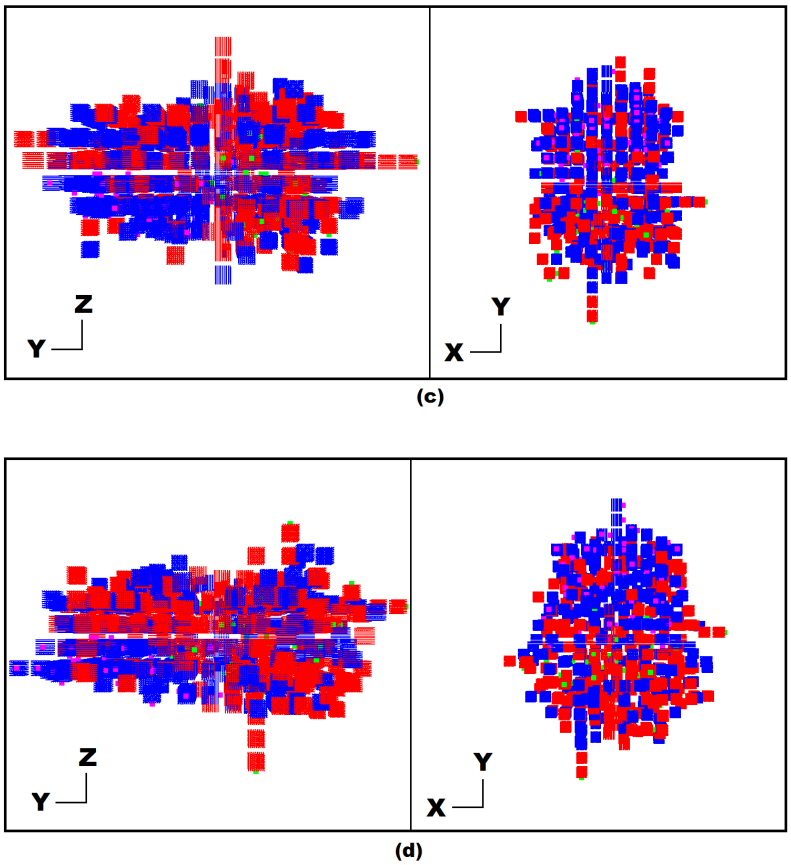

Figure 6.4: *Two views, left and right, with positive axes as labeled of a test for relative growth as directed by positive and negative fractones with neutral growth. (c-d) Examples of growth after 24 hours (200 time steps). In blue, non-proliferating cells; in red, proliferating cells; in green, positive fractones; in pink, negative fractones.*

The distances from the initial conditions are shown in Table 6.3. Again, with the random neutral growth and random fractone distributions, the distances are very similar across all three tests. Of note the negative fractone distances are small compared to the positive fractone distances. This should be expected since positive fractones move due to the growth they promote, while the negative fractones remain relatively stationary since their associated cells should not grow. They move, however, due to pushes caused by the growth of other cells.

To more clearly observe the effect, we can remove the random neutral growth from the model and rerun the simulation, see Fig. 6.5. Note here that without neutral growth, the negative fractones do not have any growth to block, so we remove them from the test. While this alters the

Test	D_H	D_F^+	D_F^-	D_a	D_B
b	72	72	36	1132.5	1312.5
c	72	73.239	49.497	1148	1342.7
d	72	72	30	1151.2	1325.2

Table 6.3: *Table of distances for the three tests of accelerated and blocked growth with neutral growth, positive and negative fractones. Tests (b), (c), (d) refer to the images in Fig. 6.4.*

Test	D_H	D_F^+	D_a	D_B
b	48	48.374	1124.5	1220.9
c	48	48	1135.5	1231.5
d	60	60.299	1139.7	1260

Table 6.4: *Table of distances for the three tests of accelerated growth with no neutral growth and only positive fractones. Tests (b), (c), (d) refer to the images in Fig. 6.5.*

diffusion mechanics (since the negative fractones are no longer present to absorb growth factors), this test is meant to examine the relative growth mechanics. All other parameters remain the same.

The results of three different randomized distributions of positive fractones are shown in Fig. 6.5(b-d). The results are as intended, with growth only in the area with positive fractones. Note that cell positions change even on the opposite end from the fractones due to the pushing algorithm, demonstrating that growth can affect all parts of the cell mass, even far from the growth. As in case 1, the existence of strands of cells in the growth is noticeable, especially in the right-side images in Fig. 6.5(b-d). This occurs frequently when fractones are left to grow near the exterior of a mass. Their rapid growth occurs because once fractones are near the exterior, close to meningeal cells, growth factor flows quickly to them. Thus once the rest period ends, accelerated growth is immediately triggered again, pushing the strand out further. This causes a rapid growth of cells along a single axis.

The distances from the initial conditions are shown in Table 6.4. The results are similar to previous tests, with no particular test growing much more than another. The third test (d) does have larger distances, and this can be observed in Fig. 6.5, where (d) has a longer strand of cells extending out in the negative y axis direction than the other test simulations.

To observe the effects of negative fractones, we can restore the random neutral growth, and rerun the simulation with only negative fractones. In Fig. 6.6, we use the same initial cell

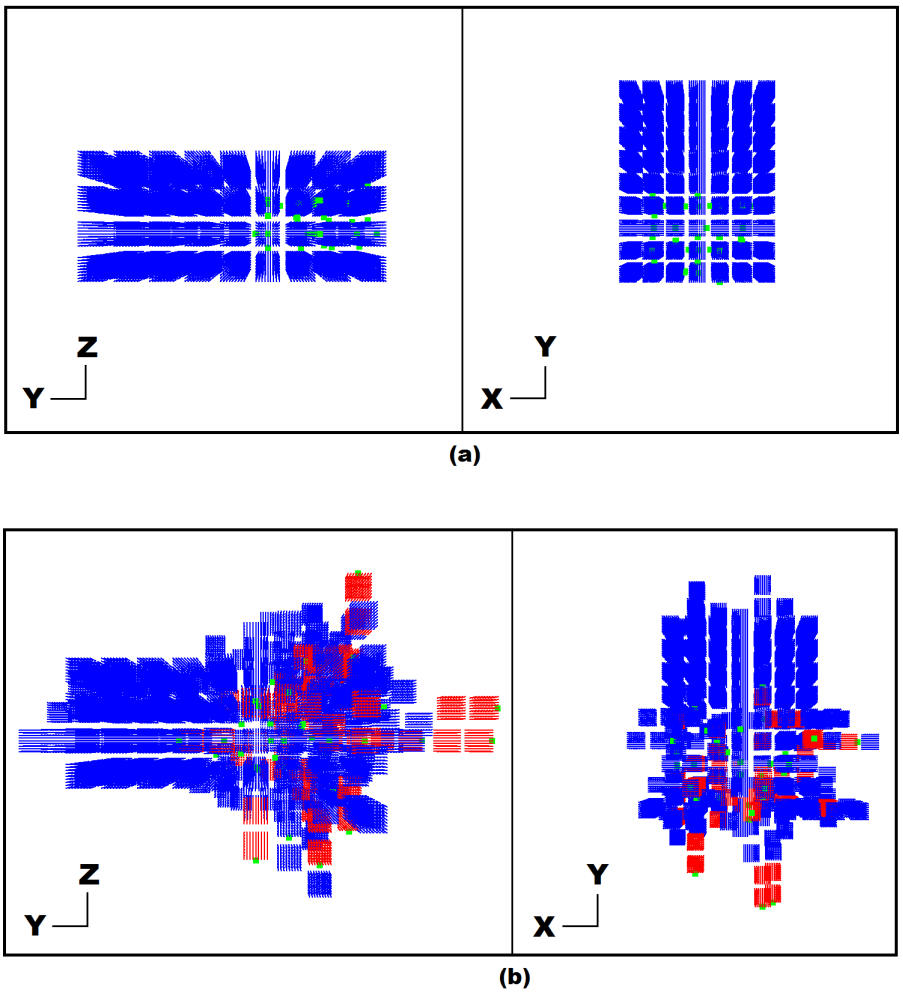

Figure 6.5: *Two views with positive axes as labeled of a test for relative growth as directed by positive fractones only, and no neutral growth. (a) The initial cell mass, a rectangular prism of cells with dimensions* $7 \times 9 \times 4$ *cells. Positive fractones are randomly distributed in an area as shown. Fractones size is enlarged for visibility. (b) Example of growth after 24 hours (200 time steps). In blue, non-proliferating cells; in red, proliferating cells; in green, fractones (enlarged for visibility).*

distribution, but now have no positive fractones and distribute negative fractones randomly to cells in the lower half (along the z-axis) of the prism. Each cell has a 75% chance of receiving a negative fractone on one of its faces.

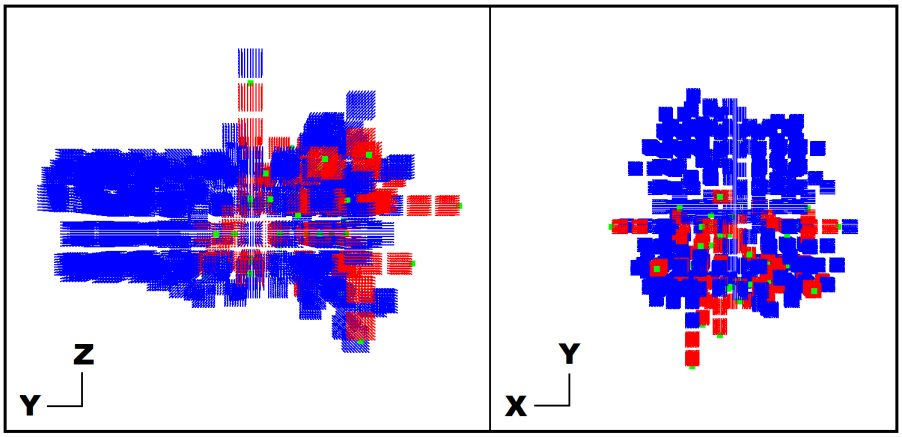

(c)

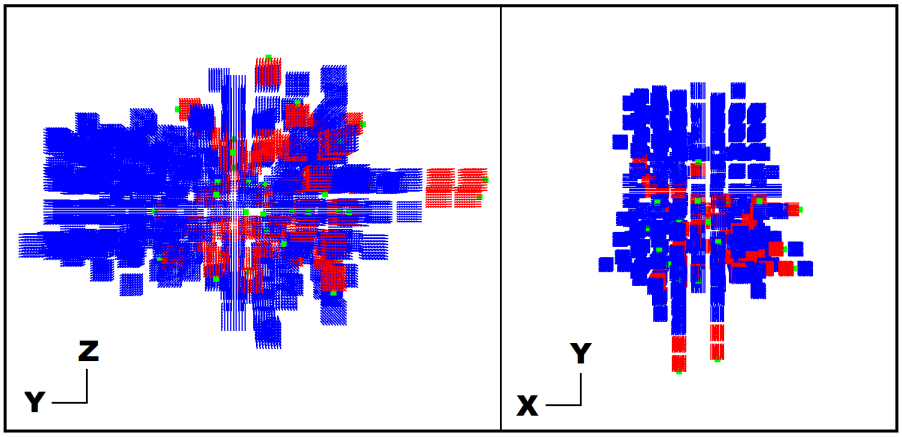

(d)

Figure 6.5: *Two views with positive axes as labeled of a test for relative growth as directed by positive fractones only, and no neutral growth. (c-d) Examples of growth after 24 hours (200 time steps). In blue, non-proliferating cells; in red, proliferating cells; in green, fractones (enlarged for visibility).*

The results after 24 hours (200 time steps) for three tests with different randomized distributions of negative fractones are shown in Fig. 6.6(b-d). Notice the predominance of growth on the upper half of the cell mass, while the negative fractones keep growth in the bottom half relatively low. Despite this, deformation occurs in all directions due to the pushing algorithm. Thus, again, growth in one area can case a change on the other side of the cell mass. This is an important observation when attempting to develop an algorithm to direct growth. One must be very precise about what growth occurs in order to prevent a chain reaction of pushes from deforming the cell

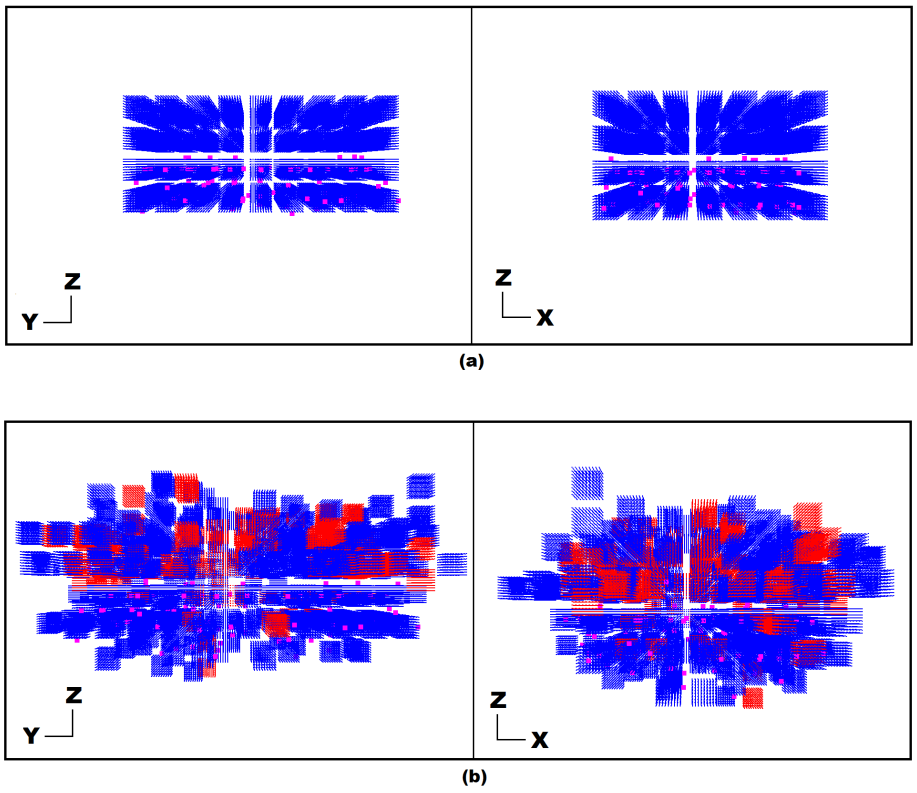

Figure 6.6: *Two views with positive axes as labeled of a test for relative growth as directed by negative fractones with neutral growth. (a) The initial cell mass, a rectangular prism of cells with dimensions* $7 \times 9 \times 4$ *cells. Negative fractones (pink) are randomly distributed in an area as shown. Fractones size is enlarged for visibility. (b) Examples of growth after 24 hours (200 time steps). In blue, non-proliferating cells; in red, proliferating cells; in pink, negative fractone (enlarged for visibility).*

mass too far. It also demonstrates why we will pursue the controllability question in the following section without the random growth since it is very difficult to account for the random pushes that may occur.

The distances from the initial conditions are shown in Table 6.5. Note that the negative fractone distances are relatively small compared to the distances in other tests we have run. As mentioned for the original tests in this case, negative fractones are expected not to move very much.

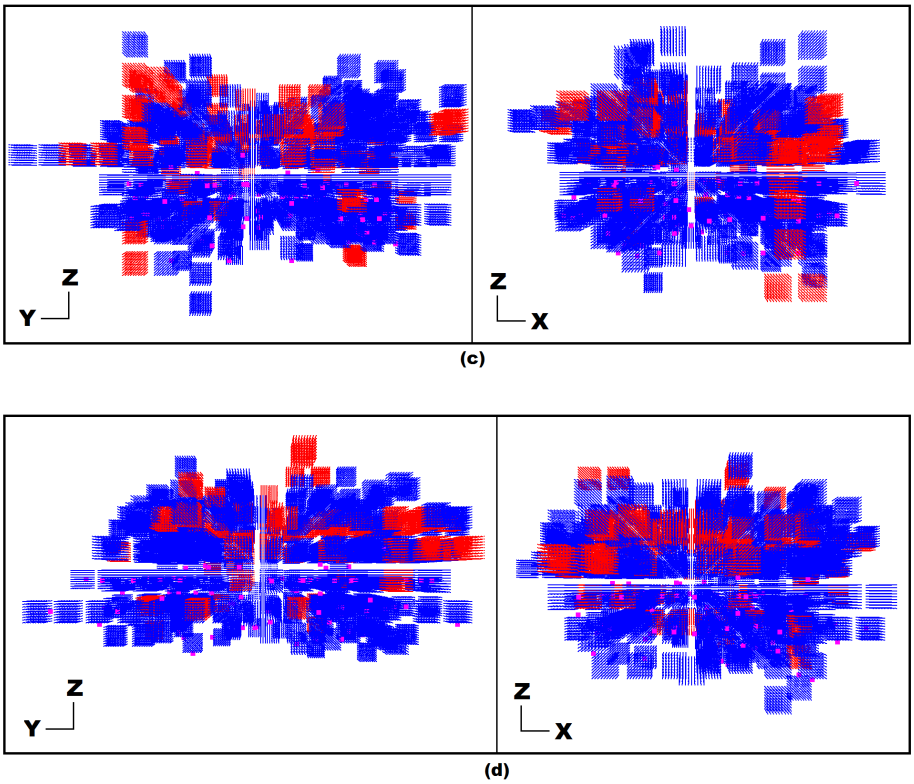

Figure 6.6: *Two views with positive axes as labeled of a test for relative growth as directed by negative fractones with neutral growth. (c-d) Examples of growth after 24 hours (200 time steps). In blue, non-proliferating cells; in red, proliferating cells; in pink, negative fractone (enlarged for visibility).*

Test	D_H	D_F^-	D_a	D_B
b	42	30	1140	1212
c	48	21.954	1149	1219
d	48	35.355	1130.7	1214.1

Table 6.5: *Table of distances for the three tests of accelerated growth with neutral growth and only negative fractones. Tests (b), (c), (d) refer to the images in Fig. 6.6.*

6.1.4 Case 4: Diffusion Rate

Since the capture of growth factor drives the accelerated growth of cells, it is important to examine the rate of growth factor capture. In most of our simulations, the diffusion constant is set at $\nu^+ = \nu^- = 0.12$. This is due to the way in which the numerical diffusion is implemented in the code. Each time step, the diffusion into unit i by neighbor unit j is given by $\nu^+ * (x_j - x_i)$, where x_i and x_j is amount of growth factor concentration units in unit i and j, respectively. Each unit has up to 6 neighboring units, so a diffusion constant much bigger than 0.14 would begin to cause unrealistic behavior in the diffusion. The actual diffusion rate of growth factor in the system is likely faster than modeled in the system, and alternative methods of implementing the diffusion are under evaluation.

Simple test cases were performed to examine the absorption of growth factor over time. In these simulations, all growth, both accelerated and neutral, was disabled, and only the diffusion and capture of growth factor occurred. Since the diffusion of the positive and negative growth factors occurs through the same mechanics, we look only at positive growth factor ans positive fractones, with diffusion constant 0.12 and absorption rate of 0.9. In each simulation, only one fractone was placed in the system at a time, so no other fractones interfere with the diffusion. The arrangement for each test and the amount of growth factor captured over time are shown in the figures.

When the number of meningeal cells is relatively small, and thus a relatively small amount of growth factor is produced in the system, diffusion occurs very slowly, as can be seen in Figure 6.7. Here there is no growth factor initially present in the system. A fractone 3 units from the single meningeal cell (Fig. 6.7(a)) captures a large amount of growth factor - about 2000 of the 3000 total growth factor concentration units introduced by the meninges over the 200 time steps. However, when the fractone is relocated to the opposite side of the cell (6.7(c)), it captures less than 3 growth factor units in the same time period. This again shows that a fractone sitting on the exterior of the cell mass, near the meninges, will trigger accelerated growth very quickly as it absorbs a large amount of growth factor, and the resulting series of growth will produce the strands of cells that we have previously seen. When the fractone is adjacent to one of the remaining four faces (6.7(b)), the amount of growth factor captured is slow, but still enough to trigger growth (assuming the threshold amount is 100 growth factor concentration units, as we typically use), at about 120 growth factor concentration units.

Tests with small groups of cells were also performed, see Figures 6.8 and 6.9. In these tests, a $2 \times 2 \times 2$ block and $3 \times 3 \times 3$ block of cells, respectively, were used and meninges placed

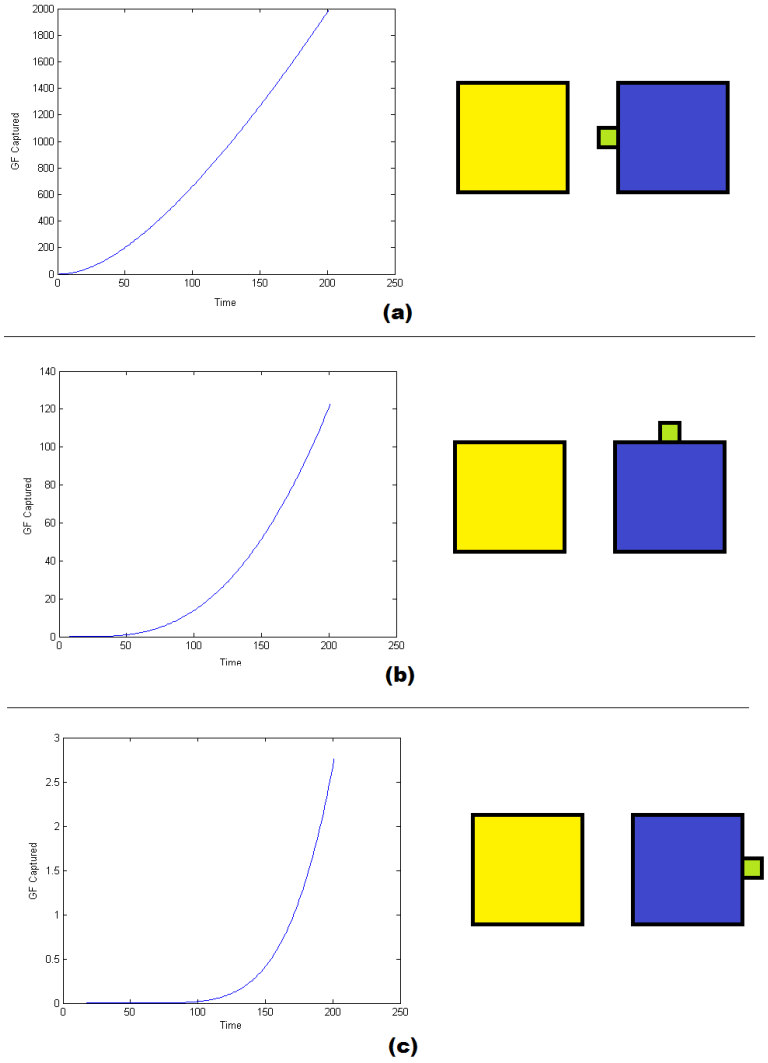

Figure 6.7: *Growth factor captured by a single fractone over time. The cell is centered at* $(12, 12, 12)$*, and the meningeal cell centered at* $(0, 12, 12)$*. (a) Fractone placed on side facing the meninges,* $(7, 12, 12)$*. (b) Fractone placed on lateral side,* $(12, 17, 12)$*. (c) Fractone placed on far side of the cell from the meninges,* $(17, 12, 12)$*.*

around the cubes. The figures show a cross-section of the set-ups. No growth factor was initially present in the diffusion space. Here again, it is clear that fractones close to the meninges absorb a great deal more than fractones placed anywhere else. In fact, from these small cell mass tests, it seems like accelerated growth should not trigger at all for fractones in the center of the mass

due to a very small amount of growth factor reaching inside. However, larger cell masses also have more meningeal cells producing growth factor, and so more growth factor reaches the interior. Furthermore, once growth is triggered (either neutral or accelerated), the deformation of the cell bodies can push cells with fractones closer to the meninges or into areas with higher concentrations of growth factor. The pushing action itself redistributes growth factor at the end of a push and this also concentrates growth factor (see Fig 5.8), making fractones at the end of the push even more likely to absorb enough growth factor to trigger mitosis again. This is another contributing factor to the strands that we have seen in previous test cases.

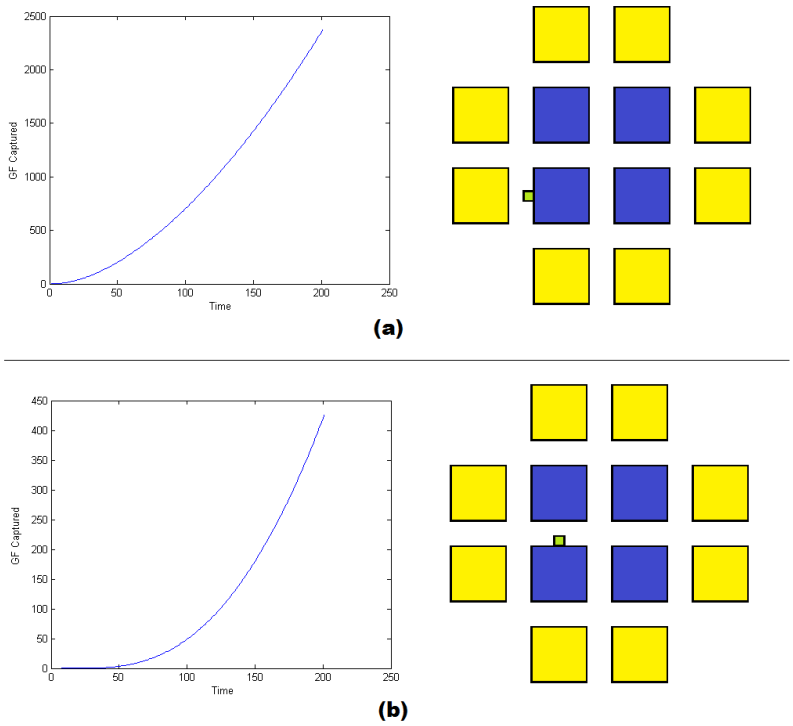

Figure 6.8: *Growth factor captured by a single fractone over time, and associated cross-section of fractone location. Cell configuration is a symmetric* $2 \times 2 \times 2$ *block surrounded by meningeal cells. (a) Fractone placed facing the meninges. (b) Fractone placed on lateral side.*

Although growth factor diffuses slowly in the system, as shown in Fig. 6.9, when the same configuration is used and a small amount of growth factor added initially (a uniform 5 growth factor concentration units in the diffusion space), the amount of growth factor absorbed is much higher (Fig. 6.10). This is explored in more detail in the next test case.

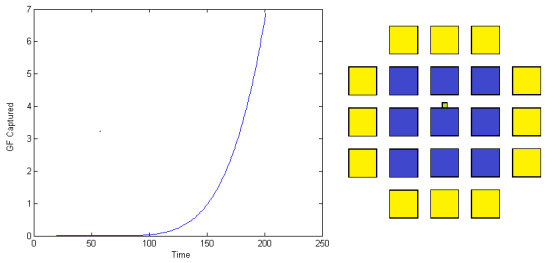

Figure 6.9: *Growth factor captured by a single fractone over time, and associated cross-section of fractone location. Cell configuration is a symmetric* $3 \times 3 \times 3$ *block surrounded by meningeal cells. Fractone is placed adjacent to the center cell.*

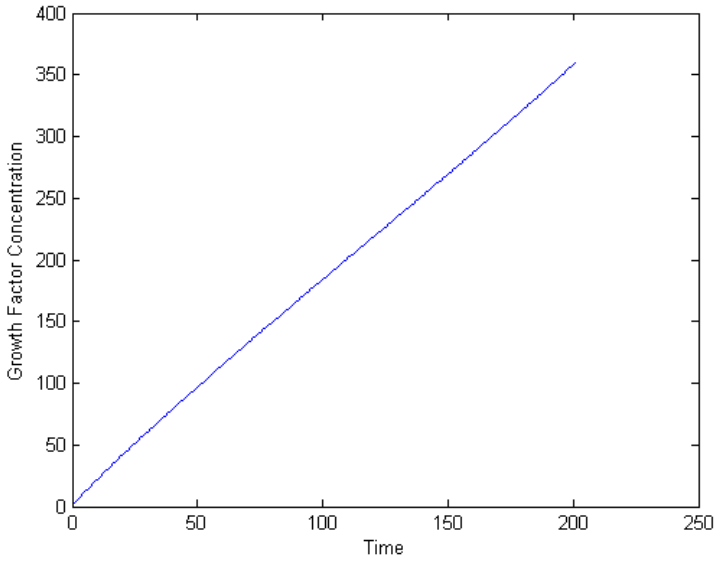

Figure 6.10: *Growth factor captured by a single fractone over time, with* 5 *growth factor concentration units uniformly distributed to each unit in the diffusion space. Cell and fractone set-up is the same as in Fig. 6.9.*

Finally, we examine the effect of fractones interfering with the growth factor diffusion. We set up two cells and one meningeal cell along the same axis, as in Fig. 6.11. In Fig. 6.11(a), a single positive fractone is set adjacent to the cell furthest from the meninges. In Fig. 6.11(b), two more fractones are added to the system adjacent to the cell closer to the meninges. The idea is to see if the two new fractones interfere with the amount of growth factor that reaches the original fractone. As the results show in the figure, the effect is almost negligible. The test is repeated in

Fig. 6.12 with an initial growth factor distribution of 5 growth factor concentration units in the diffusion space, and again the effect is almost negligible. Thus with the current parameter values, we do not have to worry too much about interference by other fractones in the absorption of growth factor. This also means that the exclusion of negative fractones when neutral growth is turned off will not greatly affect the system since the impact on the amount of growth factor they would absorb is negligible.

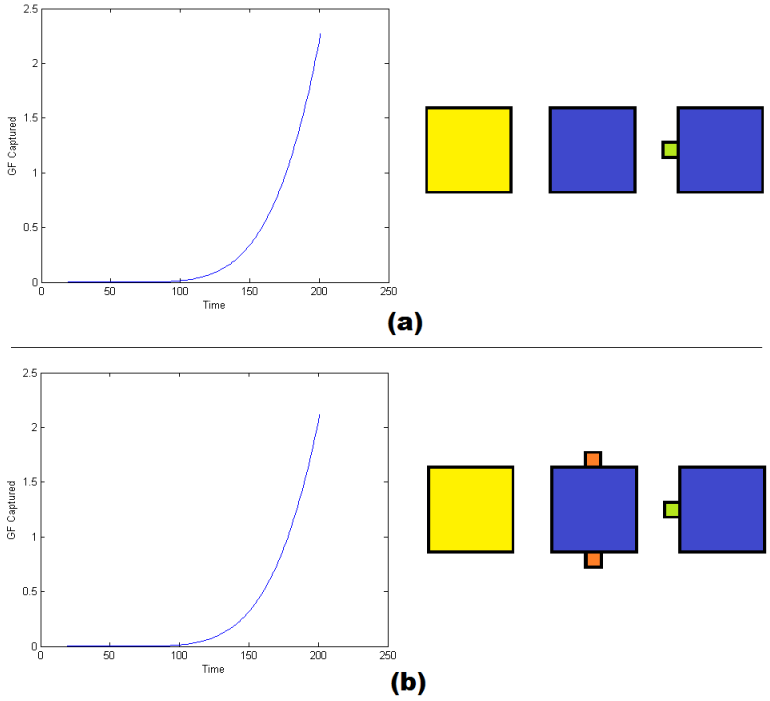

Figure 6.11: *Growth factor captured by a single fractone over time, and associated cross-section of fractone location. No growth factor was initially located in the system; all growth factor was produced by the meninges over time. Set-up is two cells (blue) and one meningial cell (yellow), as shown. (a) A single fractone (green) placed a shown. (b) Two additional fractones added (orange). Graphs show the cumulative growth factor captured by the fractone labeled in green.*

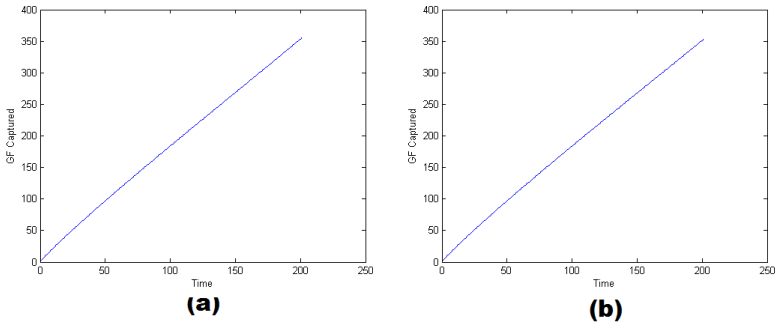

Figure 6.12: *Cumulative growth factor captured by a single fractone over time. Initially,* 5 *growth factor concentration units were uniformly distributed in each unit of the diffusion space. Set-up is two cells (blue) and one meningial cell (yellow), as shown in Fig. 6.11. (a) Graph of captured growth factor with only a single fractone present. (b) Graph of captured growth factor with two additional fractones interfering.*

6.1.5 Case 5: Initial Growth Factor Distribution

As shown in Case 4, the initial distribution of growth factor may play a large role in the timing of the growth in our model. We thus consider several test cases with different initial distribution of growth factor concentration in the diffusion space. In each case, the initial cell configuration and fractone distribution is kept constant (unlike previous cases where the fractone distribution was randomized). The initial cell configuration is a $5 \times 5 \times 5$ cube of cells, and 26 positive fractones are placed in the system. Of these 26 fractones, only 4 are placed on the exterior of cell configuration, adjacent to the cells in the middle of four of the faces of the cube. See Fig. 6.13(a) for the initial set-up. Neutral growth is turned off in order to better see the effect of the initial growth factor on positive fractones. Since there is no neutral growth, negative fractones are not used in these tests. The absorption constants of the positive fractones are set to 0.9 and 0.2 for the positive growth factor and negative growth factor, respectively. A uniform 15 growth factor concentration units are added to every unit adjacent to the meninges every 10 time steps.

Five different initial growth factor distributions were used and the system was run for 24 hours (200 time steps). The results are shown in the Fig. 6.13 and Fig. 6.13. With no growth factor initially added, Fig. 6.13(b), shows what would be expected by the diffusion rate experiments: the fractones on the exterior each trigger growth four times over the 24 hours, forming strands of cells extending from the main body. Meanwhile, fractones near the exterior trigger growth once or twice, and fractones on the interior do not trigger growth at all, as they do not absorb enough growth factor.

Turning up the initial growth factor distribution just a bit, with 5 growth factor concentration units uniformly distributed to every unit in the diffusion space for both positive and negative growth factors, we see a significant change to the 0 distribution (Fig. 6.13(c)). Now all fractones on the interior trigger growth, although each only once or twice. Adding more initially, with 10 positive and negative growth factor concentration units in each unit in the diffusion space (Fig. 6.13(d)), now interior cells trigger growth multiple times, causing significant changes and pushes, causing more strand-like structures compared to previous cases. An even more extreme distribution is shown in Fig. 6.13(e), with 50 positive and negative growth factor concentration units initially distributed. Even more growth occurs over the 24 hour period. This extreme level of growth factor distribution likely saturates the system and every fractone triggers growth four times. It is interesting to note the difference between the 10 and 50 initial growth factor cases. The former shows strands that do not appear in the latter, which has a single very long strand of cells. It is likely that the timing of the cell growths differed in the two cases, causing a different pattern of pushing. In the 50 initial growth

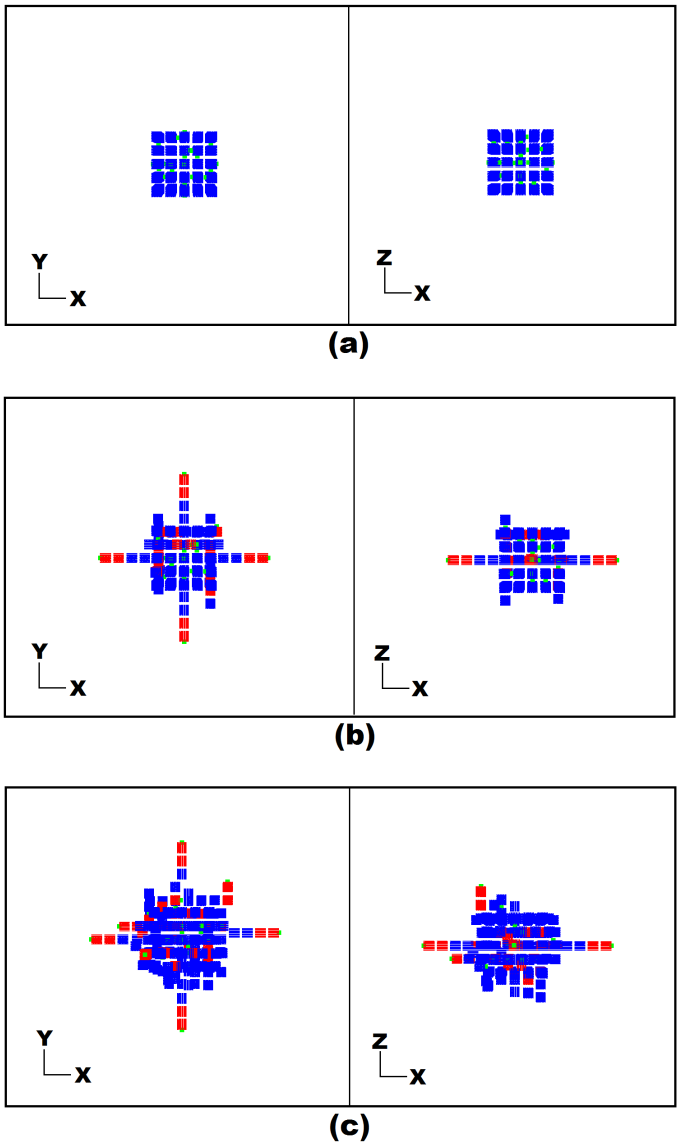

Figure 6.13: *(a) Initial set-up of the initial distribution test. A* $5 \times 5 \times 5$ *cube of cells with* 26 *fractones.* 4 *of those fractones are placed adjacent to cells in the center of the four faces perpendicular to the* x *and* y *axes; the fractones are placed such that they are* 3 *units from the meninges (not shown). (b-c) Configuration after* 24 *hours (200 time steps) for: (b)* 0 *positive and negative growth factor concentration units uniformly distributed in diffusion space; (c)* 5 *positive and negative growth factor concentration units uniformly distributed.*

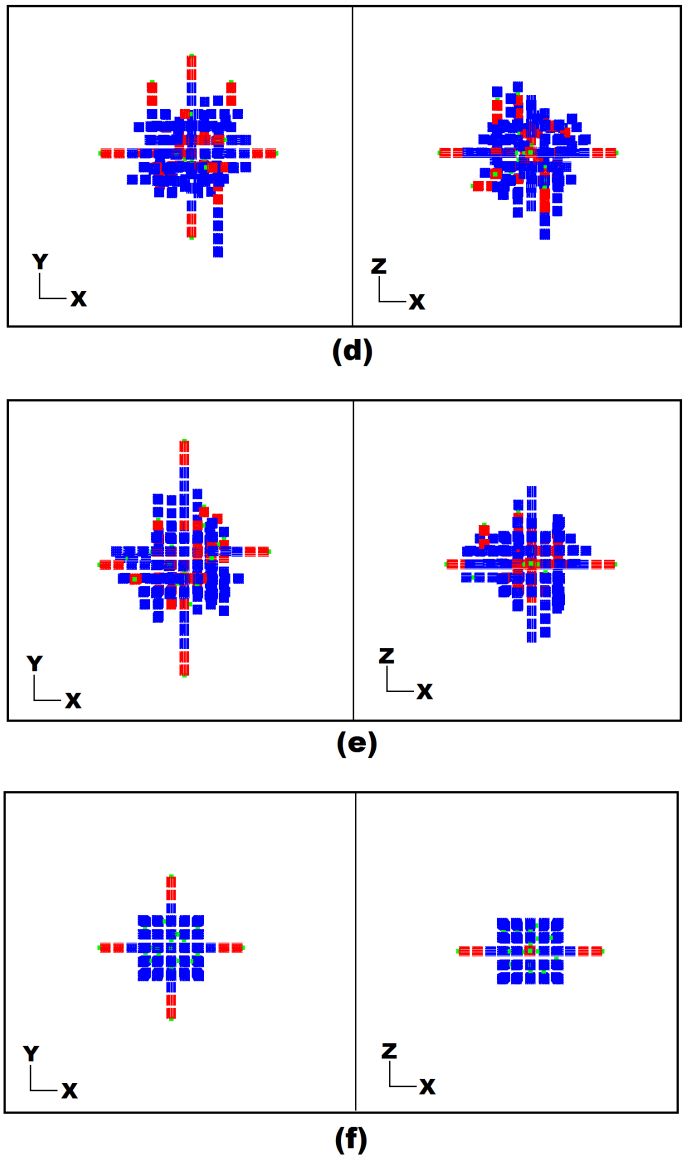

Figure 6.13: *Configuration after* 24 *hours (200 time steps) for: (d)* 10 *positive and negative growth factor concentration units uniformly distributed in diffusion space; (e)* 50 *positive and negative growth factor concentration units uniformly distributed; (f)* 10 *positive and* 50 *negative growth factor concentration units uniformly distributed.*

factor case, cell with fractones were pushed into alignment so that instead of creating two different short strand structures, a single long strand was created instead.

Test	D_H	D_F^+	D_a	D_B
0-0	48	48	1132.5	1228.5
5-5	60	60.299	1131	1251.3
10-10	66	60	1100.2	1226.2
50-50	84	84	1124.5	1292.5
10-50	36	36	981	1053

Table 6.6: *Table of distances for the initial growth factor distribution tests. Test numbers refers to the initial positive growth factor distribution and negative growth factor distribution, respectively. Corresponding images can be found in Fig. 6.13.*

Finally, Fig. 6.13(f) shows the case with 10 positive growth factor concentration units and 50 negative growth factor concentration units distributed uniformly through the diffusion space. Recall that the growth mechanic states that growth is triggered by a positive fractone when the difference between of positive growth factor captured (x^+) and negative growth captured (x^-) meets the threshold value: $x^+ - x^- \geq \tau_1 = 100$. As this test shows, when the negative growth factor is significantly more than the positive growth factor in the system, growth is stopped. Only the exterior fractones, which absorb a great deal of positive growth factor from the nearby meninges grow, and only 3 times (compared to the 4 in all other test cases.

The distances from the initial conditions are shown in Table 6.6. The distances reported relate well with our observation of the final configurations. The more initial positive growth factor in the system, the more growth occurs. And the case with 10 initial positive growth factor concentration and 50 negative growth factor concentration shows the relatively small amount of growth. The inhibited growth also means the age distance is relatively small compared to most other tests we have shown in this chapter.

6.1.6 Case 6: Growth Factor Production

We next tested the differences in growth that may occur by changing the growth factor production function, $g^+(t)$. It was theorized that altering the way in which growth factor was added might change the behavior of the growth. The actual rate at which growth factor is created by the meninges is not known. We therefore wish to test the difference between constant addition of growth factor and a sinusoidal pattern of production. The initial set-up was the same as used in Case 5, but with the absorption of the positive fractones set to 0.9 and 0.2 for positive and negative growth factor, respectively, and 0 initial growth factor concentration in the diffusion space. Neutral growth is again turned off.

The growth factor production functions used were chosen so that the total amount of growth factor added into the system after 24 hours would be the same. The functions tested (for both the positive and negative growth factor production) were:

$$g_1(t) = 15$$

$$g_2(t) = 15(\sin(\frac{\pi}{50}t) + 1)$$

$$g_3(t) = 15(\sin(\frac{\pi}{25}t) + 1)$$

$$g_4(t) = 15(\sin(\frac{\pi}{12.5}t) + 1)$$

$$g_5(t) = 7.5(\sin(\frac{\pi}{50}t) + 2)$$

$$g_6(t) = 7.5(\sin(\frac{\pi}{25}t) + 2)$$

$$g_7(t) = 7.5(\sin(\frac{\pi}{12.5}t) + 2)$$

These 7 functions feature constant production in g_1, sinusoidal production that oscillates between 0 and 30 with differing periods in g_2, g_3, g_4, and sinusoidal production that oscillates between 7.5 an 22.5 with differing periods in g_5, g_6, and g_7. Growth factor was added to each unit in the diffusion space adjacent to the meninges every 10 time steps. Testing with these 7 functions,

however, revealed no difference in the cell and fractone positions after 24 hours. The resulting cell configuration is shown in Fig. 6.14(a).

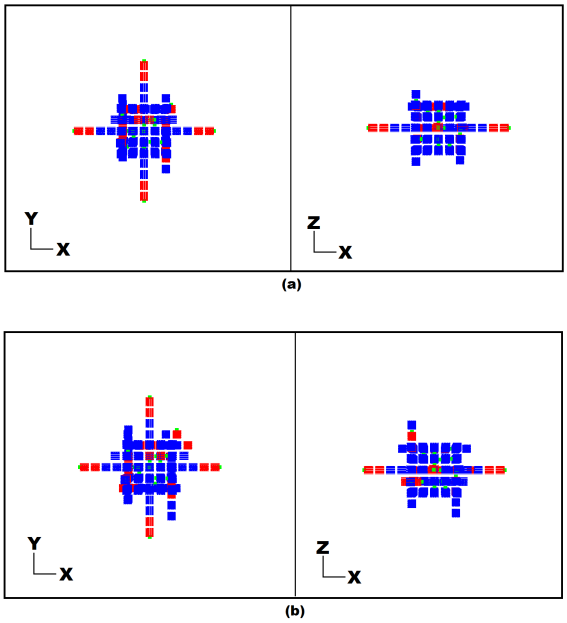

Figure 6.14: *Results of tests on growth factor production. (a) Cell and fractone distribution after* 24 *hours (200 time steps) for growth factor production functions* $g_1(t)$ *through* $g_7(t)$*. All gave the same final distribution. (b) Cell and fractone distribution after* 24 *hours for growth factor production function* $g_8(t)$*. In blue, non-proliferating cells; in red, proliferating cells; in green, positive fractone (enlarged for visibility).*

Although the final configurations were the same, cells grew at different times, depending on the growth factor production function. Table 6.7 shows the age distances between the final cell distributions of some of the tests. In particular, we look at tests where the positive and negative growth factor production functions were g_1 or g_2, the constant production and the slow large-amplitude production functions, respectively. These two are chosen since they are the most dissimilar of the 7 tested growth factor production functions. The age distances show that the greatest distances occur when the positive growth factor productions are different between the two simulations. The age distance are relatively close when the positive growth factor productions are the same. The greater variation being due to the positive growth factor production is unsurprising since only positive fractones are in the test systems and they are much more sensitive to positive

Test 1	Test 2	D_a
g_1-g_1	g_2-g_2	63
g_1-g_1	g_1-g_2	22.5
g_1-g_1	g_2-g_1	90
g_1-g_2	g_2-g_1	90
g_1-g_2	g_2-g_2	85.5
g_2-g_1	g_2-g_2	27

Table 6.7: *Table of age distances, D_a between final cell configurations. Columns Test 1 and Test 2 denote the particular simulations we are comparing. As an example, g_1-g_2 refers to the simulation with positive growth factor production given by $g_1(t)$ and negative growth factor production given by $g_2(t)$.*

growth factor due to a much larger absorption constant for positive growth factor (0.9) compared to negative growth factor (0.2).

In an effort to show that the growth factor production function can cause a change in the final cell configuration, an eighth growth factor production function was chosen, which adds significantly more growth factor to the system.

$$g_8(t) = 50$$

The results of using this function are shown in Fig. 6.14(b). With this production function, there is slightly more growth that occurs compared to the other functions.

6.1.7 Case 7: Growth Factor Absorption

The next test case looks at the absorption constant parameters. The set-up is the same as in Case 5 for the cell and fractone locations and the growth factor production. A uniform 10 positive and negative growth factor concentration units are distributed throughout the diffusion space. Again, we turn neutral growth off and do not include negative fractones.

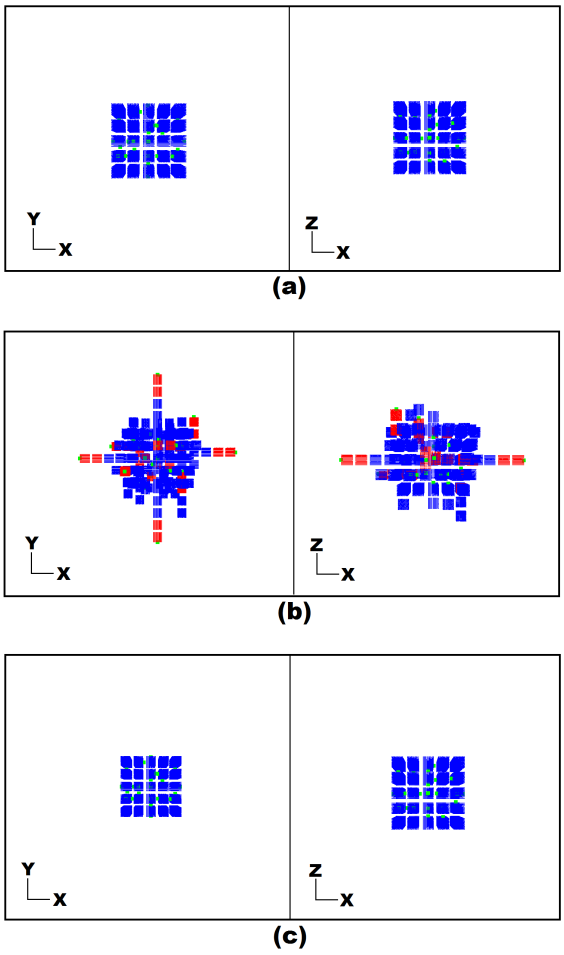

Figure 6.15: *Two views, left and right, with positive axes as labeled of a test for relative growth with varying absorption constants. (a) The initial cell mass, a* $5 \times 5 \times 5$ *cube of cells with* 26 *positive fractones. (b) Absorption constants* $\alpha_1^+ = 0.5$, $\alpha_1^- = 0.2$. *(c) Absorption constants* $\alpha_1^+ = 0.5$, $\alpha_1^- = 0.5$. *In blue, non-proliferating cells; in red, proliferating cells; in green, positive fractone (enlarged for visibility).*

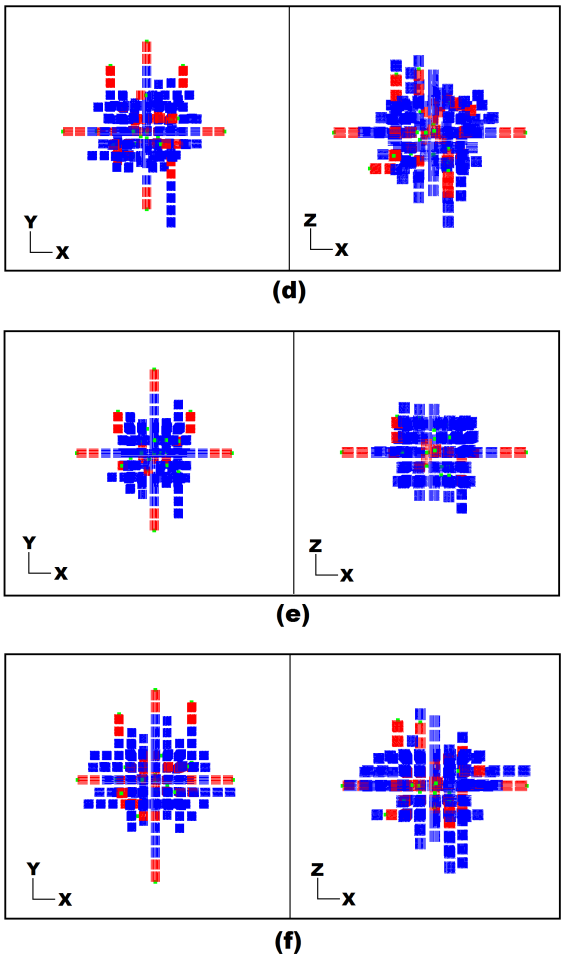

Figure 6.15: *Two views, left and right, with positive axes as labeled of a test for relative growth with varying absorption constants. (d) Absorption constants* $\alpha_1^+ = 0.9$, $\alpha_1^- = 0.2$. *(e) Absorption constants* $\alpha_1^+ = 0.9$, $\alpha_1^- = 0.5$. *(f) Absorption constants* $\alpha_1^+ = 1.0$, $\alpha_1^- = 0$. *In blue, non-proliferating cells; in red, proliferating cells; in green, positive fractone (enlarged for visibility).*

Figure 6.15(a) shows the initial set-up. Five different tests were performed altering the absorption constants for positive and negative growth factors, α_1^+ and α_1^-, respectively. Figure 6.15(b) sets $\alpha_1^+ = 0.5$ and $\alpha_1^- = 0.2$. Figure $\alpha_1^+ = 0.5$, $\alpha_1^- = 0.2$(c) sets $\alpha_1^+ = 0.5$ and $\alpha_1^- = 0.5$. As might be expected in this case, the amount of positive and negative growth factor absorbed is exactly the same, so the threshold value, τ_1 is never reached, so growth never occurs. The third test, Fig. 6.15(d), sets $\alpha_1^+ = 0.9$ and $\alpha_1^- = 0.2$, and we see significantly more growth compared to the first test due to more positive growth factor being absorbed. Comparatively, when more negative

Test	D_H	D_F^+	D_a	D_B
0.5-0.2	54	54	1134	1242
0.5-0.5	0	0	0	0
0.9-0.2	66	60	1100.2	1226.2
0.9-0.5	54	54	1125	1233
1.0-0.0	72	72	1126.5	1270.5

Table 6.8: *Table of distances for the absorption constant tests. Test numbers refers to the absorption constants α_1^+ and α_1^-, respectively. Corresponding images can be found in Fig. 6.15.*

growth factor is absorbed in the fourth test, Figure 6.15(e), with $\alpha_1^+ = 0.9$ and $\alpha_1^- = 0.5$, the amount of growth is reduced. The fifth test, Fig. 6.15(f), brings things to an extreme with $\alpha_1^+ = 1.0$ and $\alpha_1^- = 0$, and shows more growth than any other test.

The distances from the initial conditions are shown in Table 6.8. The results are as we observed, with greater α_1^+ corresponding to more growth and greater α_1^- corresponding to less growth.

6.1.8 Case 8: Relative Growth Rates of Meninges and Cells

Our final test gathers data on positive and negative growth factor production and the relative rate of cell and meningeal cell growth. The initial cell set up is the same octahedron as in Case 1. For each cell, there is probablity $1/3$ that a single positive fractone is placed next to the cell (with a random choice of side). There is also a $1/3$ chance for a negative fractone instead, and a $1/3$ chance for no fractone. The growth factor production, initial distribution, and absorption constants are as in Case 1. Neutral growth is active. The amount of uncaptured growth factor and the numbers of cells and meningeal cells over time are shown in Fig. 6.16.

Because meningeal cells are always arrayed around the exterior of the set of cells, the number of menigeal cells can decrease when the arrangement of the cells changes. In particular, this can occur when concave portions of the surface are filled in. The number of fractones in the system was too small to have a significant impact on the amount of uncaptured growth factor, and as the number of meningeal cells increased, the amount of growth factor added every 10 time steps also increased. This caused the almost quadratic trend in the growth factor graphs. Also noticeable in Fig. 6.16(c) are the sudden jumps in cell numbers around $t = 25, 75, 125, 175$. These are caused by the positive fractones, which have a 6 hour (50 time step) period between accelerated growth.

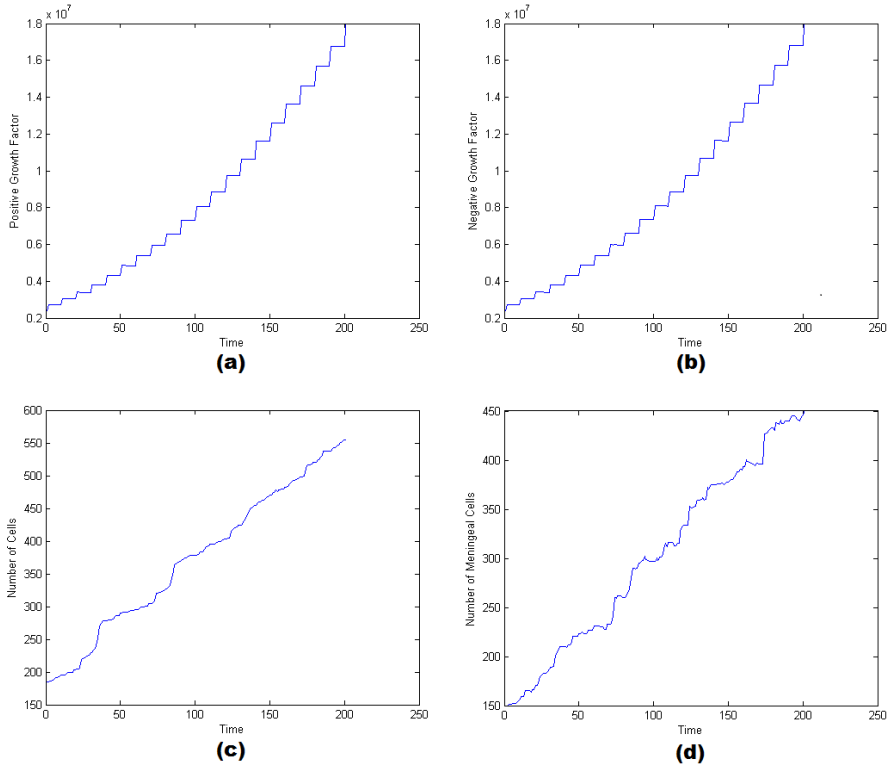

Figure 6.16: *Graphs over time of of (a) Positive Growth Factor (uncaptured). (b) Negative Growth Factor (uncaptured). (c) Number of cells in the system. (d) Number of meningeal cells in the system.*

6.2 Image Processing and System Initialization of Biological Data

When biological maps are made available, we wish to be able to convert them to states in our discretized system in order to initialize the model. To do this, a program was written by University of Hawai'i undergraduate student Zachary Deweese which analyzes an image file and identifies clusters of replicating cells, fractones, and empty holes. To create his program, Mr. Deweese used MATLAB and the available functions in the Mathworks Archive. The program takes a two-dimensional image and generates a two-dimensional discretized map of cell and fractone locations by going through the colored biological image and locating areas of sufficient size and brightness as fractones and replicating cells, and placing them in a three-dimensional matrix array that represents our discretized cell space. Fractones located within 17 units of a replicating cell center were labeled as positive fractones, and all others as negative fractones. This is based off of the assumptions that positive fractones cause growth, so positive fractones should have proliferating cells nearby. Other fractones without replicating cells nearby are possibly inhibiting growth, and so are chosen as negative fractones. The 17 unit radius we choose is arbitrary - just short of one and a half cell lengths - and something we may alter based on future experimentation.

Once proliferating cells and fractones are placed in the array, the remaining space in the array is filled with non-proliferating cells that align to the $6 \times 6 \times 6$ grid that we use. A second pass of the array is then made by the program that aligns the proliferating cells to the grid, and ensures the fractones are adjacent to the middle of one of the cube faces of a cell. It also ensures that no cell has both positive and negative fractones associated to it. This rearrangement of the proliferating cells to the grid causes pushing of the non-proliferating cells.

The sort of biological data we hope to receive is a series of images taken of one location in a developing rat embryo. Each two-dimensional image depicts a very thin layer of the location under study; essentially the $x - y$ plane for some z coordinate. This can be done with the Zeiss Pascall confocal laser scanning microscope (CLSM) at the John A. Burns School of Medicine, which is able to record the image of a very thin slice of a sample at a variable depth set by the user. Each of these two-dimensional images can be run through our conversion program to create a map for our model. Then these maps can be "stacked" together and a three-dimensional map for our model generated.

Fig. 6.17 shows an example of the mapping program, with an experimentally-obtained map and the discretized 2D map created by the mapping program. The original map used is not ideal, as it captures too thick of a slice of the tissue. Overlapping of cells is visible and causes

overlapping of cells in the computer model that is fixed by the program. The uneven border of the cell mass is due to the pushing algorithm that creates room for the overlapping proliferating cells to align to our $6 \times 6 \times 6$ grid. Note that this is not an ideal solution as it possibly inaccurately squishes cells into the same two-dimensional plane while in a more realistic three-dimensional map they might be quite separate. An ideal map, and what we aim to achieve from the CLSM, is a slice approximately 1 μm thick. This would eliminate most overlap issues since, recall, a fractone is between 1 and 4 μm in length, and a cell is much larger than that at about 10 μm in diameter. The image in Fig. 6.17 shows a slice of tissue well over 10 μm in thickness.

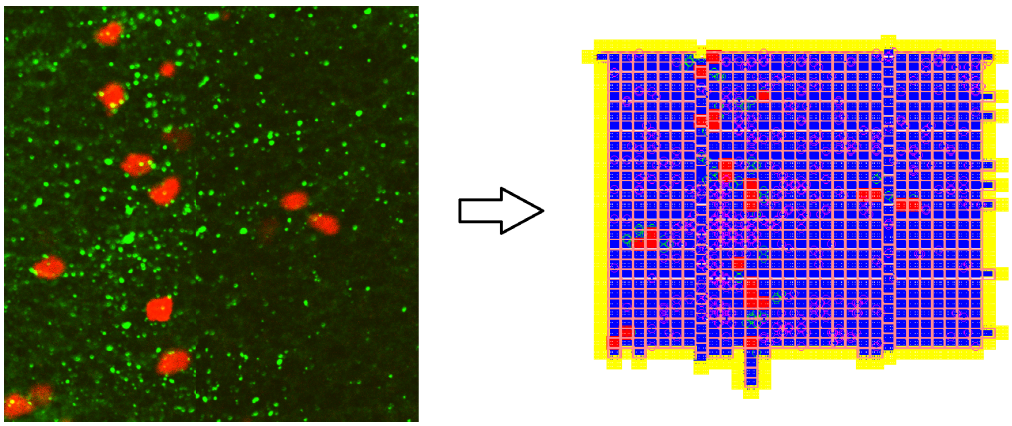

Figure 6.17: *Left: A portion of a rat brain. In red are proliferating cells. The bright green puncta represent fractone locations. Right: The resulting discretized map used to initialize the model. Red squares, proliferating cells; blue squares, non-proliferating cells; yellow squares, meninges; green circles, positive fractones; pink circles, negative fractones.*

Also, we note another simplification for these biological data tests. The meninges has merely been added around the exterior of the cells, and are not in biologically accurate positions. In the future, this is something that will be more carefully placed according to the biology. Their addition around the entire cell configuration for now, however, allows us to preview an evolution of the system, as shown in Fig. 6.18.

A second example of the mapping program on a different biological image can be seen in Fig. 6.19.

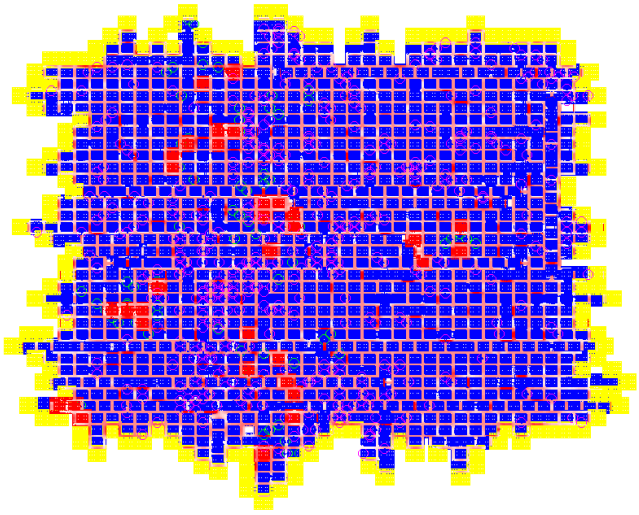

Figure 6.18: *The evolution of the system initialized in Fig. 6.17 after* 6 *hours (*50 *time steps). Red squares, proliferating cells; blue squares, non-proliferating cells; yellow squares, meninges; green circles, positive fractones; pink circles, negative fractones.*

6.3 Controllability

We restate the controllability question posed earlier: Given an admissible initial set of cell bodies, E_0; a target admissible set of cell bodies, E_f, with $E_0 \subset E_f$; an initial growth factor distribution, $x_0 \in \mathbf{X}$; and ignoring random neutral growth, can we find a control $u(x,t)$ and initial $q_0 \in \mathbf{Q}$, where q_0 has the set of cell bodies E_0, such that for the resulting hybrid control system H, $\exists(q_f, X_f) \in End_H$, where q_f has the set of cell bodies, E, and $D_H(E, E_f) \leq 12$?

As we will ignore the random neutral growth when considering the controllability question, the growth in the model is deterministic and the evolution of the biological structure is controlled by the fractone locations given by $u(x,t)$. The answer to the controllability problem as stated is clearly "No". Since growth can only occur once every 6 hours, we can, at best, only quadruple the number of cells in the system in one day. Thus a target configuration could be too large to get to in 24 hours. However, if we replace End_H with $Reach_H$ in the problem statement, then it is always possible to find a solution.

The existence of a solution to this problem is readily apparent for most simple cases. Since the initial structure is a subset of the final structure, we can approach the problem with the following algorithm:

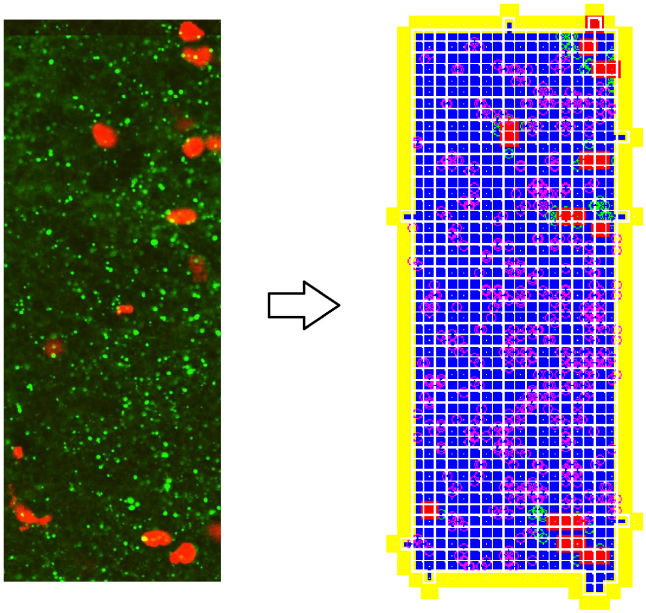

Figure 6.19: *Left: A portion of a rat brain. In red are proliferating cells. The bright green puncta represent fractone locations. Right: The resulting discretized map used to initialize the model. Red squares, proliferating cells; blue squares, non-proliferating cells; yellow squares, meninges; green circles, positive fractones; pink circles, negative fractones.*

1) We start by defining a new target structure. We adjust the cells in the final mass that are not part of the initial mass so that they are aligned with a neighboring cell. This means that the cell centers align to a $12 \times 12 \times 12$ grid. Because one adjustment may cause a cascade of such adjustments, we start adjusting those cells that are neighboring the initial cell mass. An adjustment may cause an overlap, which is handled by moving the overlapped cell so that it is in-line with a neighboring cell. This may cause further overlaps which are handled in the same way.

2) Next, we choose a cell neighboring the initial mass as the one we wish to grow, and place a fractone on the exterior of initial cell mass such that the triggered growth will occur in that direction, producing a cell in the location we chose.

3) After growth has occurred, remove the fractone and repeat the previous step: choose a neighboring cell to grow and place a fractone in the appropriate place. Repeat until the final target is reached.

For more complicated E_f, the first step in the above procedure may fail. It may not always be possible to slide cells into alignment such that they are always within a Hausdorff distance of 12. For example, in Fig. 6.20(a), the cells cannot simply be moved within 12 units of their initial positions so that a path of growth is obvious. However, by placing new cells (Fig. 6.20(b)), we can find a solution within 12 units. This gives rise to a more general procedure for the first step:

> 1*) Starting with E_0, begin "tiling" the space by placing cells aligned with each other in the three-dimensional space. Depending on E_0, small gaps may have to exist in the tiling. Keep tiling until every cell in E_f intersects a cell in the new space, and every tiling cell that could be placed within 12 units of E_f has been placed.

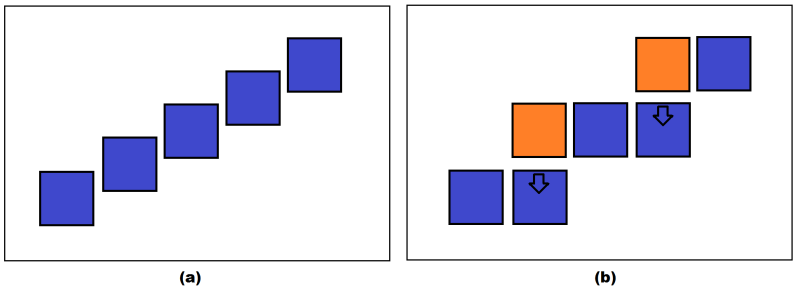

Figure 6.20: *(a) A two-dimensional configuration of cells that cannot simply be translated to form a new target cell configuration within our allowed* 12 *unit bound. (b) A new target cell configuration within our bound formed by translating cells (indicated by arrows) and creating new cells (in orange).*

This new space now has several important features. First, every cell is in-line with a neighbor. Second, no cell in this space is greater than 12 units from a cell in E_f, and every cell in E_f intersects a cell in the new space so the Hausdorff distance must be less than 12 between these two sets. Three, the space is admissible - separation between cells in the space could only occur if there was separation in E_f, but E_f is admissible. And four, this set can always be grown simply using the above single-fractone algorithm since every the tiling was created progressively with in-line cells from the initial E_0. Therefore, this new space suffices for our new target and the algorithm can proceed. See Fig. 6.21 for an example of this first step. We note that the different tilings can produce several different target spaces, all within Hausdorff distance 12. Thus solutions to the controllability problem exist, and they are not necessarily unique.

Proposition 6.3.1 *Given an admissible initial set of cell bodies, E_0; a target admissible set of cell bodies, E_f, with $E_0 \subset E_f$; an initial growth factor distribution, $x_0 \in \boldsymbol{X}$; and ignoring random neutral growth, there exists a control $u(x,t)$ and initial $q_0 \in \boldsymbol{Q}$, where q_0 has the set of cell bodies E_0, such that for the resulting hybrid control system H, $\exists(q_f, X_f) \in Reach_H$, where q_f has the set of cell bodies, E, and $D_H(E, E_f) \leq 12$.*

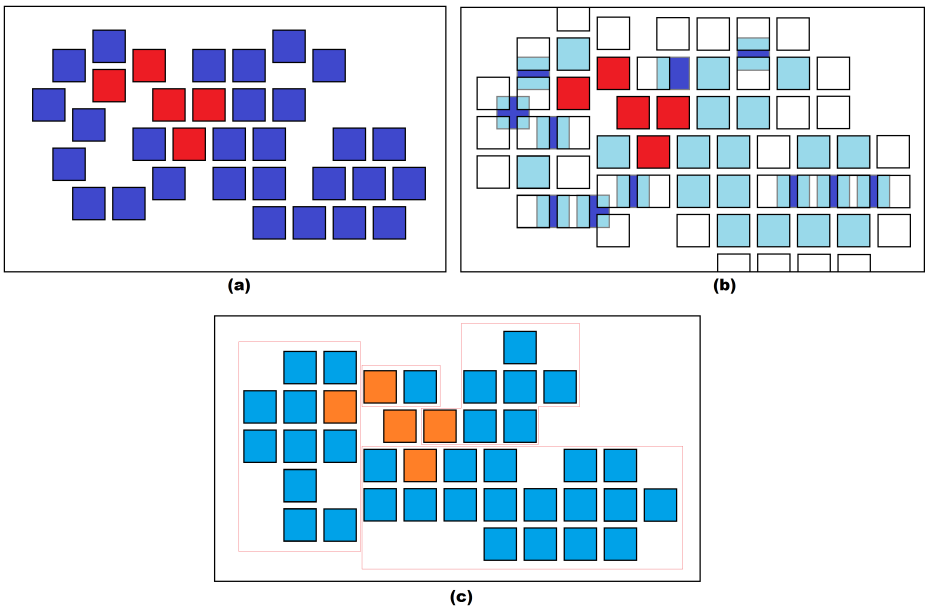

Figure 6.21: *An example of the tiling procedure in two dimensions. (a) An initial cell configuration (red) and a final target cell configuration (blue). (b) A tiling overlaid over the final cell configurations. The initial cell configuration is preserved. Each new cell is placed aligned with a neighboring cell - that is, the neighboring cell centers align to the 12×12 grid. (c) The new target space. Note that some of the cells were removed from (b) as they were unnecessary to complete the growth. Red boxes demonstrate regions that are aligned to the 12×12 grid and can therefore be grown with controlled placement of a single fractone.*

Growth in this fashion will never be blocked and never cause pushing because of our choice of fractone position and our modification of the target structure. This algorithm provides a solution that is very slow, as it only allows one fractone at a time, and we must wait for growth to occur (see Fig 6.22). However, since the fractone is always placed facing the exterior of the cell mass, it is also very close to the meninges, so growth factor reaches it very quickly to trigger the accelerated growth.

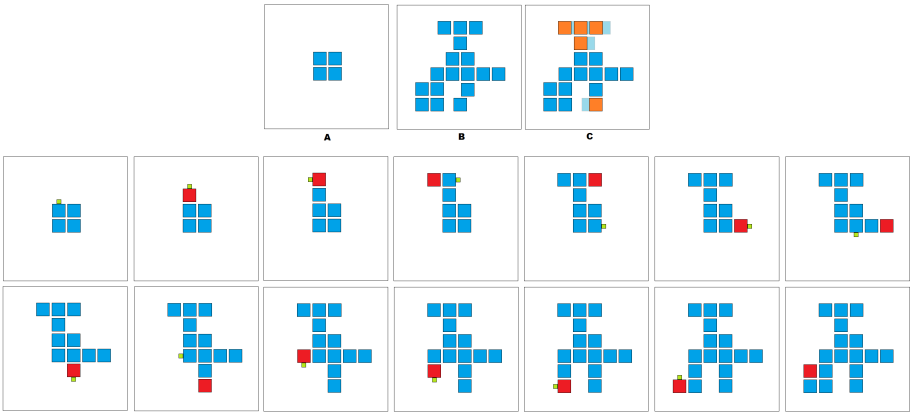

Figure 6.22: *A: An initial cell mass in two dimension. B: A final cell mass. C: The adjusted final cell mass. Bottom: solution using one fractone.*

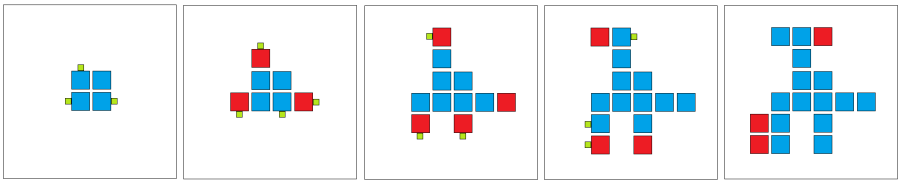

Figure 6.23: *Alternative faster solution using multiple fractones.*

It is easy to see that for some given initial and final structures, it is possible to increase the speed of reaching the target structure by allowing more than one fractone at a time - one just requires that the subsequent growths will not potentially overlap and thus cause pushing in the structure (see figure 6.23). It is also fairly simple to see that instead of avoiding pushing of the cells altogether, in some cases it may be more accurate or faster to take advantage of the pushing algorithm. However, it is difficult in a general sense to create an algorithm that will intelligently predict when to take advantage of pushing.

6.3.1 A Controlled Example

Although algorithmically it is difficult to determine an efficient solution for controlled growth, an intelligent user can create one with a little bit of work. We offer an example of a initial set of cells, E_0, and final set of cells, E_f, and a control that guides us from one to the other. This control solution is not unique, but we do have some goals in creating it. First, of course, we want accuracy, so we will ensure that our final set of cells is within a Hausdorff distance 12. Second, we

want to be biologically-feasible. This means we will not constantly create and destroy fractones; we will try to maintain the same fractones in the system for as long as possible. Our target and initial cell configurations are shown in Fig. 6.24.

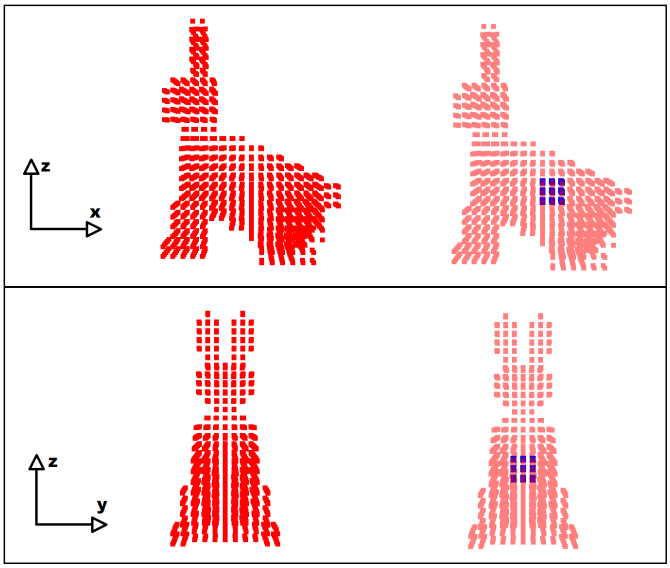

Figure 6.24: *Left: Final target cell configuration. Right: Transparency of target cell configuration showing relative location of initial cell configuration in blue. Positive axes are as shown.*

We generate the approximation to the final state with a control, $u(x,t)$. At the start of the simulation, $u(x,0)$ describes the initial fractone positions, and the simulation runs, following the normal algorithms of diffusion and growth. Only at specific times (shown in Fig. 6.25) do we set $u(x,t)$ to not follow the usual growth and displacement algorithm for relocating fractones and instead create and remove fractones in specific locations to generate the approximation to the final state.

To create the control that generated this final target configuration of a rabbit, fractone positions were set by the author and growth allowed to proceed until the growing cell configuration exceeded the target cell configuration's dimensions. The state of the system was saved at every 5 time steps, allowing the author to then look through the evolution of the growth and choose a point in time to alter the fractone distribution (these are the exact times shown in Fig. 6.25) in order to avoid exceeding the target cell configuration's bounds, and produce a reasonable approximation of the rabbit. Note that early on, a large amount of time (200 time steps) passes before fractones are

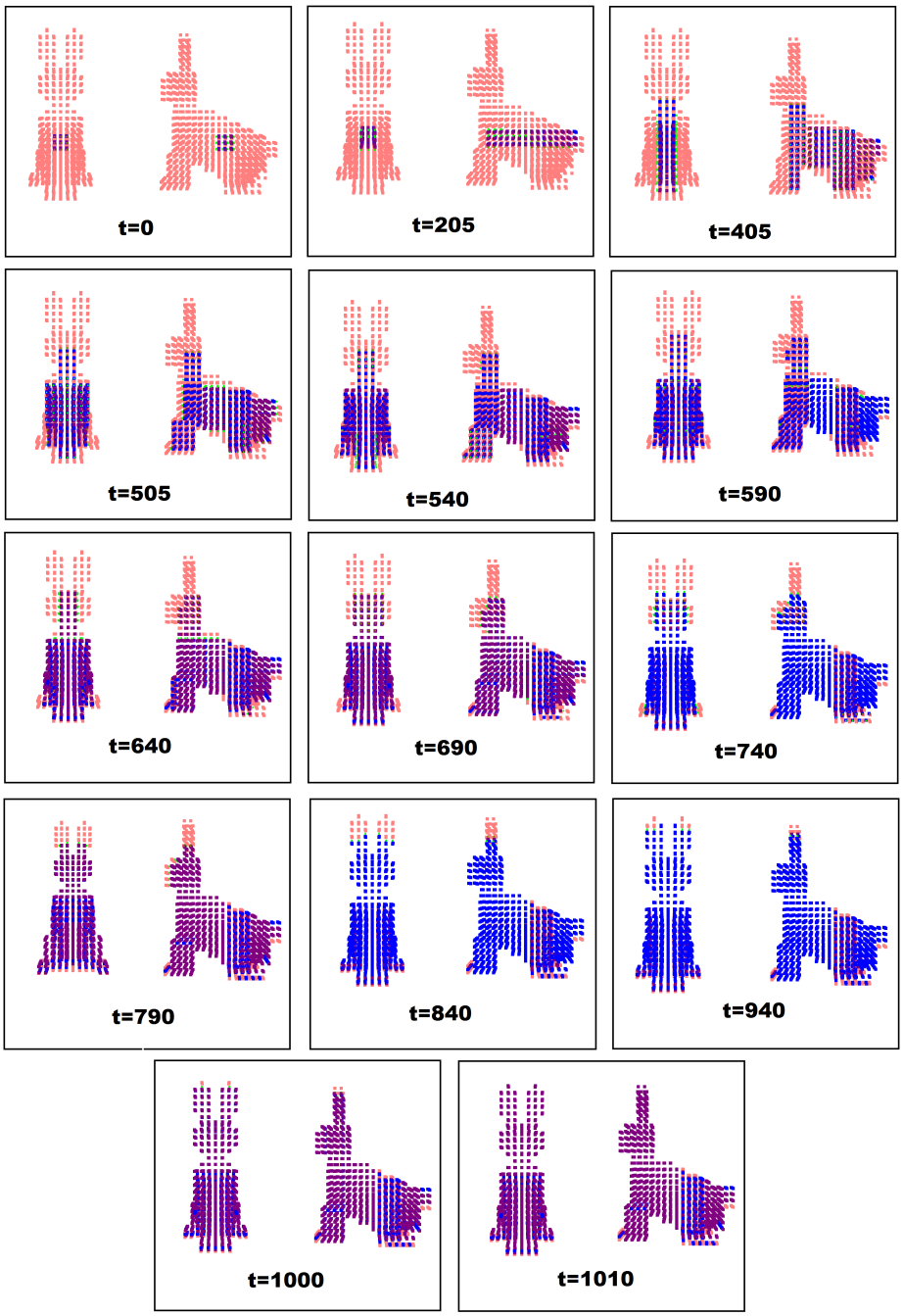

Figure 6.25: *Progression of growth of cells (blue) compared to target space (red) over time. Images shown correspond to times at which the control exerted a change on the position of fractones.*

altered, but as more detailed growth is required, the time between changes shrinks to about 50 time steps. The final cell configuration and the target cell configuration have a Hausdorff distance of 12.

The control shown is not optimal in the sense of time. Since the author set the fractone locations, the control was not guided by any algorithm beyond what he judged to look proper. This control is not unique, either. Different controls could have produced the same final target configuration (although the timing of the growths may have been different). Fractone positions could have been changed at every single time step to produce a final configuration that was exactly the same as the target, however this would be contrary to our hope to find a control that only exerted itself a small amount.

6.3.2 A Discussion on Time Optimization

The observations from the beginning of this chapter lead to a more interesting question: Since we know solutions exist, and these solutions need not be unique, is there a "best" solution for a given initial and final structure? "Best" in this sense may be defined in several ways. We could seek the solution which concludes in the smallest time, t, or we could seek the solution which minimizes the number of fractones we create and destroy. The latter case is more in line with a minimal cost solution, since the developing organism would expend energy to create or destroy a fractone. We focus on the time optimization problem in this section.

In developing a general algorithm to get from an initial cell configuration to a final target cell configuration efficiently, it is important to discuss holes in the cell mass. For discussion purposes, the holes may be thought of in a very natural way; they are gaps between cells large enough that growth factor can diffuse freely without interaction with fractones or cell walls. In terms of the model, in our definition of the diffusion space, we defined C_H: the union of the connected components in $A \setminus \hat{C}$ that are separated from the boundary of A. Then C_H represents the holes in our biological structure. We will denote the individual components of C_H by $C_{h1}, C_{h2}, \ldots$. The pushing algorithm, specifically pushes into off-set cells (see Figures 5.5 and 5.6, can cause holes to appear in the cell mass. While in practice, these holes tend to be small (not much larger than one cell in size), it is possible to make them quite large by precise control of where growth is allowed to occur. For an example of this, see Fig. 6.26.

In our model, the only way to open holes is by taking advantage of the pushing mechanism, however other biology-related processes also exist. In particular, cell motility and cell death can contribute to the generation of holes in a tissue. In fact, similar to the interaction of the cells

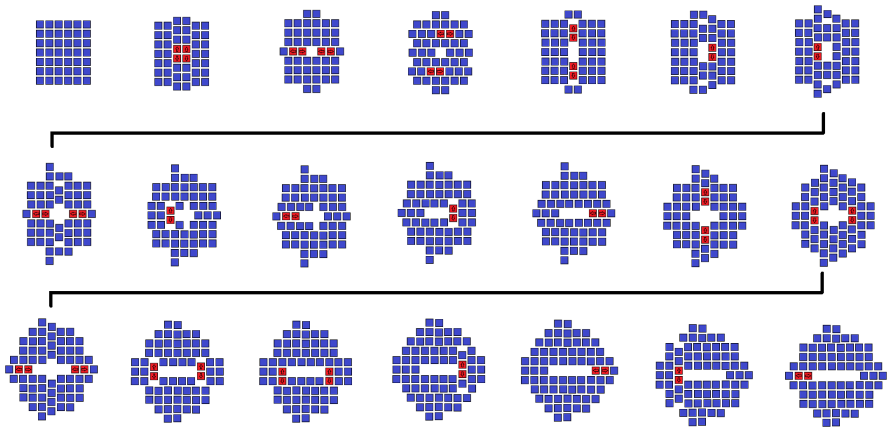

Figure 6.26: *A two-dimensional example of hole formation. A sequence of growths that use the growth and displacement algorithm to generate an increasingly large hole. Cells in red represent the cells undergoing mitosis that cause the pushing. The hole could be made larger with further careful selection of growths. Three-dimensional sets of cells can use similar techniques to generate three-dimensional holes.*

with growth factors, motility and cell death may be triggered by exposure to chemical signal as well. These mechanism are not in the current iteration of the model, however.

Intentionally creating large holes in the cell mass can be time-consuming. There is also a significant amount of pushing involved. Both of these reasons suggest that if the final target cellspace has holes in it, then in most cases it is faster to generate growth around the hole than to fill the hole and try to recreate it later. Since the initial cell configuration is a subset of the final, we will also never start with any of the final target configuration's holes filled in.

We can now proceed with a plan to generate a solution to the question posed. We approach first the time-optimal problem: how do we get to an approximation of the final cell mass in the fastest time possible? One key point to consider is the six hour period that new daughter cells are unable to undergo mitosis. Thus it will be faster to allow every cell in the initial cell mass to grow instead of choosing only a few - this allows us to quickly create the cell numbers needed. The caveat is that we do not want to exceed the boundaries of the final cell mass by more than one cell length. As we have seen, growth on the interior of the mass can cause pushing that affects every part of the mass, thus as the developing biological structure comes close to the final target structure, it is important to be more discerning with fractone placement. Another consideration for speed is to try to prompt

growth from older cells rather than from cells that have just undergone mitosis because of the six hour waiting period.

Thus a simple strategy is if the existing cell mass and the target cell mass are far enough apart, then fractones should be placed on every cell, and rapid growth should be allowed. Once the existing cell mass and the target cell mass grow close enough in their boundaries, then in a second phase, fractones should be relocated to the exterior cells of the cell mass in order to direct growth without pushing the rest of the mass. Since this second phase is time-consuming and slow, we wish to make it as short as possible by making our fractone placement choices in the first phase intelligently so that the cell mass boundaries get as close as possible.

We note that generally, although rapid growth and lots of pushing can create holes, we do not have to be too concerned about creating holes where none exist in the final structure. Any hole the size of a cell or larger can easily be filled by placing a fractone on a cell adjacent to the hole on the appropriate side to generate growth to fill the hole, and any hole less than the size of a cell is within our approximation bound. In fact the creation of a hole may be beneficial in the time-optimal solution, as this may push the boundary of the cell mass out further to better match the target mass. Then in the second phase, the holes can be filled in simultaneously with the final detailed growth.

The shape of the target cell mass is important as well. Blocks and masses of cells that are relatively uniform in size on all axes are relatively quick to grow since we can take advantage of the pushing algorithm. However more detailed or spindly structures of cells take a long time to grow since the growth must be directed by fractones on the exterior of the cell mass in order to prevent abnormal growths. In addition, cell masses that are longer along one axis than the others make placing fractones along that axis preferable in order to keep within the approximation bounds.

We split our algorithm into two phases, as previously discussed. The first phase involves growing as rapidly as possible, while the second phase is slower more detailed growth. The second phase's purpose is to complete the growth without pushing the rest of the cell mass, thus requiring that all growth be into empty space and not into other cells.

The second phase is significantly easier than the first phase to algorithmically determine since we consider only one growth at a time. We essentially use the same algorithm as given in the beginning of this chapter: Adjust the target space using the tiling procedure to ensure the new target can be reached without any further pushing. Then compare the existing cell mass to the new target cell mass, locating cells in the target mass that are not present in the existing mass and adjacent to cells in the existing mass. Then place fractones in the appropriate locations to promote growth of the missing cells. If more than one fractone location is viable, then we choose the location adjacent

to the oldest cell - this will ensure that growth happens as fast as possible and is not delayed while we wait for a cell to reach the 6 hour maturity needed for accelerated growth. As growth occurs, fractone positions should be constantly updated until the target is reached. Recall that the tilings are not unique, and the tiling chosen may affect the speed.

The first phase is more difficult as we wish to intelligently choose the growth as to minimize the amount of time we spend in the second phase. This means looking several growths ahead and compensating for any pushing that may occur. Timing is important since each mitosis event can deform the entire system, causing all subsequent growths to further deform the system, and we wish to control these chains of pushes to benefit the speed and accuracy of our execution. Fortunately, removal of the random growth from the system means that the evolution of the system is deterministic. Thus it is possible to adopt a system of trial and error, testing several likely distributions of fractones and choosing the best one. We generate these distributions using the following guidelines already discussed:

- Place fractones along the exterior of the set of cells as long as the subsequent growth will not lie outside the target cell configuration.
- If the current cell mass is far from the boundaries of the target cell configuration, then place fractones on cells in the interior of the cell configuration.
- If the target cell mass is elongated along some axis, then place fractones preferentially along that axis.

Then the idea of the algorithm to generate solutions is:

1. Generate distributions of fractones to test using the above guidelines for the initial cell configuration E_0.
2. (Phase 1) Test a distribution, F_i by simulating the growth until a mitosis event would cause the cell configuration, E_i, to have a directed Hausdorff distance $d(E_i, E_f) \geq 12$. Halt the simulation just before this growth can occur, and refer to the resulting cell configuration as E_i'.
3. If the intermediate cell configuration, E_i', from part (2) does not satisfy the $D_H(E_i', E_f) \leq 12$ (where D_H is the Hausdorff distance), and might benefit from fractones placed on its interior, then repeat steps 1 and 2 for E_i', creating further intermediate cell configuration, E_{ij}', E_{ijk}',

etc. where the subscripts denote each fractone distribution used. Repeat until we are within Hausdorff distance 12 or interior fractones will no longer benefit the speed of the growth.

4. (Phase 2) Generate several new target configurations using the tiling procedure.

5. Test the target configurations, placing fractones as described and generating growth until the target configuration is achieved.

6. Repeat steps 1-5. This will generate a set of sequences of fractone distributions and tilings. Choose the sequence with the shortest time to completion. The sequence defines the control we want.

Note this algorithm does not guarantee time-optimality, it is merely an organized way of finding time-efficient controls.

As mentioned, time optimality is not the only sort of optimization we might pursue. Indeed, other sorts of optimality may be more interesting to study as they may reveal biological mechanisms that have evolved to be highly efficient by some measure.

Chapter 7

Conclusion & Future Work

We have presented a new control hybrid model of morphogenesis and demonstrated many of its key features through a numerical version. We have framed the model as a controlled hybrid system with stochastic elements. The important mechanics of the model, including the diffusion and capture of growth factor, the deformation of the cell mass caused by meninges, the ability to implement real-world experimental data, and the control asserted by fractone placement, have been shown. We have demonstrated the effect of several parameter value changes in order to develop a better intuition of the behavior of the model as parameters change. This is in preparation for the next phase of the work when we must tune the parameters around actual biological data. We have also examined the question of controllability on the non-stochastic model and offered some insights into the optimization question.

While much has been done in preparation, the biological extent of a fractone's ability to control growth will not be known until further laboratory experimentation is completed. Once experimentally-determined three-dimensional maps of developing rat embryos are available, we can begin testing the fractone hypothesis by initializing the model using a map and comparing the results to maps of embryos which are 24 hour older. This process will also allow us to refine the parameter values we have thus far assumed. This includes the growth factor production functions, the timing of the growth factor production, the threshold values for the positive and negative growth factors, the delay between mitosis events, the diffusion constant, the absorption constants, and the initial growth factor distribution.

The MATLAB code for the model has also not been optimized. We would like to examine larger biological structures and reduce the size of the time step to produce better results, however with the current code this is excessively time-consuming. Better hardware and more efficient coding

would help to deliver effective results. The current approach to numerically approximating diffusion shall also be reconsidered to see if a more realistic method can be found.

Finally, determining optimal strategies for growth and finding optimal controls given any pair of initial and final sets of cell bodies is a very interesting problem. While the naive methods introduced in this paper may lead to efficient executions, they are fairly slow as they require repeated trial and error. Further study of the system may reveal better insights leading to more refined methods and results, as well as algorithms to automate the selection of good control of fractone positions (as compared to an intelligent user sitting down and setting the control as was done in the rabbit example). Understanding of the optimal methods in the model may lead to better understanding of the biological system and grant better insight into how all lifeforms takes on their particular form. Our model focuses on fractone-directed morphogenesis, where fractones are responsible for accelerated and directed growth of cells. A common question posed then is "What directs the fractones?" While this is currently unknown, it is our hope that understanding the questions of controllability and optimization may lead us in the right direction to answer this question.

Appendix A

Hybrid Automata

Hybrid model describe systems with both continuous and discrete dynamics over time. Hybrid systems have been studied more in recent years due to their application to digital technology and automated computer systems. Digital technology operates very quickly, and controls can change and toggle their operation nearly instantaneously. As technology moves towards robotics and automated safety systems (consider Google's new automatic cars), understanding the behavior and control of these systems becomes more and more important.

A hybrid automata has sets of continuous variables and discrete variables. In general, the continuous dynamics evolve the continuous state, the values of the continuous variables, like a typical continuous dynamical system. This occurs until specific conditions are met. At that point, an instantaneous change occurs in the discrete state (the values of the discrete variables). At that point, an instantaneous switch occurs. This discrete switch may alter the continuous state, and the continuous dynamics may depend on the discrete state.

As a thought experiment to illustrate a simple hybrid automata, imagine a rocket ship traveling through space with two thrusters that can be switch ON or OFF independently. Then switching a thruster ON or OFF is a change to the discrete state, of which there are four: (OFF,OFF), (OFF,ON), (ON,OFF), (ON,ON). We can assume the discrete change is instantaneous. The continuous variable(s) in this case represent the position of the rocket, and the continuous dynamics (the acceleration of the rocket) are given by simple Newtonian mechanics. Note that the acceleration in the continuous dynamics is dependent on the discrete state (the more thrusters active, the faster the rocket will accelerate).

We define a hybrid automata using the notation from [38]. A hybrid automata is a collection $H = (Q, X, f, Init, D, E, G, R)$:

- Q: A finite set of discrete variables. By $\mathbf{Q}$, we denote the set of values these variables can take.
- X: A finite set of continuous variables. We will always choose the continuous variables to be real-valued, although any smooth manifold can be used. We denote the set of valuations of n such variables $\mathbf{X} = \mathbb{R}^n$.
- $f : \mathbf{Q} \times \mathbf{X} \to T\mathbf{X}$. The vector field describing the evolution of the continuous vector. Here $T\mathbf{X}$ denotes the tangent bundle of $\mathbf{X}$. We will assume for all $q \in textbfQ$ that $f(q, \cdot)$ is globally Lipschitz continuous.
- $Init \subseteq \mathbf{Q} \times \mathbf{X}$. A set of initial continuous and discrete states. By $\mathbf{Q} \times \mathbf{X}$, we denote the set of valuations on $Q \times X$.
- $D : \mathbf{Q} \to P(\mathbf{X})$. Here $P(\mathbf{X})$ denotes the set of all subsets of $\mathbf{X}$. D is a "domain". For $q \in \mathbf{Q}$, $D(q)$ is the subset of $\mathbf{X}$ in which the continuous evolution $\dot{x} = f(q, x)$ occurs.
- $E \subseteq \mathbf{Q} \times \mathbf{Q}$ is the set of "edges". The edge $(q_i, q_j) \in \mathbf{Q} \times \mathbf{Q}$ represents the instantaneous change in discrete state from q_i to q_j. We note that not every pair of discrete states will be in E, as the dynamics of the system may not allow every discrete state to be reached by every other discrete state.
- $G : E \to P(\mathbf{X})$. The "guard conditions" for each edge - the subset of $\mathbf{X}$ which will cause a switch in the discrete state, along the given edge.
- $R : E \times \mathbf{X} \to P(\mathbf{X})$. The "reset map" for each edge. When a discrete switch occurs along edge E, X may change, causing a discontinuous jump in the continuous dynamics.

We illustrate a hybrid automata with a simple example.

Example A.1 Consider the following system in Figure A.1: A ball is placed in a cylindrical container of height L filled with a viscous fluid. One end of the cylinder is red, and the other end is blue. The cylinder is initially placed so that the red side is up. A sensor that can detect the ball is placed at height r. The ball drops at a constant rate through the fluid due to the balance between the viscous drag forces and gravity. When the sensor detects the ball, it flips the container at its center, causing the ball to reverse direction and now fall toward the opposite end of the container.

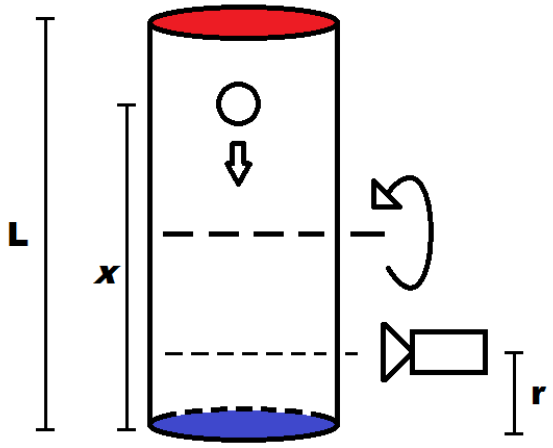

Figure A.1: *The system set-up for hybrid automata Example A.1*

In this system, there is one discrete variable that tracks the orientation of the container, $Q = \{q\}$, with valuation $\mathbf{Q} = \{\text{RED}, \text{BLUE}\}$, representing whether the red side or the blue side of the cylinder is up, respectively, and one continuous variable that tracks the distance of the ball from the blue side, $X = \{x\}$, which takes values in the real numbers, $\mathbf{X} = \mathbb{R}$.

The ball falls at constant rate of ν, so the vector field $f(q, x)$ that describe the motion in the continuous variable are:

$$f(\text{RED}, x) = -\nu$$

$$f(\text{BLUE}, x) = \nu$$

We will always start with the container red side up, and the ball above the sensor. Thus

$$Init = \{(q, x) | q = \text{RED},\ x \in (r, L]\}$$

Since the system undergoes a discrete switch when the ball is detected by the sensor, the domain, D, is given by:

$$D(\text{RED}) = \{x \in \mathbb{R} : x \geq r\}$$

$$D(\text{BLUE}) = \{x \in \mathbb{R} : x \leq L - r\}$$

Two edges exist: $E = \{(\text{RED}, \text{BLUE}), (\text{BLUE}, \text{RED})\}$, and the associated guard conditions for the switch are:

$$G(\text{RED}, \text{BLUE}) = \{x \in \mathbb{R} : x = r\}$$

$$G(\text{BLUE}, \text{RED}) = \{x \in \mathbb{R} : x = L - r\}$$

In this example, the reset map is trivial since the ball does not move in relation to the bottom of the cylinder when the flip occurs.

$$R((\text{RED}, \text{BLUE}), x) = \{x\}$$

$$R((\text{BLUE}, \text{RED}), x) = \{x\}$$

Example A.2 We consider a slightly more interesting example of a hybrid automata. Consider the following system in Figure A.2: Consider a pair of channel locks, which we will call Lock 1 and Lock 2. Each lock has two water pumps, one that moves water in and one that moves water out of the lock. There is a gate between the locks that can be opened or closed.

We will model a simplified automated process for moving a ship up from Lock 1 to Lock 2: Initially, Lock 1 has low water level, and Lock 2 has a high water level. A ship enters Lock 1, and water is pumped in at rate ν, raising the ship. The gate is opened when the water levels in the two locks are similarly high, this resets the water levels in the two locks to be equivalent. The ship moves into Lock 2, the gate is closed and water is pumped out of Lock 1 at rate μ to reset the system, while water is pumped into Lock 2 to further raise the ship.

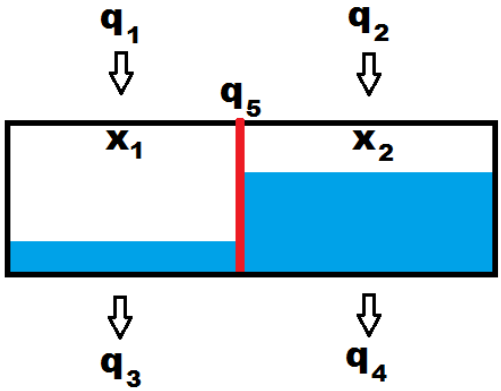

Figure A.2: *The system set-up for hybrid automata Example A.2. The x_i represent water level in the two locks. The discrete variables q_1, q_2, q_3, q_4, takes values of ON or OFF, depending on whether their respective water pumps are active to move water in or out of the locks. Discrete variable q_5 takes values of OPEN or CLOSED, depending on the state of the gate.*

In this example, there are five discrete variables, referring to the four pumps and the gate: $Q = \{q_1, q_2, q_3, q_4, q_5\}$. The state of the pumps for adding water into Locks 1 and 2 are

given by q_1 and q_2, respectively. And the state of the pumps for removing water into Locks 1 and 2 are given by q_3 and q_4, respectively. The state of the gate is given by q_5. Then $\mathbf{Q} = \{\{\text{ON}, \text{OFF}\}, \{\text{ON}, \text{OFF}\}, \{\text{ON}, \text{OFF}\}, \{\text{ON}, \text{OFF}\}, \{\text{OPEN}, \text{CLOSED}\}\}$

There are two continuous variables in this system, $X = \{x_1, x_2\}$, which track the water level in Lock 1 and 2, respectively. Naturally, $\mathbf{X} = \mathbb{R}^2$.

There are 32 combinations for the discrete variables, but we will show f for only those combinations that are relevant to traversing the lock. The three phases, and their associated continuous dynamics are:

- Raising the ship:

$$f\left((\text{ON}, \text{OFF}, \text{OFF}, \text{OFF}, \text{CLOSED}), x\right) = \begin{bmatrix} \nu \\ 0 \end{bmatrix}$$

- Opened lock:

$$f\left((\text{ON}, \text{ON}, \text{OFF}, \text{OFF}, \text{OPEN}), x\right) = \begin{bmatrix} \nu \\ \nu \end{bmatrix}$$

- Resetting the locks:

$$f\left((\text{OFF}, \text{ON}, \text{ON}, \text{OFF}, \text{CLOSED}), x\right) = \begin{bmatrix} -\mu \\ \nu \end{bmatrix}$$

We will consider only one initial condition, as we begin raising the ship, with water levels 10 and 100 in Locks 1 and 2, respectively. $INIT = \{((\text{ON}, \text{OFF}, \text{OFF}, \text{OFF}, \text{CLOSED}), (10, 100))\}$.

The domains for the three phases are:

- Raising the ship:

$$D\left((\text{ON}, \text{OFF}, \text{OFF}, \text{OFF}, \text{CLOSED})\right) = \left\{x \in \mathbb{R}^2 : x_1 \leq 90\right\}$$

- Opened lock:

$$D\left((\text{ON}, \text{ON}, \text{OFF}, \text{OFF}, \text{OPEN})\right) = \left\{x \in \mathbb{R}^2 : x_2 \leq 100\right\}$$

- Resetting the locks:

$$D\left((\text{OFF}, \text{ON}, \text{ON}, \text{OFF}, \text{CLOSED})\right) = \left\{x \in \mathbb{R}^2 : x_1 \geq 10\right\}$$

The edges we consider are naturally, the ones that move us through the three phases. The relevant guard conditions are:

$$G\left(((\text{ON}, \text{OFF}, \text{OFF}, \text{OFF}, \text{CLOSED}), (\text{ON}, \text{ON}, \text{OFF}, \text{OFF}, \text{OPEN}))\right) = \left\{x \in \mathbb{R}^2 : x_1 = 90\right\}$$

$$G\left(((\text{ON}, \text{ON}, \text{OFF}, \text{OFF}, \text{OPEN}), (\text{OFF}, \text{ON}, \text{ON}, \text{OFF}, \text{CLOSED}))\right) = \left\{x \in \mathbb{R}^2 : x_2 = 100\right\}$$

The reset map is largely trivial except when the gates is opened. When this occurs, the water levels in the two locks equalize at their average.

$$R\left(((\text{ON}, \text{OFF}, \text{OFF}, \text{OFF}, \text{CLOSED}), (\text{ON}, \text{ON}, \text{OFF}, \text{OFF}, \text{OPEN})), x\right) = \left(\frac{1}{2}(x_1 + x_2), \frac{1}{2}(x_1 + x_2)\right)$$

Further examples may be found in, [28], [36], and [38].

In our description of the hybrid automata, H, we have very few restrictions on the discrete mechanics described by the guard conditions, edges, and domains. It is generally incumbent on the model creator to ensure that the hybrid automata will operate as intended. We introduce the following two definitions to help us account for a properly working hybrid automata.

Definition We define the *hybrid time trajectory*, τ, as the collection of intervals for continuous growth: $\tau = \{I_i\}_{i=0}^{N}$ such that:

- $I_i = [\tau_i, \tau_i']$ for all $i < N$
- Either $I_N = [\tau_N, \tau_N']$, or $I_N = [\tau_N, \tau_N')$
- $\tau_i \leq \tau_i' = \tau_{i+1}$ for all i.

The idea is that a hybrid time trajectory gives us the time period in which we are in a sequence of discrete states. Note that discrete changes are assumed to occur at $\tau_i' = \tau_{i+1}$, and this notion can easily be extended to $N = \infty$ cases.

We further define $\langle\tau\rangle = \{0, 1, \ldots, N\}$, the indices of the intervals in τ. And we denote $|\tau| = \sum_{i \in \langle\tau\rangle}(\tau_i' - \tau_i)$

Definition An *execution* of a hybrid automaton, H, is a collection $\chi = (\tau, \hat{q}, \hat{x})$, where τ is a hybrid time trajectory, $\hat{q} : \langle\tau\rangle \to \mathbf{Q}$, and $\hat{x} = \{\hat{x}^i(t) : i \in \langle\tau\rangle\}$ is a collection of differentiable maps $\hat{x}^i : I_i \to \mathbf{X}$, such that

- $(\hat{q}(0), \hat{x}^0(0)) \in Init$
- $\forall t \in [\tau_i, \tau_i'), \dot{\hat{x}}^i(t) = f\left(q(i), \hat{x}^i(t)\right)$ and $\hat{x}^i(t) \in D(\hat{q}(i))$
- $\forall i \in \langle\tau\rangle \setminus \{N\}, e \equiv (\hat{q}(i), \hat{q}(i+1)) \in E$, and $\hat{x}^i(\tau_i') \in G(e)$, and $\hat{x}^{i+1}(\tau_{i+1}) \in R(e, \hat{x}^i(\tau_i'))$

Thus an execution, if one exists, describes a "proper" path in the system where we start in a discrete state, the continuous dynamics flow according to f until we hit a guard condition at the boundary of the domain of the discrete state, and this immediately changes our discrete state and our continuous state changes (or in some cases remains the same) so that we are in the domain of the new discrete state, and the continuous dynamic resumes (although potentially affected by the discrete state) until we hit another guard condition. Generally, we always want to carefully construct hybrid automata to have executions. Determining whether a hybrid automata has executions for any given initial conditions, and whether those executions are unique, is one important area of study [36]. Continuity and stability of hybrid systems can also be analyzed [37]. While typically hybrid automata are sensitive to changes in initial condition, especially as they become more complicated in modeling real-world systems, it is possible for hybrid automata to have some sense of continuity. Briefly stated, a hybrid system is continuous if two executions which are "close" remain within a given distance of each other, where this distance is determined by a given metric for $\mathbf{Q} \times \mathbf{X}$ and the difference between the total time $|\tau|$ of the executions.

In examining the behavior of the executions of a system, we make the following brief definitions to categorize executions of a hybrid automata.

Definition

- An execution is *finite* if τ is a finite sequence ending with a compact interval. We denote by $\varepsilon_H^*(q_0, x_0)$ the set of all finite executions.
- An execution is *infinite* if either τ is an infinite sequence, or $|\tau| = \infty$. We denote by $\varepsilon_H^\infty(q_0, x_0)$ the set of all infinite executions.
- An execution is *zeno* if τ is infinite and $|\tau| < \infty$.
- We denote $\varepsilon_H(q_0, x_0)$ as the set of all execution of H with initial condition (q_0, x_0).

A zeno execution, named after the philosopher Zeno and his well-known paradoxes, is one that takes finite time but has an infinite number of switches. For example, in the classic math problem of a bee flying back and forth between two colliding trains, if the discrete states are the directions the bee travels, then the bee makes an infinite number of switches in the discrete state over the finite period of time before the trains collide. Lygeros and Johansson and their colleagues have examined zeno executions [28] [29] , specifically examining ways to extend the zeno executions beyond their zeno time (the finite time of the execution). This is important because in simulating hybrid automata, zeno executions create problems when they begin to switch very quickly - lots of computations occur due to the switching, but no real progress is made since time barely moves. Methods for breaking the zeno behavior have been proposed in order to extend a zeno execution to an infinite execution.

Related to the question of existence of executions, there is also the question of what is reachable by those executions. We therefore make the following definition:

Definition We define the set of all *reachable* states by H: $Reach_H = \{(q,x) \in \mathbf{Q} \times \mathbf{X} : \exists(\{[\tau_i, \tau_i']\}_{i=0}^N, \hat{q}, \hat{x}) \in \varepsilon_H^*, (\hat{q}(N), \hat{x}^N(\tau_N')) = (q,x)\}$.

Analyzing the set of reachable states is important for the next question of controllability. Several papers cited above deal briefly with the question of controllability and reachability in hybrid automata. There is also similar work done on different types of hybrid systems [68], many of which can be rewritten as hybrid automata [35], and some work on controllability for general hybrid systems [70] also exists. The general algorithms given, however, are too computationally intensive for a system as complicated as our model.

Appendix B

Fluid Mechanics

In our model, when two cells collide or when growth would cause a pushing of the cell mass, the deformation algorithm determines the motion. To lend credence to algorithm's assumptions, tests were performed with glass marbles in glycerol. All marbles were spherical and of the same size and shape. A glass marble attached to a rigid pendulum was swung into arrangements of marbles and the final resting state observed. Collisions were also filmed by digital camera. See Fig. B.1 for three examples of the set-up and result. The set-up was chosen to examine the behavior of pushing into off-set neighbors. In the algorithm we use (see Section 5.2), the off-set neighbor cells move perpendicular to the direction of the push. This was usually verified by the experimental results (see Fig B.1(b-c)), however sometimes there was significant motion parallel to the direction of the push (see Fig B.1(a)). The variation is probably due to the difficulty in setting the marbles up in the exact same way each time, so the pendulum impact and the resulting forces were distributed differently.

The experimental set-up was not particularly robust, but these very simple tests supported the intuitive choices we made in our growth algorithm. The algorithm is not perfect and as the experiment showed, there is likely some parallel motion, but as we choose to align to a grid to simplify our model, we feel the perpendicular motion is more pronounced than the parallel motion and so retain the perpendicular motion in the algorithm.

In a second experiment, water beads were used to simulate the behavior of two small daughter cells growing beside each other. Water beads start as approximately 3.5 mm diameter spheres, and when placed in water grow over the course of several hours to approximately 12 mm diameter spheres. The water beads were placed 1 to 2 mm apart underwater in a large fish tank and

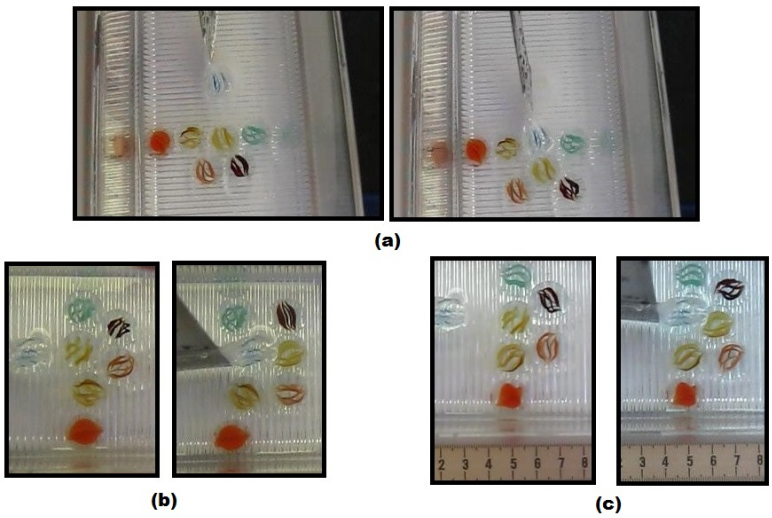

Figure B.1: *Three experimental set-ups and the results after the pendulum swing. A marble was attached to a metal ruler which was suspended above a plastic tray filled with glycerol. The ruler was allowed to swing as a pendulum. Glass marbles were set up in the tray in two rows such that the pendulum would swing in and hit a marble in the first row and push it into the marbles in the second row which are arranged to be off-set from the pushed marble. (a) An experimental set-up and result showing significant motion parallel to the direction of the push, contrary to our algorithm. (b-c) Experimental set-ups and results showing motion mainly perpendicular to the push, similar to our algorithm.*

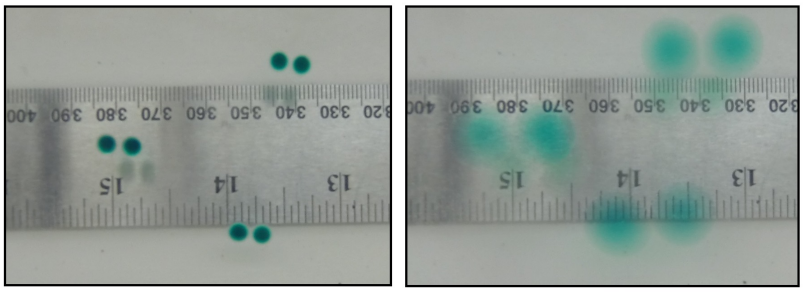

Figure B.2: *Water beads at (left) the start of the experiment and (right) two hours later. The beads push against each other, causing roughly symmetric motion along the axis of their growth, such that the center of mass of the two-bead system remains fairly constant.*

left to grow. A GoPro camera was used to take time lapse footage of their growth. Their final resting state was then observed for their relative positions to one another and their initial location.

Results showed that the water beads pushed against each other symmetrically along the axis of their growth, such that both beads move (see Fig. B.2). This growth pattern is different from what we use in our growth algorithm for unblocked growth, in which one cell remains where the mother cell was located and the second cell is created 12 units away along the axis of growth. While the result is intuitive and contrary to our algorithm, we choose to keep our algorithm as is because the unblocked growth algorithm provides an important directional growth component that allows us to control the development of the cell mass. Future iterations of the model, which may incorporate other means of generating directional growth, may alter the unblocked growth algorithm to be more in-line with the experimental results. Examples of future model components that may cause directional growth include pulling of cells caused by a deformation of the meninges, considering the relative cell mass that must be pushed in each direction during growth, and implementation of cell migration.

Finally, to examine the assumption that cells maintain a 3 unit separation during pushes and after growth, we model the relationship of two spheres growing next to one another in a fluid using some basic fluid mechanics. The spheres are the same size and grow at the same rate. We center our axes in the middle between the two spheres. Due to symmetry, we can reduce the system to two dimensions, and can focus on just one sphere (on the positive z-axis. Growth will occur uniformly around the sphere, so there will be no net motion due to growth as the sphere boundary pushes against the fluid. We use the following notation:

$b(t)$: Position of the center of the sphere

$Q(r,t)$: Volume Flux

α : Growth rate of sphere

R_0 : Initial sphere radius

$R(t) = R_0 + \alpha t$: Radius of the sphere at time t

$h(r,t)$: height of ball boundary at r at time t

$p(r,t)$: pressure

$u(r,z,t)$: Fluid velocity

ρ : density of the fluid

We start with the following governing equations due to negligible inertia and ignoring gravity:

$$\mu \frac{\partial^2 u}{\partial z^2} - \frac{\partial p}{\partial r} = \rho \frac{\partial u}{\partial t} = 0 \tag{B.0.1}$$

$$\frac{\partial p}{\partial z} = -\rho g = 0 \tag{B.0.2}$$

We also have the following boundary conditions:

No slip: $u = 0$ at the sphere boundary $h(r, t)$

Fluid flow maximized between the balls: $\frac{\partial u}{\partial z} = 0$ at $z = 0$.

We note that $h(r,t) - b(t) = -\sqrt{R(t)^2 - r^2}$. We use a Taylor approximation to get $h(r,t) = b(t) + R(t) - \frac{r^2}{2R(t)}$. Only force from fluid pressure will push the ball, but we assume no acceleration, so:

$$\int_0^{R(t)} p 2\pi r \ dr = mb'' = 0$$

$$\int_0^{R(t)} pr \ dr = 0 \tag{B.0.3}$$

We integrate Equation B.0.1 with respect to z, noting that p has no z dependence by Equation B.0.2. Applying our boundary conditions we obtain:

$$u(r, z, t) = \frac{\partial p}{\partial r} \left[\frac{1}{2\mu} z^2 - \frac{1}{2\mu} h(r,t)^2 \right] \tag{B.0.4}$$

We now consider the volume-flux:

The general continuity equation for volume flux is:

$$-\frac{\partial Q}{\partial x} = \frac{\partial h}{\partial t} \tag{B.0.5}$$

We alter this for the volume flux in polar coordinates:

$$-\frac{\partial (rQ)}{\partial r} = r \frac{\partial h}{\partial t} \tag{B.0.6}$$

Substituting our equation for h and integrating, we get:

$$-rQ = \int \left(r \frac{\partial b}{\partial t} - r\alpha - \frac{r^3 \alpha}{2R(t)^2} \right) \ dr$$

$$Q(r,t) = -\frac{r}{2} \frac{\partial b}{\partial t} + \frac{r\alpha}{2} + \frac{r^3 \alpha}{8R^2} \tag{B.0.7}$$

By definition, we know that $Q = \int_{-h(r,t)}^{h(r,t)} u(t)dz$. We substitute the result from B.0.4 and solve to obtain

$$Q(r,t) = -\frac{2}{3\mu}h(r,t)^3\frac{\partial p}{\partial r} \tag{B.0.8}$$

Combining the results from Equations B.0.7 and B.0.8, we can solve for $\frac{\partial p}{\partial r}$, obtaining:

$$\frac{\partial p}{\partial r} = \frac{\frac{r}{2}\frac{\partial b}{\partial t} - \frac{r\alpha}{2} - \frac{r^3\alpha}{8R(t)^2}}{\frac{2}{3\mu}\left(b(t) - R(t) + \frac{r^2}{2R(t)}\right)^3}$$

This can be solved with proper substitution ($w = b - R + \frac{r^2}{2R}$) to obtain:

$$p = \frac{9}{16}\mu\alpha R\frac{1}{w^2} + \frac{3}{8}\mu\alpha\frac{1}{w} - \frac{3}{16}\mu\alpha b\frac{1}{w^2} - \frac{3}{8}\mu\frac{\partial b}{\partial t}R\frac{1}{w^2}$$

We substitute this into Equation B.0.3 and integrate to obtain an equation for $\frac{\partial b}{\partial t}$

$$\frac{\partial b}{\partial t} = \frac{\alpha \ln\left|\frac{b-R/2}{b-R}\right|}{R^2\left(\frac{-1}{b-R/2} + \frac{1}{b-R}\right)} + \frac{3}{2}\alpha - \frac{1}{2}\frac{\alpha b}{R} \tag{B.0.9}$$

We note that $b(t) = h(0,t) + R(t)$. We denote $h(0,t)$ by $h_0(t)$. Then substituting into equation B.0.9, we obtain:

$$\frac{\partial h_0}{\partial t} = \frac{\alpha \ln\left|1 + \frac{R}{2h_0}\right|}{R^2\left(\frac{1}{h_0} - \frac{1}{h_0+R/2}\right)} - \frac{1}{2}\frac{\alpha h_0}{R} \tag{B.0.10}$$

We can numerically solve these differential equations for $b(t)$ and $h_0(t)$ to examine their behavior. Figures B.3 and B.4 show an example solution. Note that the sphere centers grow apart from each other, while the boundary distance initially grows then slowly shrinks. The initial parameters for the figures shown are $R_0 = 0.5$, so a relatively small initial radius (if we treat the units a microns); $\alpha = .5$; and $b(0) = 1$, so there is an initial gap between the spheres of 1 micron. Note that under the chosen α, the cell would reach its full size radius of 4.5 microns in about 8 time units, and at this time the separation between the cells is approximately 3 microns, the same as used in our algorithm.

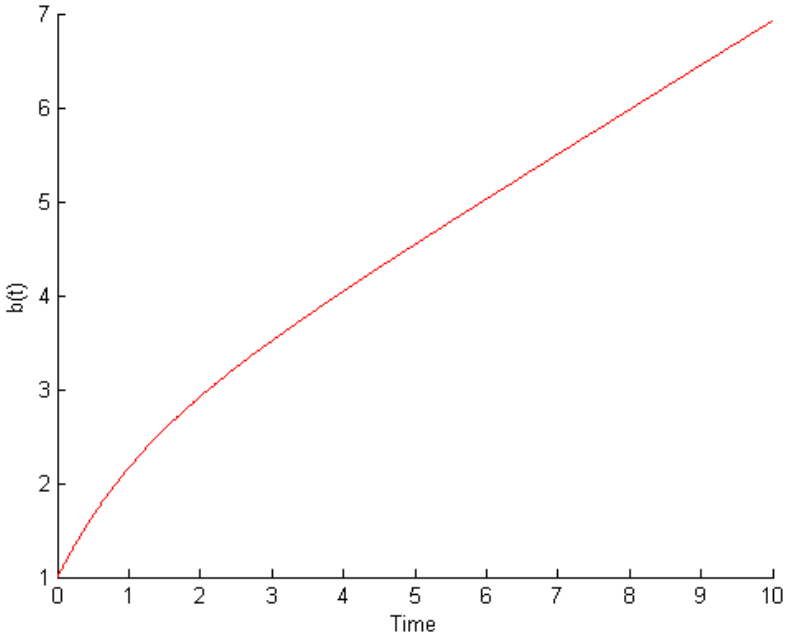

Figure B.3: *Graph of the sphere boundary separation,* $h_0(t)$*, with* $\alpha = .5$*,* $R_0 = .5$*,* $h_0(0) = 1$*.*

As a result of this analysis, we remain comfortable with the assumption that despite cells growing and pushing into each other, the separation between the cells remains at a consistent 3 units.

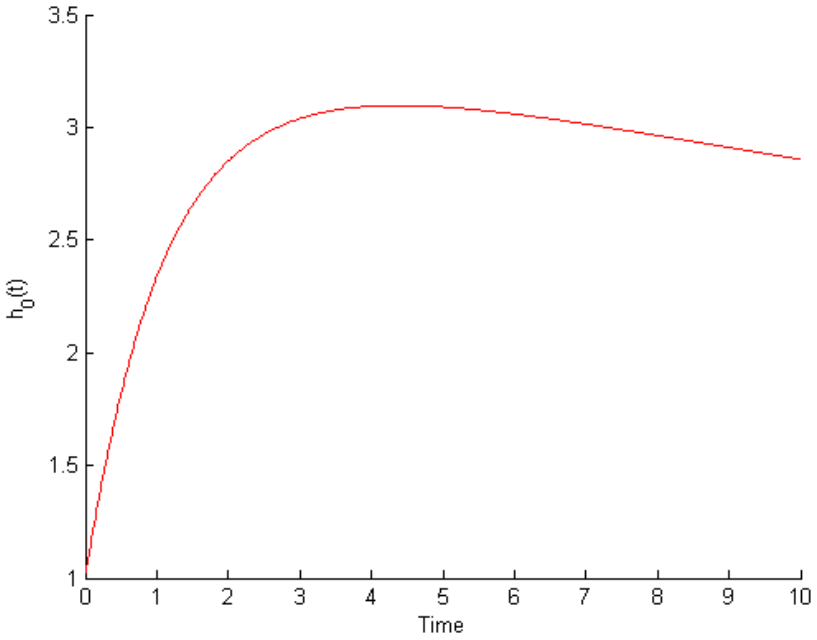

Figure B.4: *Graph of the position of the sphere center,* $b(t)$*, with* $\alpha = .5$*,* $R_0 = .5$*,* $b(0) = 1$.

Bibliography

[1] BS Abrahams and DH Geschwind. Advances in autism genetics: on the threshold of a new neurobiology. *Nature Reviews Genetics*, 9:341–355, 5 2008.

[2] AR Anderson and MA Chaplain. Continuous and discrete mathematical models of tumor-induced angiogenesis. *Bull Math Biol*, 60(5):857–899, 9 1998.

[3] PJ Antsaklis, JA Stiver, and M Lemmon. Hybrid system modeling and autonomous control systems. In RL Grossman, A Nerode, AP. Ravn, and H Rischel, editors, *Hybrid Systems*, volume 736 of *Lecture Notes in Computer Science*, pages 366–392. Springer Berlin Heidelberg, 1993.

[4] RP Araujo and DL McElwain. A history of the study of solid tumour growth: the contribution of mathematical modelling. *Bull Math Biol*, 66(5):1039–1091, 9 2004.

[5] AM Auley, Z Werb, and PE Mirkes. Characterization of the unusually rapid cell cycles during rat gastrulation. *Development*, 117:873–883, 1993.

[6] A Bafico and SA Aaronson. *Holland-Frei Cancer Medicine, 6th edition*. BC Decker, 2003.

[7] SD Banerjee, RH Cohn, and MR Bernfield. Basal lamina of embryonic salivary epithelia. production by the epithelium and role in maintaining lobular morphology. *The Journal of Cell Biology*, 73(2):445–463, 5 1977.

[8] E Bianconi, A Piovesan, F Facchin, A Beraudi, R Casadei, F Frabetti, L Vitale, MC Pelleri, S Tassani, F Piva, S Perez-Amodio, P Strippoli, and S Canaider. An estimation of the number of cells in the human body. *Ann Hum Biol*, 40(6):463–471, Nov-Dec 2013.

[9] JJB Biemond, N van de Wouw, WPMH Heemels, and H Nijmeijer. Tracking control for hybrid systems with state-triggered jumps. *IEEE Transactions on Automatic Control*, 58(4):876–890, 4 2013.

[10] GW Brodland, X Chen, P Lee, and M Marsden. From genes to neural tube defects (ntds): insights from multiscale computational modeling. *HFSP J*, 4(3-4):142–152, 6 2010.

[11] R Chaturvedi, C Huang, B Kazmierczak, T Schneider, JA Izaguirre, T Glimm, HGE Hentschel, JA Glazier, SA Newman, and MS Alber. On multiscale approaches to three-dimensional modelling of morphogenesis. *J R Soc Interface*, 2(3):237–253, 6 2005.

[12] HH Chen and GW Brodland. Cell-level finite element studies of viscous cells in planar aggregates. *J Biomech Eng*, 122(4):394–401, 8 2000.

[13] M Chyba, M Kobayashi, F Mercier, J Rader, A Tamura-Sato, G Telleschi, and Y Kwon. A new approach to modeling morphogenesis using control theory. *Special volume of the São Paulo Journal of Mathematical Sciences in honor of Prof. Waldyr Oliva,*, 5(2):281–316, 2012.

[14] P Ciarletta, M Ben Amar, and M Labouesse. Continuum model of epithelial morphogenesis during caenorhabditis elegans embryonic elongation. *Phil. Trans. R. Soc. A*, 367:3379–3400, 2009.

[15] DA Clausi and GW Brodland. Mechanical evaluation of theories of neurulation using computer simulations. *Development*, 118:1013–1023, 1993.

[16] B De Schutter, WPMH Heemels, J Lunze, and C Prieur. Survey of modeling, analysis, and control of hybrid systems. In J. Lunze and F. Lamnabhi-Lagarrigue, editors, *Handbook of Hybrid Systems Control - Theory, Tools, Applications*, pages 31–55. Cambridge University Press, 2009.

[17] I Decimo, G Fumagalli, V Berton, M Krampera, and F Bifari. Meninges: from protective membrane to stem cell niche. *American Journal of Stem Cells*, 1(2):92–105, 2012.

[18] S-I Despa and F Despa. Diffusion model for growth factorscell receptors interaction. *BioSystems*, r4:59–68, 7 1997.

[19] V Douet, E Arikawa-Hirasawa, and F Mercier. Fractone-heparan sulfates mediate bmp-7 inhibition of cell proliferation in the adult subventricular zone. *Neuroscience Letters*, 528:120–125, 2012.

[20] MT Fitch and J Silver. Glial cell extracellular matrix: boundaries for axon growth in development and regeneration. *Cell and Tissue Research*, 290(2):379–384, 10 1997.

[21] HB Frieboes, X Zheng, CH Sun, B Tromberg, R Gatenby, and V Cristini. An integrated computational/experimental model of tumor invasion. *Cancer Res*, 66(3):1597–1604, 2 2006.

[22] FH Gage. Neurogenesis in the adult brain. *The Journal of Neuroscience*, 22(3):612–613, 2 2002.

[23] DH Geschwind. Autism: Many genes, common pathways? *Cell*, 135:391–395, 10 2008.

[24] TA Henzinger. The theory of hybrid automata. *Logic in Computer Science. LICS '96. Proceedings. Eleventh Annual IEEE Symposium*, pages 278–292, 7 1996.

[25] DE Ingber, JA Madri, and JD Jamieson. Role of basal lamina in neoplastic disorganization of tissue architecture. *Proc. Natl. Acad. Sci. USA*, 78(6):3901–3905, 6 1981.

[26] AG Jacobson, GF Oster, GM Odell, and LY Cheng. Neurulation and the cortical tractor model for epithelial folding. *Journal of Embryology and Experimental Morphology*, 96:19–49, 7 1986.

[27] S et al Jamain. Mutations of the x-linked genes encoding neuroligins nlgn3 and nlgn4 are associated with autism. *Nature Genetics*, 34:27–29, 5 2003.

[28] KH Johansson, M Egerstedt, J Lygeros, and S Sastry. On the regularization of zeno hybrid automata. *System & Control Letters*, 38:141–150, 1999.

[29] KH Johansson, J Lygeros, S Sastry, and M Egerstedt. Simulation of zeno hybrid automata. *Decision and Control*, 4:3538–3543, 1999.

[30] MA Just, VL Cherkassky, TA Keller, RK Kana, and NJ Minshew. Functional and anatomical cortical underconnectivity in autism: Evidence from an fmri study of an executive function task and corpus callosum morphometry. *Cerebral Cortex*, 17(4):951–961, 6 2007.

[31] G Kempermann, L Wiskott, and FH Gage. Functional significance of adult neurogenesis. *Current Opinion in Neurobiology*, 14:186–191, 2004.

[32] A Kerever, J Schnack, D Vellinga, N Ichikawa, C Moon, E Arikawa-Hirasawa, JT Efird, and F Mercier. Novel extracellular matrix structures in the neural stem cell niche capture the neurogenic factor fibroblast growth factor 2 from the extracellular milieu. *Stem Cells*, 25(9):2146–2157, 9 2007.

[33] Y Kim, MA Stolarska, , and H Othmer. A hybrid model for tumor spheroid growth in vitro i: Theoretical development and early results. *Mathematical Models and Methods in Applied Sciences*, 17(Supplement):1773–1798, 2007.

[34] L Li, W Dong, Y Ji, Z Zhang, and L Tong. Minimal-energy driving strategy for high-speed electric train with hybrid system model. *IEEE Transactions on Intelligent Transportation Systems*, 14(4):1642–1653, 12 2013.

[35] H Lin and PJ Antsaklis. Hybrid dynamical systems: An introduction to control and verification. *Foundations and Trends in Systems and Control*, 1(1):1–172, 2014.

[36] J Lygeros, KH Johansson, S Sastry, and M Egerstedt. On the existence of executions of hybrid automata. *Decision and Control*, 3:2249–2254, 1999.

[37] J Lygeros, KH Johansson, SN Simic, J Zhang, and SS Sastry. Continuity and invariance in hybrid automata. *Decision and Control*, 1:340–345, 2001.

[38] J Lygeros, KH Johansson, SN Simic, J Zhang, and SS Sastry. Dynamical properties of hybrid automata. *Automatic Control, IEEE Transactions*, 48(1):2–17, 2003.

[39] J Lygeros, S Sastry, and C Tomlin. *Hybrid Systems: Foundations, Advanced Topics, and Applications*. Springer Verlag, 2012.

[40] J Meitzen, KR Pflepsen, CM Stern, RL Meisel, and PG Mermelstein. Measurements of neuron soma size and density in rat dorsal striatum, nucleus accumbens core and nucleus accumbens shell: Differences between striatal region and brain hemisphere, but not sex. *Neuroscience Letters*, 487:177–181, 2011.

[41] F Mercier and E Arikawa-Hirakawa. Heparan sulfate niche for cell proliferation in the adult brain. *Neuroscience Letters*, 510:67–72, 2012.

[42] F Mercier, JT Kitasako, and GI Hatton. Anatomy of the brain neurogenic zones revisited: fractones and the fibroblast/macrophage network. *J Comp Neurol*, 451(2):170–188, 9 2002.

[43] F Mercier, JT Kitasako, and GI Hatton. Fractones and other basal laminae in the hypothalamus. *J Comp Neurol*, 455(3):324–340, 1 2003.

[44] F Mercier, YC Kwon, and V Douet. Hippocampus/amygdala alterations, loss of heparan sulfates, fractones and ventricle wall reduction in adult btbr t+ tf/j mice, animal model for autism. *Neuroscience Letters*, 506:208–213, 2012.

[45] F Mercier, YC Kwon, and R Kodama. Meningeal/vascular alterations and loss of extracellular matrix in the neurogenic zone of adult btbr t+ tf/j mice, animal model for autism. *Neuroscience Letters*, 498:173–178, 2011.

[46] R Muhle, SV Trentacoste, and I Rapin. The genetics of autism. *Pediatrics*, 113(5):e472–e486, 5 2004.

[47] GF Oster. On the crawling of cells. *Journal of Embryology and Experimental Morphology*, 83:329–364, 11 1984.

[48] E Palsson. *Single-Cell-Based Models in Biology and Medicine*, chapter A 3-D Deformable Ellipsoidal Cell Model with Cell Adhesion and Signaling, pages 271–299. Mathematics and Biosciences in Interaction, 2007.

[49] JL Piovesan, CT Abdallah, and HG Tanner. Preliminary results on interconnected hybrid systems. *Control and Automation*, pages 101–106, 6 2008.

[50] JL Piovesan, CT Abdallah, and HG Tanner. Modeling multi-agent systems with hybrid interacting dynamics. *American Control Conference*, pages 3644–3649, 6 2009.

[51] JL Piovesan, HG Tanner, and CT Abdallah. Discrete asymptotic abstractions of hybrid systems. *Decision and Control*, pages 917–922, 12 2006.

[52] NJ Poplawski, M Swat, JS Gens, and JA Glazier. Adhesion between cells, diffusion of growth factors, and elasticity of the aer produce the paddle shape of the chick limb. *Physica A*, 373:521532, 1 2007.

[53] J Rader. Dynamic modelling of neural morphogenesis using mathematical control theory. Master's thesis, University of Hawai'i, 4 2011.

[54] KA Rejniak and ARA Anderson. Hybrid models of tumor growth. *Wiley Interdiscip Rev Syst Biol Med*, 3(1):115–125, 2011.

[55] C Ronse and M Tajine. Discretization in hausdorff space. *Journal of Mathematical Imaging and Vision*, 12:219–242, 2000.

[56] W Rudin. *Principles of Mathematical Analysis: Third Edition*. McGraw-Hill, Inc., 1976.

[57] JR Sanes. Extracellular matrix molecules that influence neural development. *Ann. Rev. Neurosci*, 12:491–516, 3 1981.

[58] MA Stolarska, Y Kim, and H Othmer. Multi-scale models of cell and tissue dynamics. *Phil. Trans. R. Soc. A*, 367:3525–3553, 2009.

[59] S Sun, MF Wheeler, M Obeyesekere, and CW Jr Patrick. A deterministic model of growth factor-induced angiogenesis. *Bull Math Biol*, 67(2):313–337, 3 2005.

[60] AR Teel, A Subbaraman, and A Sferlazza. Stability analysis for stochastic hybrid systems: A survey. *Automatica*, 50(10):2435–2456, 10 2014.

[61] S Tripakis and T Dang. Modeling, verification and testing using timed and hybrid automata. In Mosterman PJ Nicolescu G, editor, *Model-Based Design of Embedded Systems*, pages 383–427. CRC Press, 2009.

[62] AM Turing. The chemical basis of morphogenesis. *Philosophical Transactions of the Royal Society of London, Series B, Biological Sciences*, 237(641):37–72, 4 1952.

[63] A Voss-Bohme. Multi-scale modeling in morphogenesis: A critical analysis of the cellular potts model. *PLoS ONE*, 7(9), 2012.

[64] R Vracko. Basal lamina scaffold-anatomy and significance for maintenance of orderly tissue structure. *Am J Pathol*, 77(2):313–346, 1974.

[65] D Walker, S Wood, J Southgate, M Holcombe, and R Smallwood. An integrated agent-mathematical model of the effect of intercellular signalling via the epidermal growth factor receptor on cell proliferation. *J Theor Biol*, 242(3):774–789, 10 2006.

[66] JP Ward and JR King. Mathematical modelling of avascular-tumour growth. *IMA J Math Appl Med Biol*, 14(1):39–69, 3 1997.

[67] MA Wyczalkowski, Z Chen, BA Filas, VD Varner, and LA Taber. Computational models for mechanics of morphogenesis. *Birth Defects Res C Embryo Today*, 96(2):132–152, 6 2012.

[68] G Xie and L Wang. Necessary and sufficient conditions for controllability and observability of switched impulsive control systems. *IEEE Transactions on Automatic Control*, 49(6):960–966, 6 2004.

[69] Xu Xuping and PJ Antsaklis. Optimal control of hybrid autonomous systems with state jumps. *American Control Conference*, 6:5191–5196, 2003.

[70] Z Yang and M Blanke. A unified approach to controllability analysis for hybrid control systems. *Nonlinear Analysis: Hybrid Systems*, 1:212–222, 2007.

[71] MM Zarandi, A Bonakdar, , and I Stiharu. Investigations on natural frequencies of individual spherical and ellipsoidal bakery yeast cells. In *Proceedings of the COMSOL Conference 2010 Boston*, 2010.